GEOTECHNICAL ENGINEERING

LUNAR SURFACE ENGINEERING PROPERTIES EXPERIMENT DEFINITION

FINAL REPORT: VOLUME I OF IV
MECHANICS AND STABILIZATION OF LUNAR SOILS

by

JAMES K. MITCHELL
WILLIAM N. HOUSTON

PREPARED FOR MARSHALL SPACE FLIGHT CENTER
HUNTSVILLE, ALABAMA UNDER NASA CONTRACT
NAS 8-21432

JANUARY, 1970

SPACE SCIENCES LABORATORY

UNIVERSITY OF CALIFORNIA · BERKELEY

University of California
Berkeley
Geotechnical Engineering

LUNAR SURFACE ENGINEERING PROPERTIES EXPERIMENT DEFINITION

FINAL REPORT: VOLUME I OF IV
MECHANICS AND STABILIZATION OF LUNAR SOILS

by

James K. Mitchell
William N. Houston

Contract Number NAS 8-21432

Control Number DCN 1-8-28-00056(IF)

January, 1970

Submitted to
National Aeronautics and Space Administration
George C. Marshall Space Flight Center

Space Sciences Laboratory Series 11, Issue 10

This report was prepared by the University of California, Berkeley, under Contract Number NAS 8-21432, Lunar Surface Engineering Properties Experiment Definition for the George C. Marshall Space Flight Center of the National Aeronautics and Space Administration. The work was administered under the technical direction of the Space Sciences Laboratory of the George C. Marshall Space Flight Center.

PREFACE

This report presents the results of studies conducted during the period June 20, 1968 - July 19, 1969, under NASA research contract NAS 8-21432, "Lunar Surface Engineering Properties Experiment Definition." This study was sponsored by the Advanced Lunar Missions Directorate, NASA Headquarters, and was under the technical cognizance of Dr. N.C. Costes, Space Science Laboratory, George C. Marshall Space Flight Center.

The report reflects the combined effort of four faculty investigators, a research engineer, a project manager, and six graduate research assistants, representing several engineering and scientific disciplines pertinent to the study of lunar surface material properties. James K. Mitchell, Professor of Civil Engineering, served as Principal Investigator and was responsible for those phases of the work concerned with problems relating to the engineering properties of lunar soils and lunar soil mechanics. Co-investigators were William N. Houston, Assistant Professor of Civil Engineering, who was concerned with problems relating to the engineering properties of lunar soils; Richard E. Goodman, Associate Professor of Geological Engineering, who was concerned with the engineering geology and rock mechanics aspects of the lunar surface; and Paul A. Witherspoon, Professor of Geological Engineering, who conducted studies related to thermal and permeability measurements on the lunar surface. Dr. Karel Drozd, Assistant Research Engineer performed laboratory tests and analyses pertinent to the development of a borehole probe for determination of the in-situ characteristics of lunar soils and rocks. John Hovland, David Katz, Laith I. Namiq, James B. Thompson, Tran K. Van, and Ted S. Vinson served as Graduate Research Assistants and carried out many of the studies leading to the results presented in this report. Francois Heuzé, Assistant Specialist, served as project manager and contributed to studies concerned with lunar rock mechanics.

Ultimate objectives of this project are:

1) Assessment of lunar soil and rock property data using information obtained from Lunar Orbiter, Surveyor, and Apollo missions.
2) Recommendation of both simple and sophisticated in-situ testing techniques that would allow determination of engineering properties of lunar surface materials.
3) Determination of the influence of variations in lunar surface conditions on the performance parameters of a lunar roving vehicle.
4) Development of simple means for determining the fluid and thermal conductivity properties of lunar surface materials.
5) Development of stabilization techniques for use in loose, unconsolidated lunar surface materials to improve the performance of such materials in lunar engineering application.

The scope of specific studies conducted in satisfaction of these objectives is indicated by the following list of contents of the Detailed Final Report which is presented in four volumes. The names of the investigators associated with each phase of the work are indicated.

VOLUME I

MECHANICS AND STABILIZATION OF LUNAR SOILS

VOLUME II

LUNAR SOIL PROPERTIES FROM PHOTOGRAPHIC RECORDS

1. Soil Property Evaluations From Boulder Tracks on the Lunar Surface
   (H. J. Hovland and J. K. Mitchell)

2. Deduction of Lunar Surface Material Strength Parameters from Lunar Slope Failures Caused by Impact Events - Feasibility Study
   (T. S. Vinson and J. K. Mitchell)

VOLUME III

BOREHOLE PROBES

1. The Mechanism of Failure in a Borehole in Soils or Rocks by Jack Plate Loading
   (T. K. Van and R. E. Goodman)

2. Experimental Work Related to Borehole Jack Probe and Testing
   (K. Drozd and R. E. Goodman)

3. Borehole Jack Tests in Jointed Rock - Joint Perturbation and No Tension Finite Element Solution
   (F. E. Heuzé, R. E. Goodman, and A. Bornstein)

VOLUME IV

FLUID CONDUCTIVITY OF LUNAR SURFACE MATERIALS

1. Studies on Fluid Conductivity of Lunar Surface Materials
   (D. F. Katz, P. A. Witherspoon, and D. R. Willis)

VOLUME I OF FOUR

CONTENTS

VOLUME I OF FOUR (Cont'd) CONTENTS

VOLUME I OF FOUR (Cont'd) CONTENTS

CHAPTER 1

LUNAR SOIL SIMULATION

(W. N. Houston, L. I. Namiq, J. K. Mitchell)

I. INTRODUCTION

A simulated lunar soil has been prepared to use for the study of lunar soil properties in general and to provide background information on the feasibility of several simple geotechnical tests that have been proposed for early Apollo missions. These geotechnical tests, which have been described in a supplement prepared for the Definitive Experiment Plan for the Apollo Lunar Field Geology Experiment, rely mainly on the observation and, where possible, measurement of lunar soil behavior during (1) simple manipulations of the Apollo hand tools, (2) interactions with astronauts, and (3) interactions with spacecraft during landing.

Data obtained during the Surveyor program have provided reasonable quantitative estimates for several important lunar soil properties: e.g., composition, friction angle, cohesion, and density. A simulated lunar soil (referred to hereafter as "lunar soil simulant") with similar properties was prepared for study of other important lunar soil properties such as stress-deformation characteristics, compressibility, and trafficability parameters. Special emphasis has been placed on the variability of these properties with soil density and on the probable variation of density with depth for lunar soil.

The results of the study of the mechanical properties of the lunar soil simulant have also been used as background information for the theoretical and experimental studies of lunar "rolling stones" and

of new injection methods for possible lunar soil stabilization.

II. PREPARATION OF LUNAR SOIL SIMULANT

Selection of an appropriate terrestrial material for simulation of a lunar soil was based on a review of methods and materials used by other investigators, a study of the probable origin of lunar soils, and data provided in the reports of Surveyor missions I, III, V, and VI.

Exact limits on the grain size distribution of lunar soil could not be made using the available data, but the following considerations were used in selecting a test soil for this study.

(1) The best pre-Apollo evidence (Surveyor alpha-backscatter measurements) suggested that the lunar soil is basaltic in composition.

(2) Simulations during the Surveyor program indicated that at least 60 percent of the lunar soil particles should be finer than about 50 μ to account for the appearance of the footpad imprints.

(3) Particle size distribution counts using Surveyor photographs suggests that the lunar soil is fairly well-graded.

(4) Considerations of particle breakdown in the absence of significant chemical weathering, as is likely the case on the moon, suggest that significant numbers of particles finer than 1 μ equivalent spherical diameter are unlikely.

(5) Analyses of Surveyor data indicate that the near-surface lunar soil has a friction angle of the order of 35 to 37 degrees and a unit cohesion of about 0.05 to 0.1 psi. Density estimates vary; however, a value of about 1.5 g/cm^3 was proposed in Surveyor reports.

Selection of a lunar soil simulant involved finding a material that would best fulfill the requirements listed above.

A commercially available basalt sand was obtained. Since this sand did not contain sufficient fine particle sizes, it was necessary to crush a large quantity of the coarse material in a roller mill yielding a fine powder. These fines were mixed in various proportions with the coarse sand.

Shear strength parameters for the various gradations were determined using vacuum triaxial tests. At the same time small trenches with vertical walls were dug in samples of each mixture as a check on the cohesion. These cohesion tests are described in more detail in a later section. Very low confining pressures (0.1 kg/cm^2 and less) were used for the triaxial tests in an effort to simulate the near-surface confinement on the moon.

It was found that as the percent finer than sand size was decreased from 50 to 0, the friction angle increased from about 30° to about 40°. It was also found that densities of about 1.5 g/cm^3 could easily be obtained.

From the results of these studies it was determined that a soil with the gradations shown by Curve 1 in Figure 1-1 would best fulfill the requirements noted. Thus, this material was selected as the basic lunar soil simulant.

The medium coarse basalt sand shown as Curve 2 in Figure 1-1 was used for penetration tests to provide a comparison with the lunar soil simulant. These tests are discussed in the penetration test section.

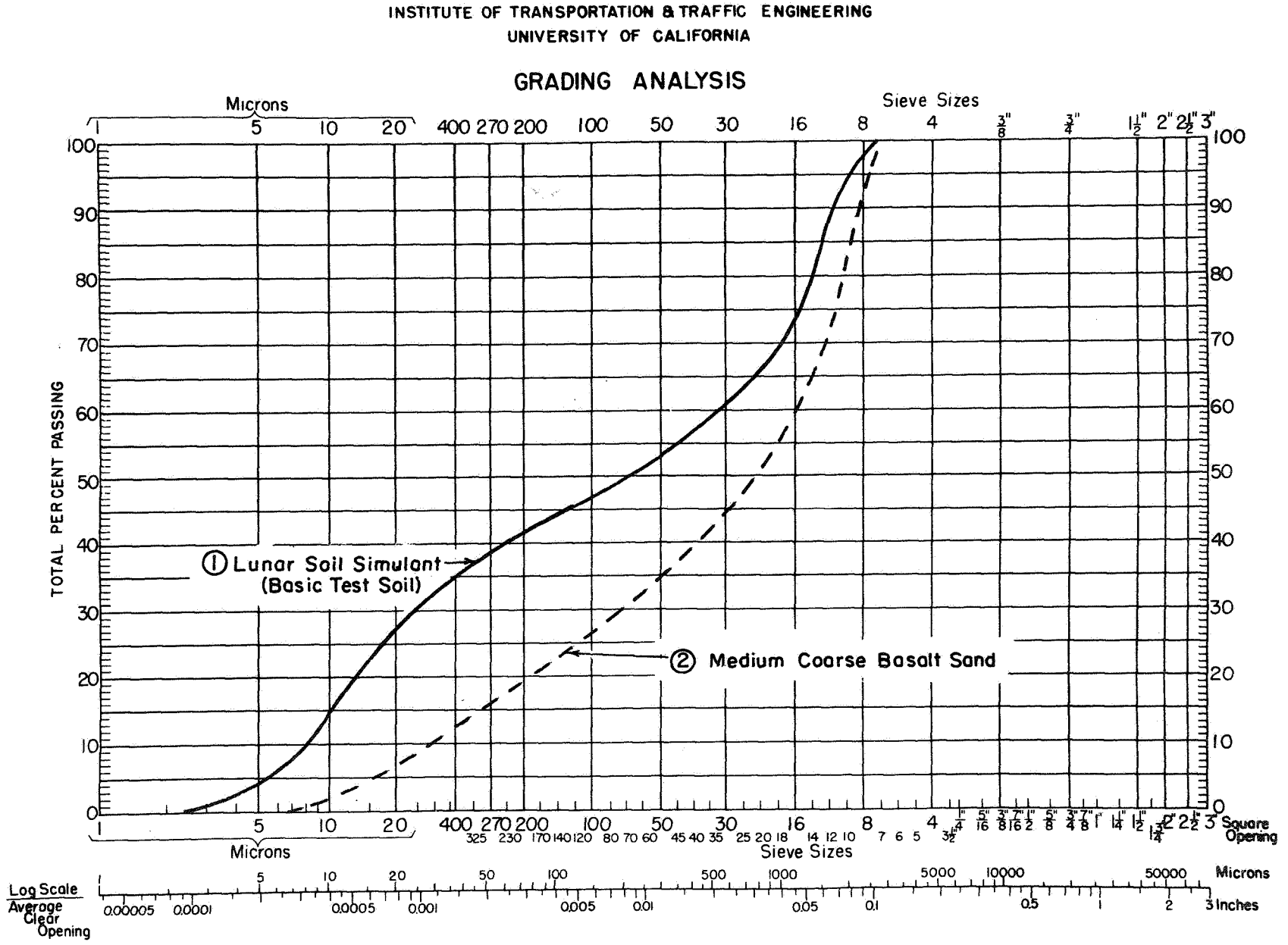

FIGURE 1-1 GRADATION CURVE FOR BASIC TEST SOIL

A large quantity (5500 lbs) of the lunar soil simulant material was shipped to the Marshall Space Flight Center for additional investigations of proposed Apollo geotechnical experiments.

Soil processing was a time-consuming operation involving both sieving and mixing. To obtain the desired gradation for the lunar soil simulant it was necessary to mix a medium-coarse basalt sand with the fine powder obtained by grinding the coarser sand in a roller mill. It was found that the percentage of plus No. 8 in the stock medium-coarse material varied erratically and that some particles as large as one inch were present. Therefore it was necessary to sieve the coarser fraction. A sieve with openings of about 3 mm was used. This process and subsequent mixing resulted in a reduction of the amount larger than the No. 8 sieve size to about 4 percent.

Mixing was accomplished by rolling sealed 55-gal drums in a drum roller for at least 30 minutes. The barrels were filled to about one-third capacity with weighed components. After mixing, the gradation was checked to determine uniformity of mixing. The percent passing the No. 200 sieve was always checked by wet sieving.

III. SOIL PLACEMENT TECHNIQUES

Several methods of placement were tried including (1) sprinkling through a sieve held just above the soil surface, (2) lifting a sieve through the soil, and (3) sprinkling directly on the soil surface from a constant height of about 3/4 inch. The third method was found to be the most satisfactory. The first method is unacceptable because contact between the sieve and the placed soil is unavoidable. This contact causes disturbance and compression of the deposited soil.

The second method is unsatisfactory because the arching and cohesive properties of the soil require that the sieve be extremely coarse or it will not pass through the soil. The third method seems slightly preferable to deposition from a mechanical hopper if very low densities are required, because the quantity of material to be sprinkled must be low and the height of drop small to obtain low initial densities. The sprinkling method described gives an average density of about 1.32 g/cm^3 for the top 1-1.5 inches. The lateral uniformity of density obtained was checked by filling four containers, side by side, to a depth of 1-1.5 inches. The lateral variation in density was only about 1 percent which is quite acceptable.

The sprinkling method was tried with heights of drop up to 6 inches. The relationship between height of drop and average density for the top 1-1.5 inches is shown in Figure 1-2.

IV. FRICTION ANGLE, ϕ

The variation of ϕ with average density has been determined by means of vacuum triaxial tests and vacuum plane strain tests on air-dried material at confining pressures ranging from 0.04 kg/cm^2 to 0.15 kg/cm^2. The lowest confining pressure used was 0.04 kg/cm^2 because the membrane corrections became too large compared to the strength for lower confining pressures. A confining pressure larger than 0.15 kg/cm^2 causes too much densification during isotropic consolidation prior to shearing. Confining pressures less than 0.15 kg/cm^2 must be used for the very loose specimens if excessive densification is to be avoided. The reported densities are the values obtained after consolidation but before shearing.

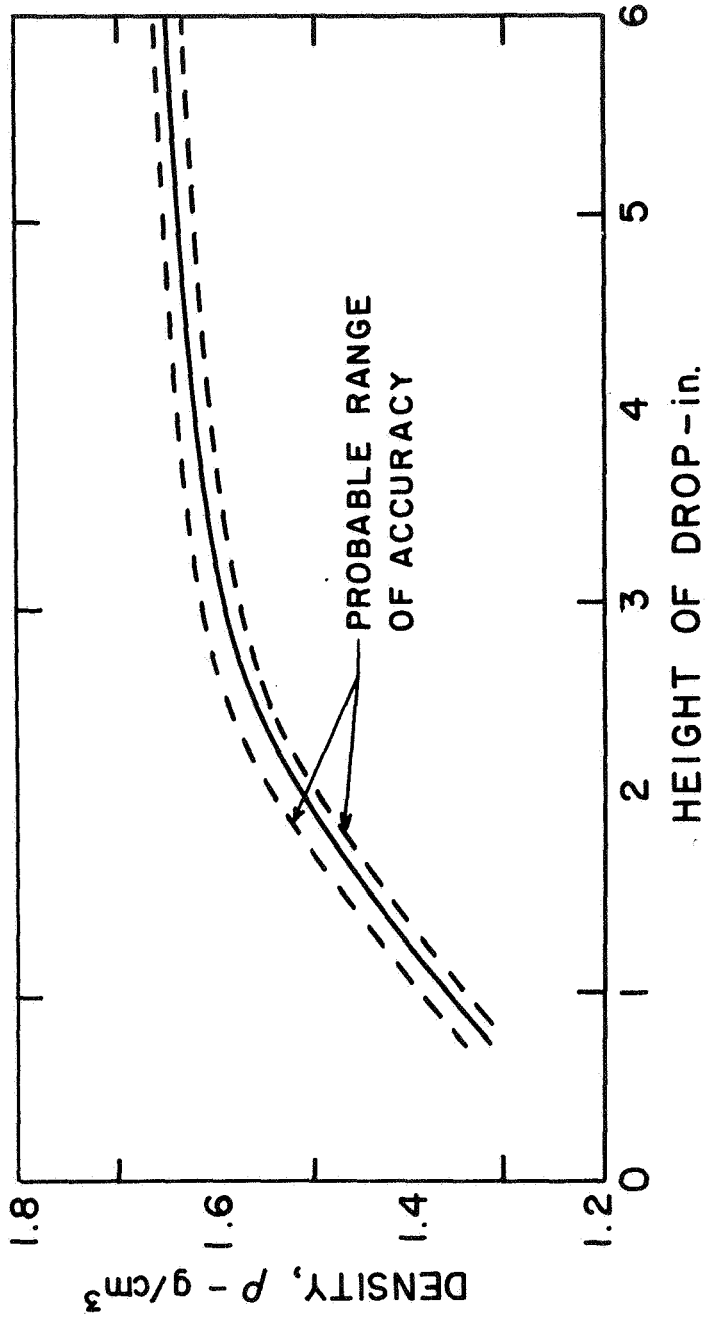

FIGURE 1-2 VARIATION OF DENSITY WITH HEIGHT OF DROP DURING PLACEMENT

As expected, the stress-strain curves for most of the specimens, especially the looser ones, exhibited a plastic-type behavior. A typical stress-strain curve for a triaxial test is shown in Figure 1-3.

The test results are summarized in Figure 1-4, in the form of a plot of tan ϕ vs 1/e. Other sands have shown a straight line plot through the origin when these parameters are used, and the simulated lunar soil appears to conform to this behavior as well. Figure 1-4 shows that a straight line through the origin provides a good fit for the plane strain data and a fair fit for the triaxial data. These data indicate that ϕ for plane strain is about 3 degrees higher than for triaxial conditions for densities between 1.5 and 1.9 g/cm^3. This result is similar to that which has been obtained for other sands.

A high degree of accuracy for ϕ values is difficult to obtain in testing very loose specimens at very low confining pressures, due to the relatively low strengths. It is quite difficult to perform a triaxial test on a specimen with an initial density less than 1.6 g/cm^3 because even small confining pressures cause densification. Probable values of ϕ for densities less than 1.6 g/c^3 have been obtained by extrapolation as shown in Figure 1-4.Nonetheless, the ϕ values obtained for plane strain are very near those suggested for actual lunar soil as a result of Surveyor tests.

V. DETERMINATION OF COHESION

The variation of cohesion with average density has been determined by excavating trenches with vertical walls in samples with different density. This method is preferable to obtaining the cohesion from the Mohr envelope (the usual method) because of the difficulties in

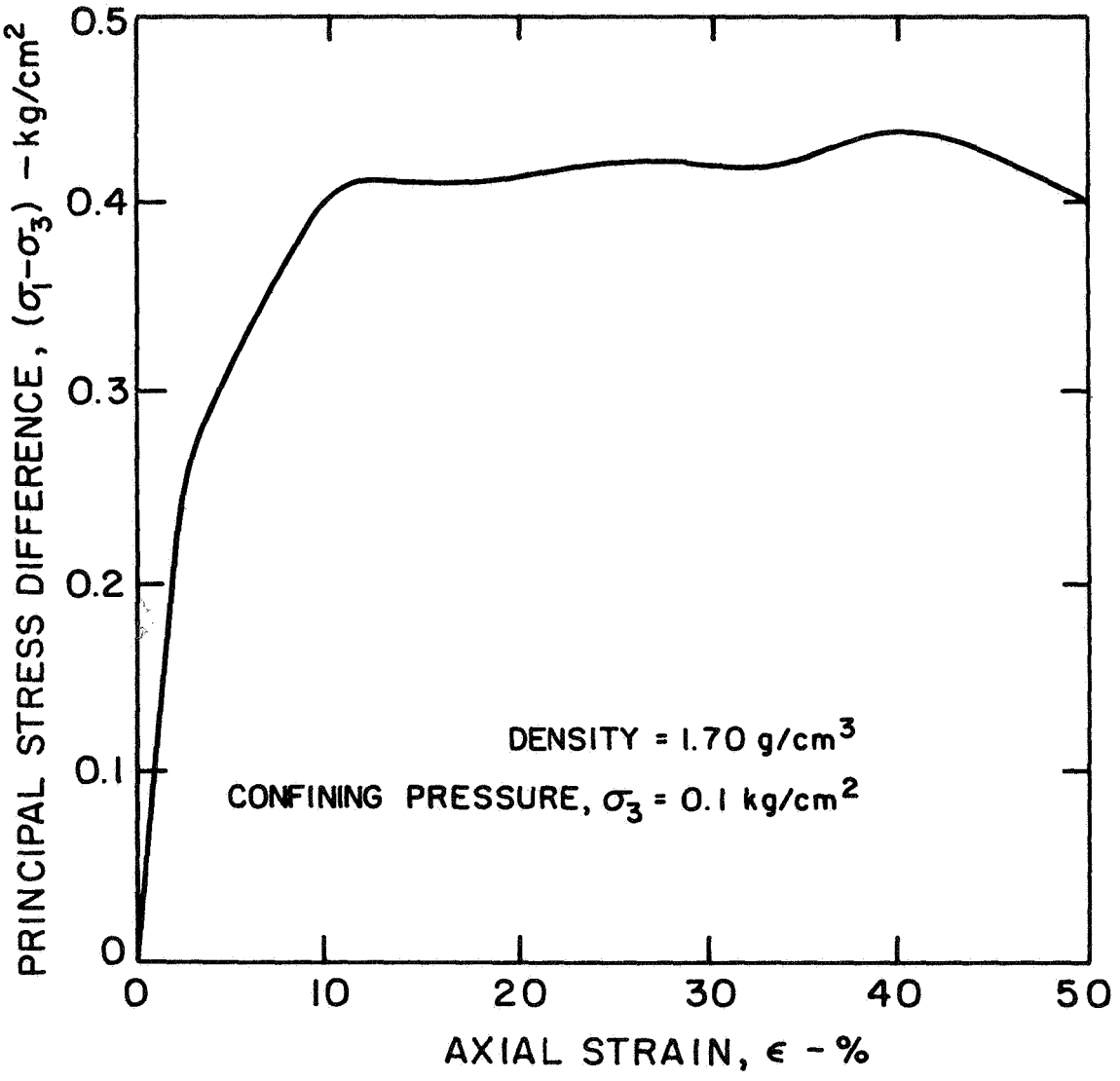

FIGURE 1-3. TRIAXIAL STRESS-STRAIN CURVE

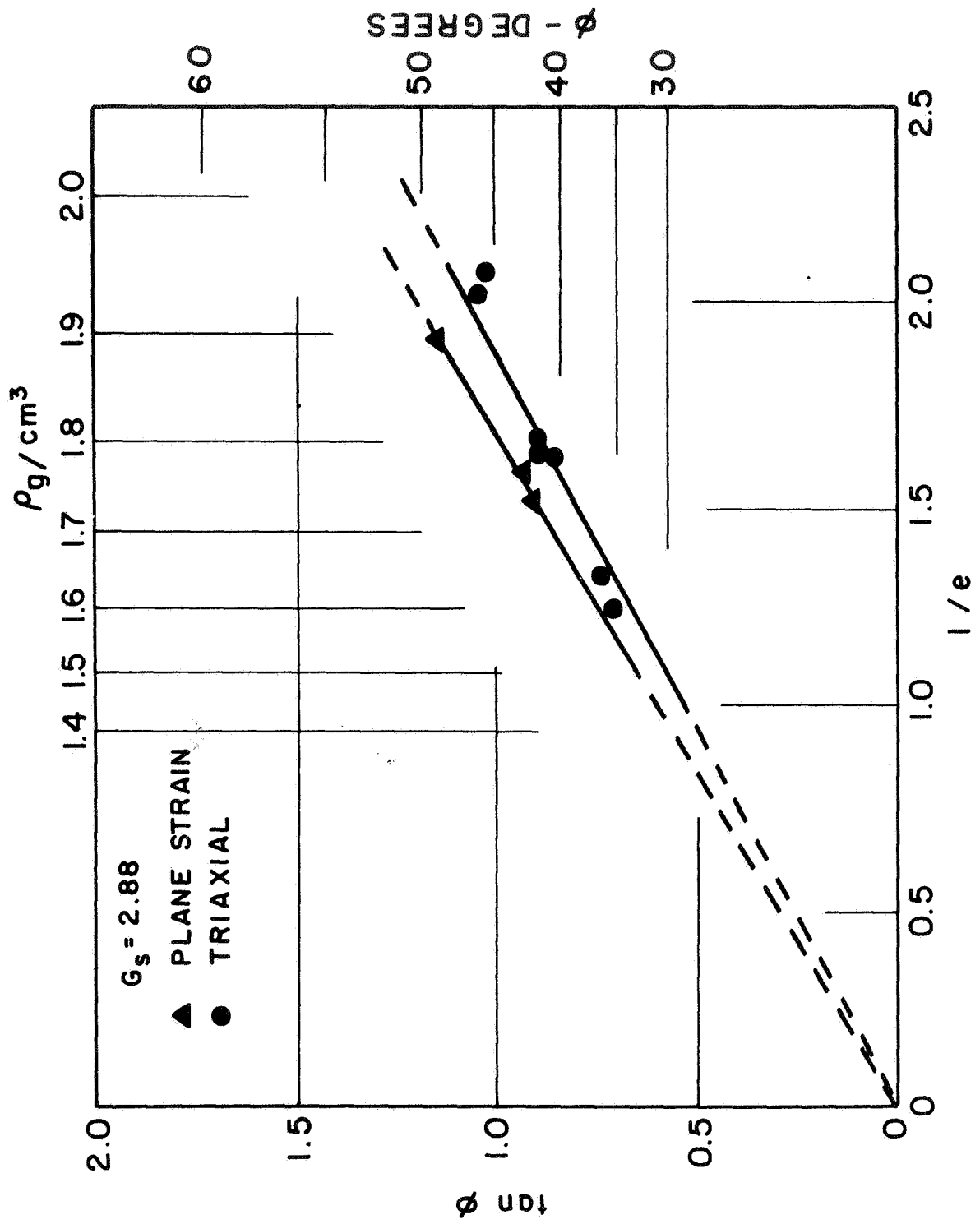

FIGURE 1-4 PLOT OF TAN ϕ VS 1/e FOR BOTH TRIAXIAL AND PLANE STRAIN TESTS

determining strengths of materials with very low cohesion at very small confining pressures, where the failure envelope intercept may be in error by as much as 100 percent. By using the vertical trench wall method, it is believed that errors may be kept much lower.

Many failures of vertical trench walls were studied, and it was found that the sliding block was essentially a Coulomb wedge. Tension cracks usually appeared at the surface, but they did not appear to cover an appreciable percentage of the slip surface. Figure 1-5 shows a photo of a trench excavation for cohesion determination. A tension crack appears about midway along the length of the wall. The wall height shown in the photo is about 2 inches. Failure has occurred along part of the wall. The procedure for calculating the cohesion consisted of (1) measuring the wall height and the distance to the tension crack at which failure developed (2) assuming a plane slip surface, (3) assigning an appropriate value of ϕ and calculating the shearing resistance force due to friction, and (4) assigning the remaining resistance required for stability to cohesion. The calculated value of cohesion was found not to be highly sensitive to either the value of ϕ assigned or the inclination of the failure surface.

It should be noted that the value of cohesion is dependent on the value of the air-dry water content. For water contents near 2 percent, the cohesion increases with air-dry water content. Relationships between cohesion, c, and density, ρ, for various values of air-dry water content are shown in Figure 1-6.

The conclusion appears warranted that the lunar soil simulant exhibits cohesion values appropriate for the range of 0.05 to 0.1 psi estimated for the actual lunar soil from Surveyor test results.

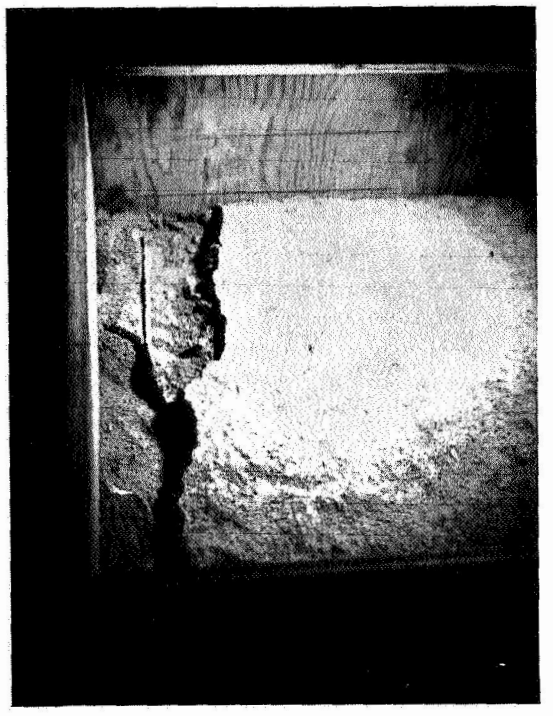

FIGURE 1-5 TRENCH EXCAVATION FOR COHESION DETERMINATION

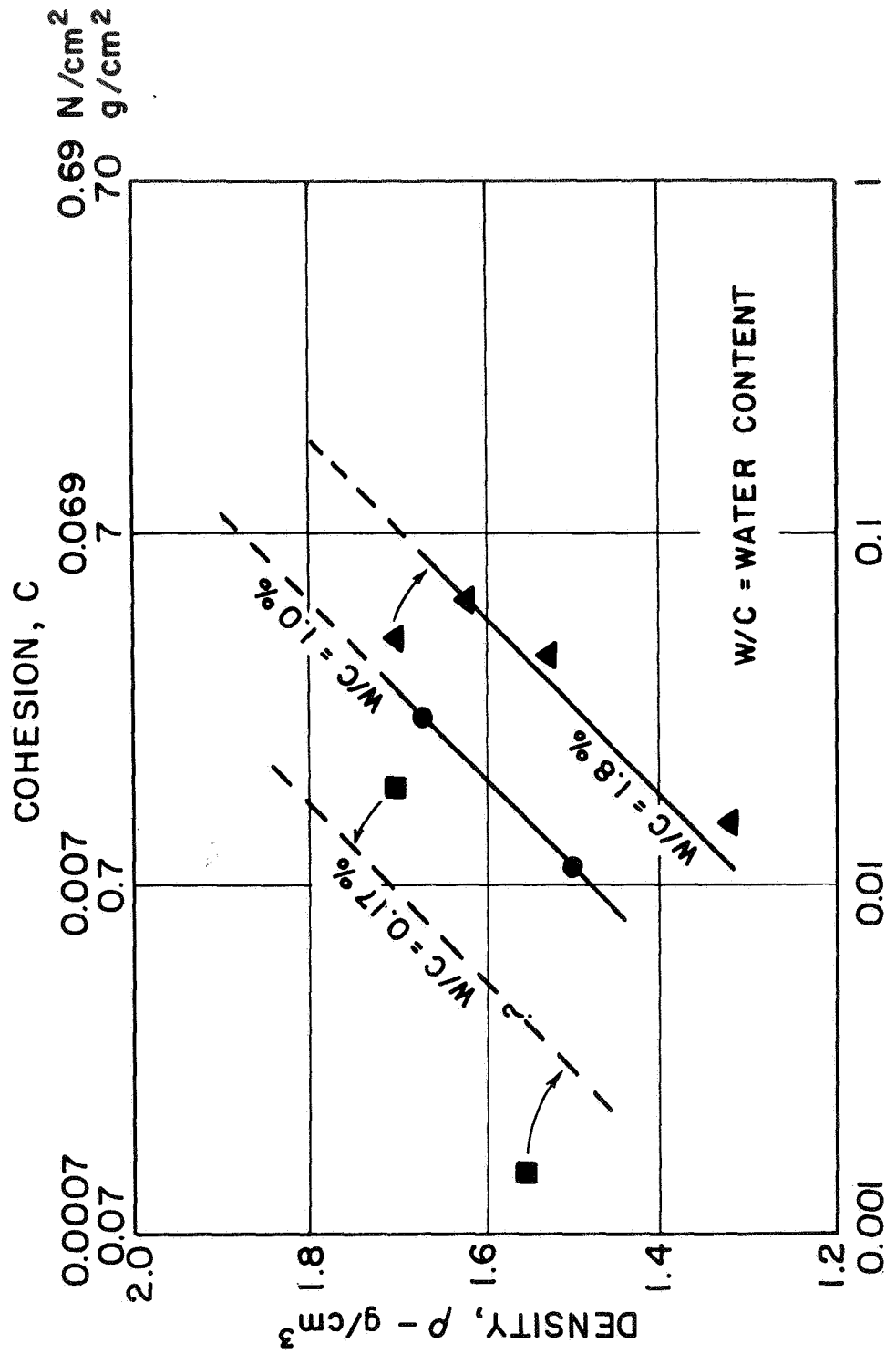

FIGURE 1-6 VARIATION OF COHESION WITH DENSITY AND WATER CONTENT AS DETERMINED BY TRENCHING TESTS

It is of interest to note that a vertical, 2-inch wall for terrestrial soil corresponds to a vertical wall of about 12 inches on the moon for lunar soil of the same density and cohesion, due to reduced gravity stresses. This observation indicates that it will probably not be difficult to excavate around a "cake" of lunar soil, forming four vertical walls. However, the fragile nature of the lunar soil simulant indicates that it may be very difficult to scoop the "cake-like" piece of soil up for a density determination without breaking it apart.

VI. SPECIFIC GRAVITY

The average value of specific gravity, G_s, for the lunar soil simulant was found to be 2.88. This is a reasonable value for basalt.

VII. PERMEABILITY

Two permeability tests were performed on dense specimens of the lunar soil simulant. The test results are shown in Figure1-7. It was necessary to make the test specimens dense to prevent piping and heaving during saturation. The data in Figure1-7indicate that the permeability to water at 20°C varies from about 9×10^{-4} cm/sec at a density of 1.70 g/cm^3 to about 20×10^{-4} cm/sec at a density of 1.50 g/cm^3. However, because of the extrapolation used, these values cannot be regarded as precise.

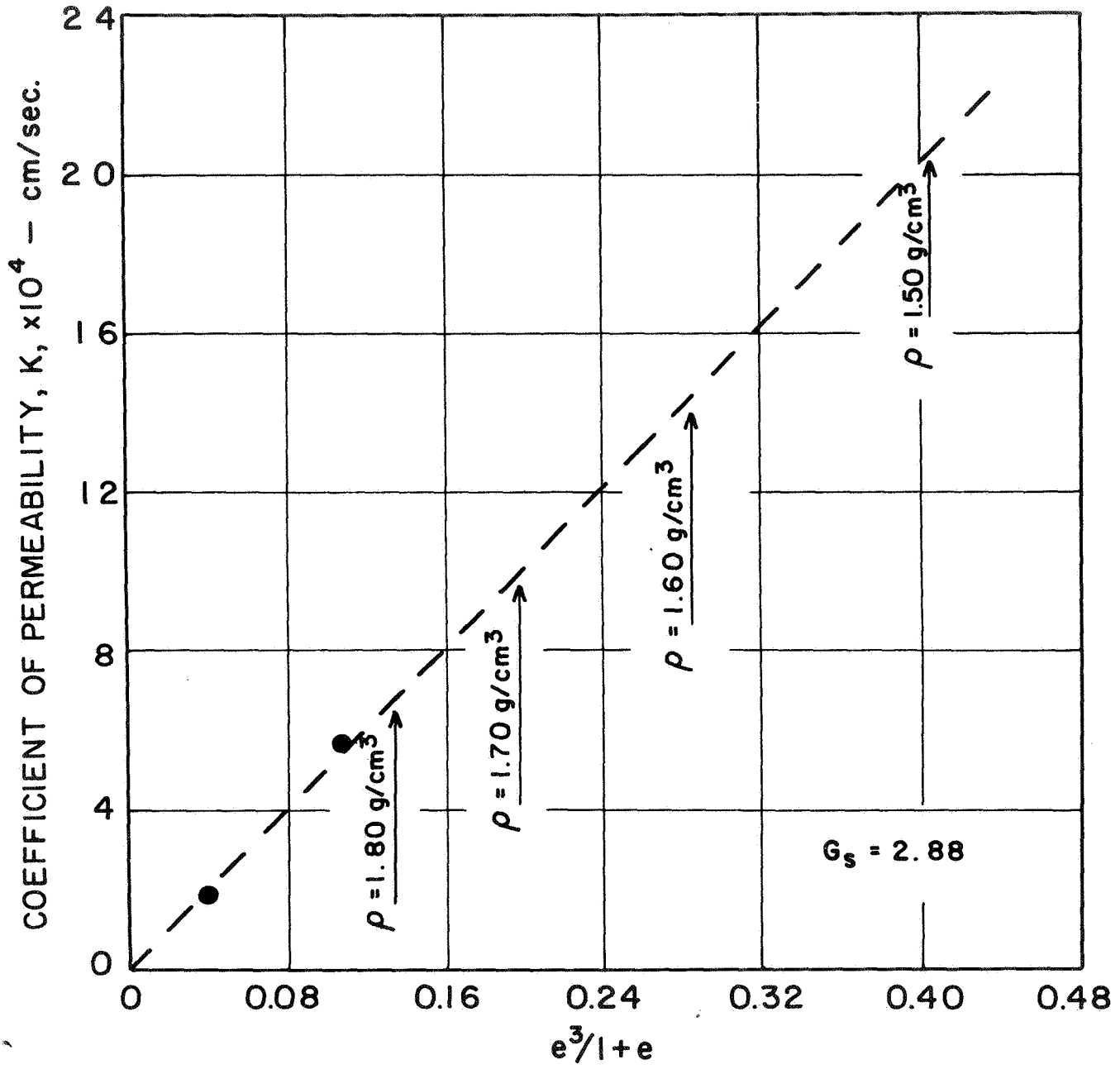

FIGURE 1-7 VARIATION OF PERMEABILITY WITH $e^3/1+e$

VIII. COMPRESSIBILITY CHARACTERISTICS OF LUNAR SOIL SIMULANT

Confined compression tests were performed on specimens with different initial densities to study the compressibility characteristics of the lunar soil simulant. The tests were carried out using a 2.8-inch-diameter teflon-lined consolidation ring. The initial specimen height was 1 inch.

The compression curves obtained from these tests are shown in Figure 1-8. The values of initial density, ρ_i, are shown on the figure. The curves show that the rebound on load release is extremely small. The same data plotted in terms of stress and density are shown in Figure 1-9. One additional compression curve is included in Figure 1-9. The curves marked L and T were obtained by extrapolation and are discussed in the following section.

It is of special interest to note that all the curves for initial densities of 1.76 g/cm^3 and less merge at a stress of 1000 g/cm^2 and a density of about 1.9 g/cm^3, and that the semi-log plot shown on Figure 1-9 indicates a linear variation of density with log pressure for densities greater than the placement density, ρ_i. These facts make extrapolation and interpolation for other initial densities possible.

The straight-line compression curves shown in Figure 1-9 have equations of the form:

$$\rho = K_1 + K_2 \log_{10} \sigma \qquad (1\text{-}1)$$

where σ = vertical compressive stress

ρ = corresponding density

K_1 = value of ρ for $\sigma = 1$ (obtained by extrapolation)

K_2 = change in ρ for one log cycle change in σ.

Equation (1-1) can be written in exponential form giving:

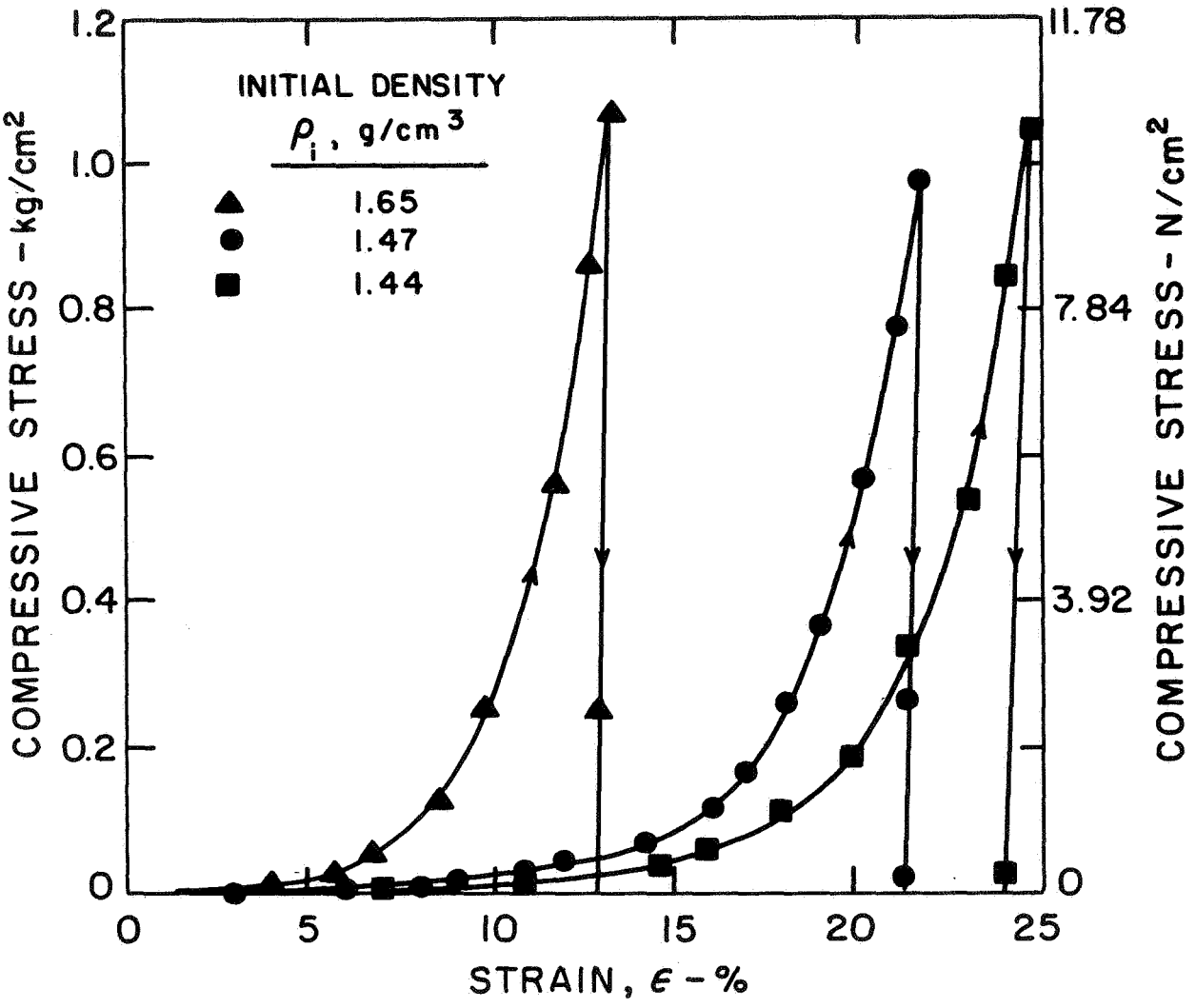

FIGURE 1-8 CONFINED COMPRESSION STRESS-STRAIN CURVES FOR DIFFERENT INITIAL DENSITIES

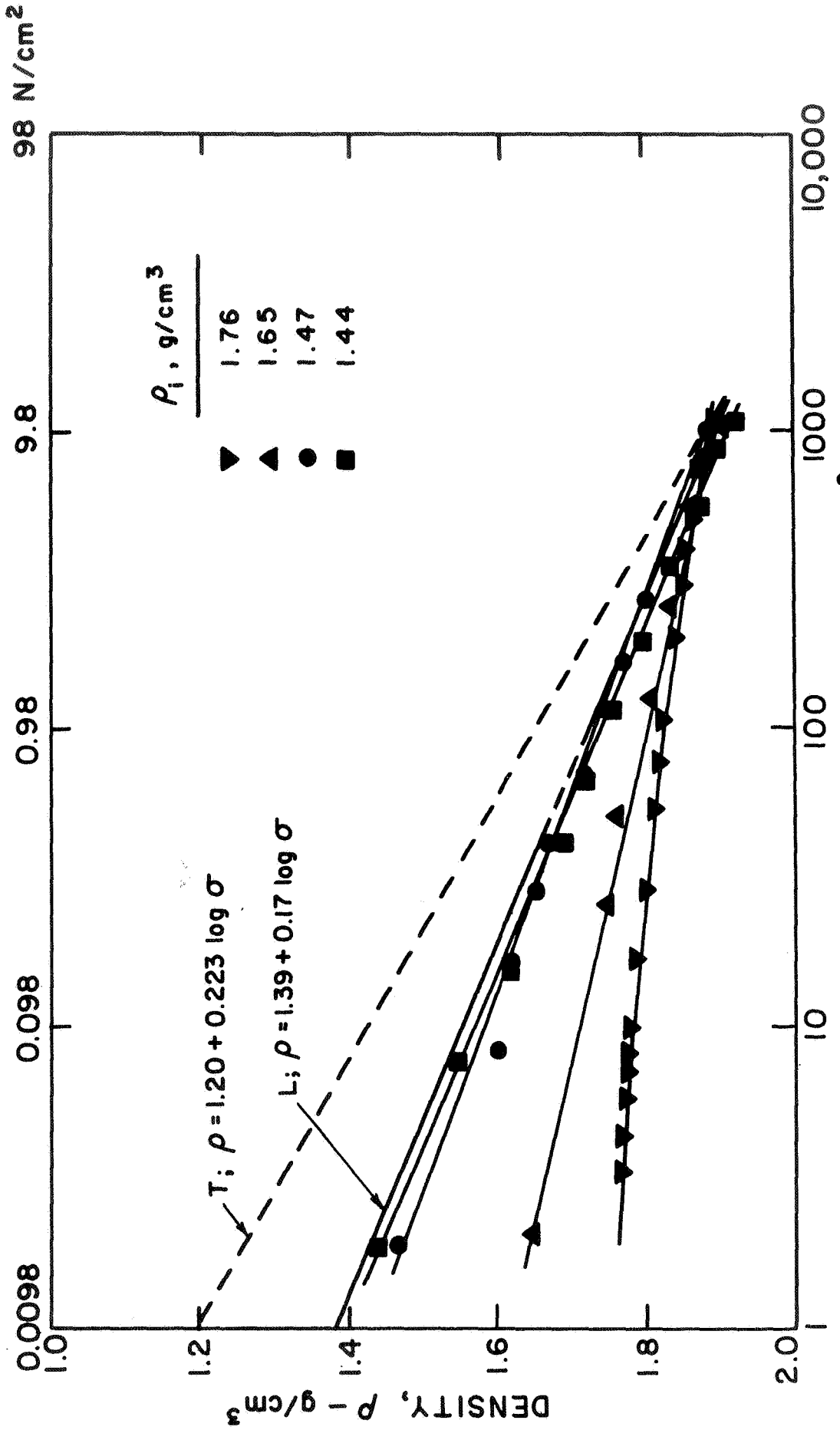

FIGURE 1-9 CONFINED COMPRESSIVE STRESS VS DENSITY

$$\sigma = e^{K_3(\rho - K_1)} \qquad (1\text{-}2)$$

where $K_3 = \frac{2.303}{K_2}$

It should be noted that the form of Equation (1-2) is valid only for initial densities lower than about 1.75 g/cm^3. At higher initial densities the relationship between density and stress deviates slightly from a straight line on the semilog plot. It should also be noted that, although densities less than the initial density, ρ_i, obviously cannot be obtained by compression, the compression curves have been extrapolated back to a stress of 1 g/cm^2 to facilitate mathematical description.

IX. DETERMINATION OF DENSITY, VERTICAL STRESS, AND SHEAR STRENGTH VARIATIONS WITH DEPTH FOR LUNAR SOIL SIMULANT IN TERRESTRIAL ENVIRONMENT

In order to analyze the test data (presented in sections X, XI, and XII) it is necessary to know the initial stresses, shear strengths, and density variations with depth.

It is possible to relate the density to the depth of deposit as follows: First, it may be assumed that a layer of soil of differential thickness, dz, is deposited on the bottom of a test bin at an initial density, ρ_i, and that subsequent densification is due only to the compressive stresses applied by the weight of additional material placed on top. The increase in stress, $d\sigma$, due to the addition of a layer of thickness dz is equal to the thickness of the layer times its density, ρ_i.

$$d\sigma = \rho_i dz \qquad (1\text{-}3)$$

In order to develop a relationship between density and depth, it is necessary to substitute an expression for $d\sigma$ in terms of ρ obtained by differentiating Equation (1-2).

$$d\sigma = K_3 e^{K_3(\rho - K_1)} d\rho \qquad (1\text{-}4)$$

Substitution in Equation (1-3) gives

$$K_3 e^{K_3(\rho - K_1)} d\rho = \rho_i dz$$

Integration gives the following expression

$$\frac{1}{\rho_i} e^{K_3(\rho - K_1)} = z + c_1 \qquad (1\text{-}5)$$

The constant of integration, c_1, can be evaluated by applying the boundary condition that $\rho = \rho_i$ for $z = 0$; therefore,

$$c_1 = \frac{1}{\rho_i} e^{K_3(\rho_i - K_1)} \qquad (1\text{-}6)$$

Equation (1-5) can be rewritten as,

$$\rho = \frac{\ln[\rho_i(z + c_1)]}{K_3} + K_1 \qquad (1\text{-}7)$$

Equation (1-7) is the desired relationship between density, ρ, and depth, z. The validity of this relationship can be verified by placing soil in a test bin and comparing the predicted densities with the measured densities. The most easily measurable quantity for a test bin of soil is the average density, ρ_{ave}, for a given depth of soil, which is determined by measuring total volume and weight after placement. An expression for ρ_{ave} in terms of ρ_i and z can be obtained by integrating Equation (1-7) with respect to z and dividing the result by z.

$$\left(\rho_{ave}\right)_z = \frac{\int \left\{ \frac{\ln[\rho_i(z + c_1)]}{K_3} + K_1 \right\} dz}{z}$$

Integration gives

$$\left(\rho_{ave}\right)_z = \frac{1}{K_3}\left\{\left(1 + \frac{c_1}{z}\right)\left(\ln[\rho_i(z + c_1)] - 1\right) - \frac{c_1}{z}\left(\ln\rho_i c_1 - 1\right)\right\} + K_1 \qquad (1\text{-}8)$$

Equation (1-8) is the desired relationship between ρ_{ave}, ρ_i, and z.

To check the validity of these relationships a 39.8-cm (15.7-inch) layer of lunar soil simulant was placed in a 2' x 2' x 2' test bin* by sprinkling from a height of about 3/4 inch. The average density after placement was measured and found to be 1.50 g/cm^3.

The placement method used produced a density near the surface of about 1.30 to 1.32 g/cm^3, as shown by Figure 1-2. Therefore, it was desirable to obtain a compression curve with this initial density. Although confined compression specimens could be placed at this initial density, they could not be tested without significantly increasing the initial density, because the process of scraping a plane surface on the top of the compression test specimen produces densification. Therefore it was necessary to obtain the probable position of this compression curve by extrapolation. Fortunately, the data in Figure 1-9 show that the desired curve should be a straight line merging with the other curves at a stress of about 1000 g/cm^2. A second point on the curve was obtained by using the known value of initial average density at the surface and assigning an average value of vertical stress due to the weight of a surficial layer. The compression curve thus obtained is shown in Figure 1-9 and marked "T" to signify its applicability to the terrestrial soil in the text bin. Examination of curve "T" in Figure 1-9 shows that $K_1 = 1.20$ and $K_2 = 0.223$ from which $K_3 = 10.32$ can be calculated. Using these

*For the soil simulation studies described in this report a standard soil layer depth of 40 cm was adopted.

compression parameters and ρ_i = 1.30 g/cm^3 and z = 39.8 cm (15.7 inches), solution of Equation (1-9) for ρ_{ave} gives ρ_{ave} = 1.50 g/cm^3, which agrees with the measured value, 1.50 g/cm^3. If a value of ρ_i = 1.32 g/cm^3 is used a value of ρ_{ave} = 1.52 g/cm^3 is obtained for z = 39.8 cm. A value of ρ_i = 1.30 g/cm^3 was then used in Equations (1-7) and (1-8) to compute the variations of ρ and ρ_{ave} with depth. The results are shown in Figure 1-10(a).

The vertical stress at any depth z is given by

$$\sigma = z \cdot (\rho_{ave})_z \qquad (1\text{-}9)$$

Equation (1-9) and the data in Figure 1-10(a) were used to compute the vertical stress variation with depth shown in Figure 1-10(b). The agreement between the computed and measured values of ρ_{ave} for the test bin of soil indicates that the assumptions made and the methods used are reasonable.

The agreement between the computed stresses and the densities shown in Figures 1-10(a) and (b) and the stress-density relationships given by curve "T" of Figure 1-9 indicates that curve "T" is consistent with the density profile obtained.

It should be noted that precise agreement between the computed density-depth relationship shown in Figure 1-10 and that implied by the confined compression curve shown in Figure 1-9 should not be expected for very small depths and for densities less than ρ_i because two modes of densification are involved. The actual soil placement process involves densification due largely to vibration - resulting in a layer of finite thickness at the surface with essentially constant density. This surface layer is then subsequently compressed in accordance with the relationships depicted in Figure 1-9. However, the calculated density-depth relationship shown in Figure 1-10(a) is based on the assumption that all densification is by static compression alone; i.e., the initially deposited surface layer of density ρ_i has only

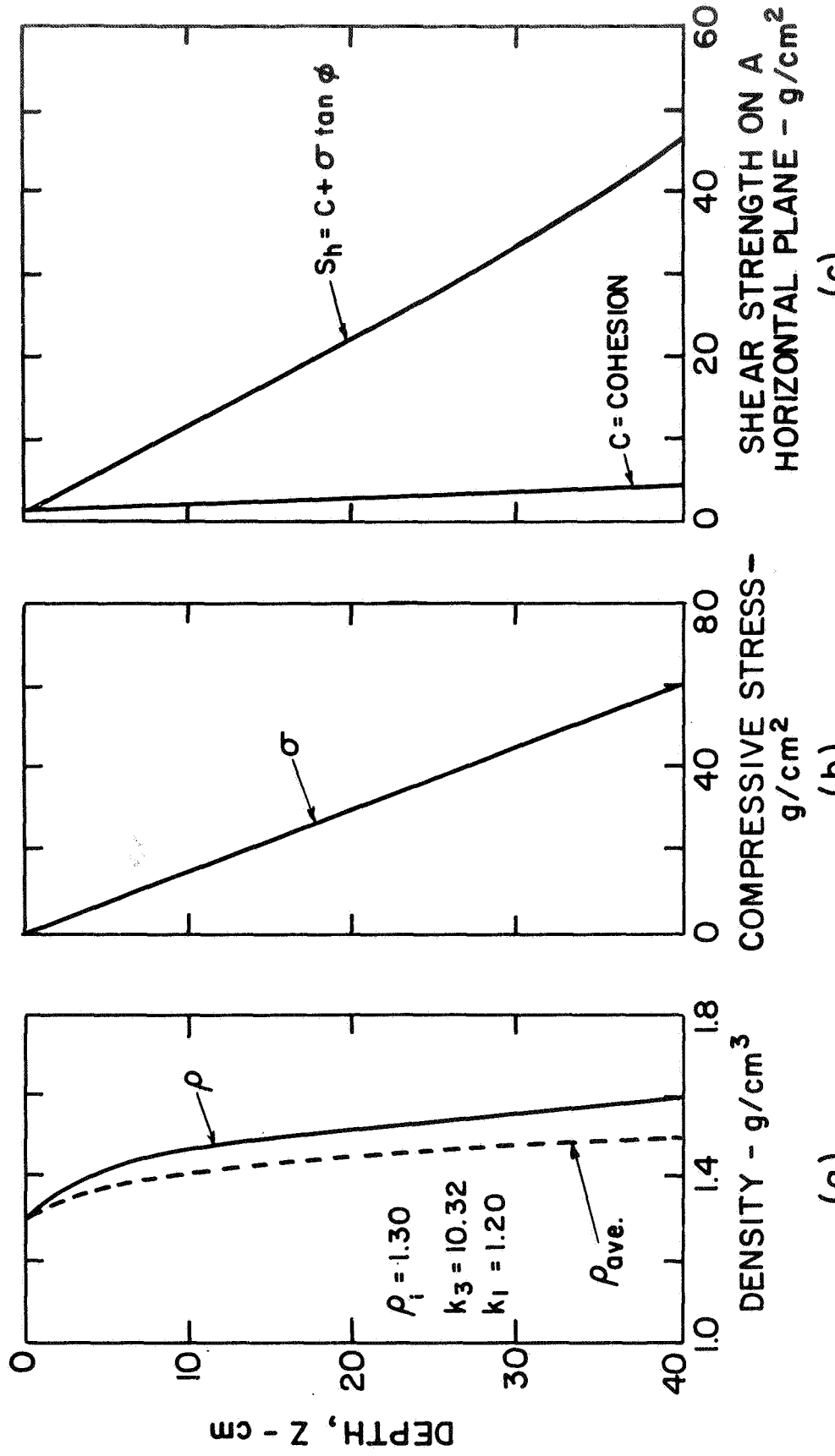

FIGURE 1-10 VARIATION OF DENSITY, VERTICAL STRESS, AND SHEAR STRENGTH WITH DEPTH FOR SIMULATED LUNAR SOIL

differential thickness. The difference caused by this assumption becomes negligible after the compressive stress exceeds a few grams per cm^2 and ρ exceeds ρ_i.

Using the data presented in Figures 1-4, 1-6 (w/c = 1.8%), and 1-10(a, b) it was possible to compute the variation of cohesion, c, and shear strength on a horizontal plane, s_h, with depth, as shown in Figure 1-10(c). Figure 1-10(c) shows that the shear strength variation with depth is nearly linear, although not precisely so, and that the contribution due to cohesion is appreciable for the first 10 to 15 cm.

Similar analyses can be made for 40-cm layers of lunar soil simulant with different values of ρ_{ave}. By choosing a value of ρ_i and interpolating (or extrapolating) in Figure 1-9 to find the appropriate compression curve (as was done in the case just discussed where ρ_i = 1.30 g/cm^3), it is possible to to calculate a corresponding value of ρ_{ave} from Equation (1-8) . Trial and error solutions of this type were made in order to relate ρ_i and ρ_{ave} for the 40-cm layer of lunar soil simulant in the test bin. Typical compression curves with their respective values of ρ_i are shown in Figure 1-11. The corresponding values of ρ_{ave} (which were later calculated from Equation (1-8) are also shown for future reference.

From these compression curves it was possible to compute relationships between ρ_i and K_1, K_3, and c_1 as shown in Figures 1-12, 1-13, and 1-14, respectively. Note that c_1 may also be readily calculated from Equation (1-6) after ρ_i, K_1, and K_3 have been evaluated. Equation (1-8) was used to calculate the relationship between ρ_i and ρ_{ave} shown in Figure 1-15.

The relationships in Figures 1-11 through 1-15 may be used to facilitate the determination of the variation of ρ and ρ_{ave} with depth for various intermediate values of ρ_{ave} for the top 40 cm. For example, Figure 1-16

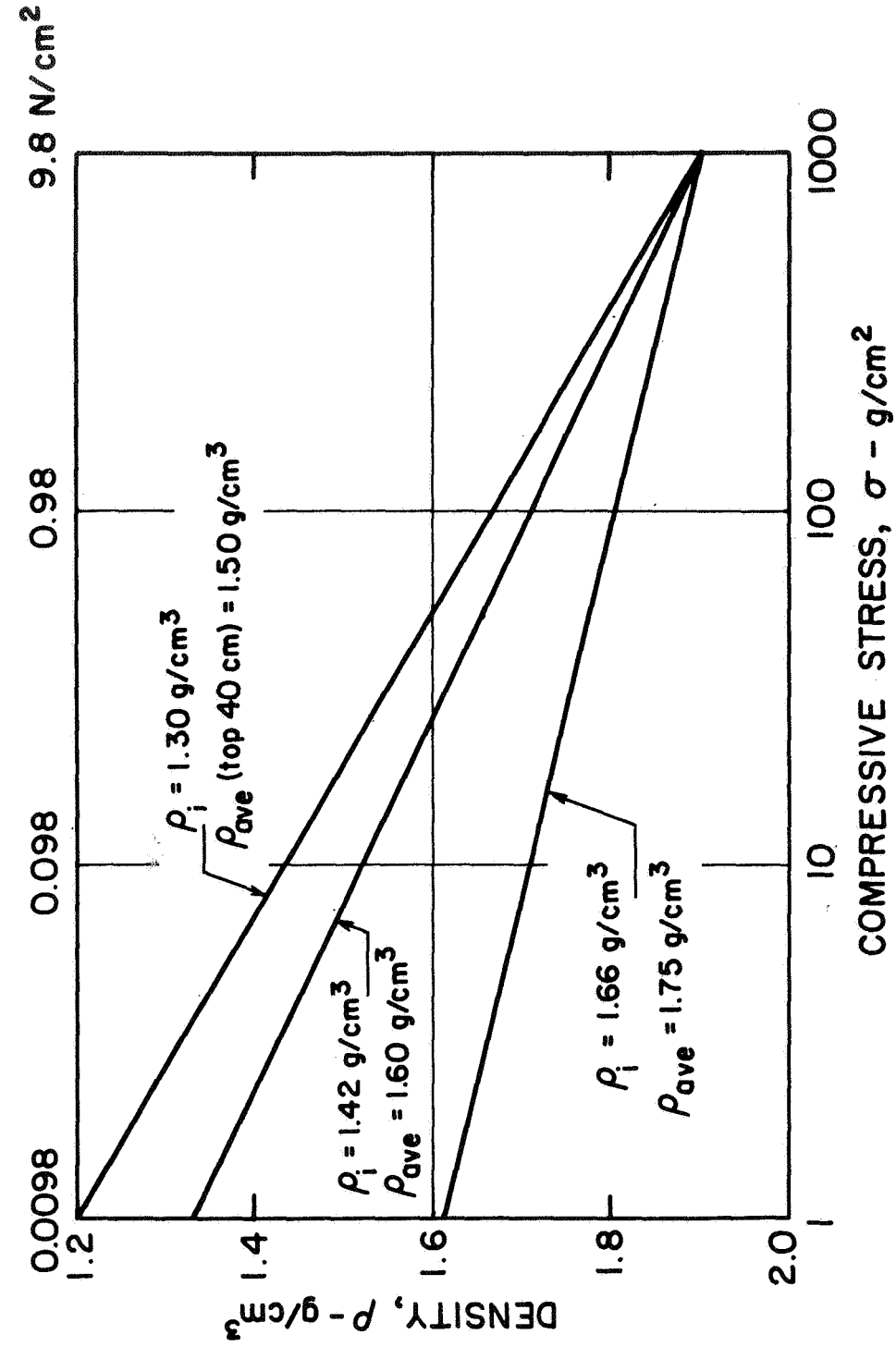

FIGURE 1-11 TYPICAL COMPRESSION CURVES FOR LUNAR SOIL SIMULANT PROFILES WITH VARIOUS VALUES OF ρ_i

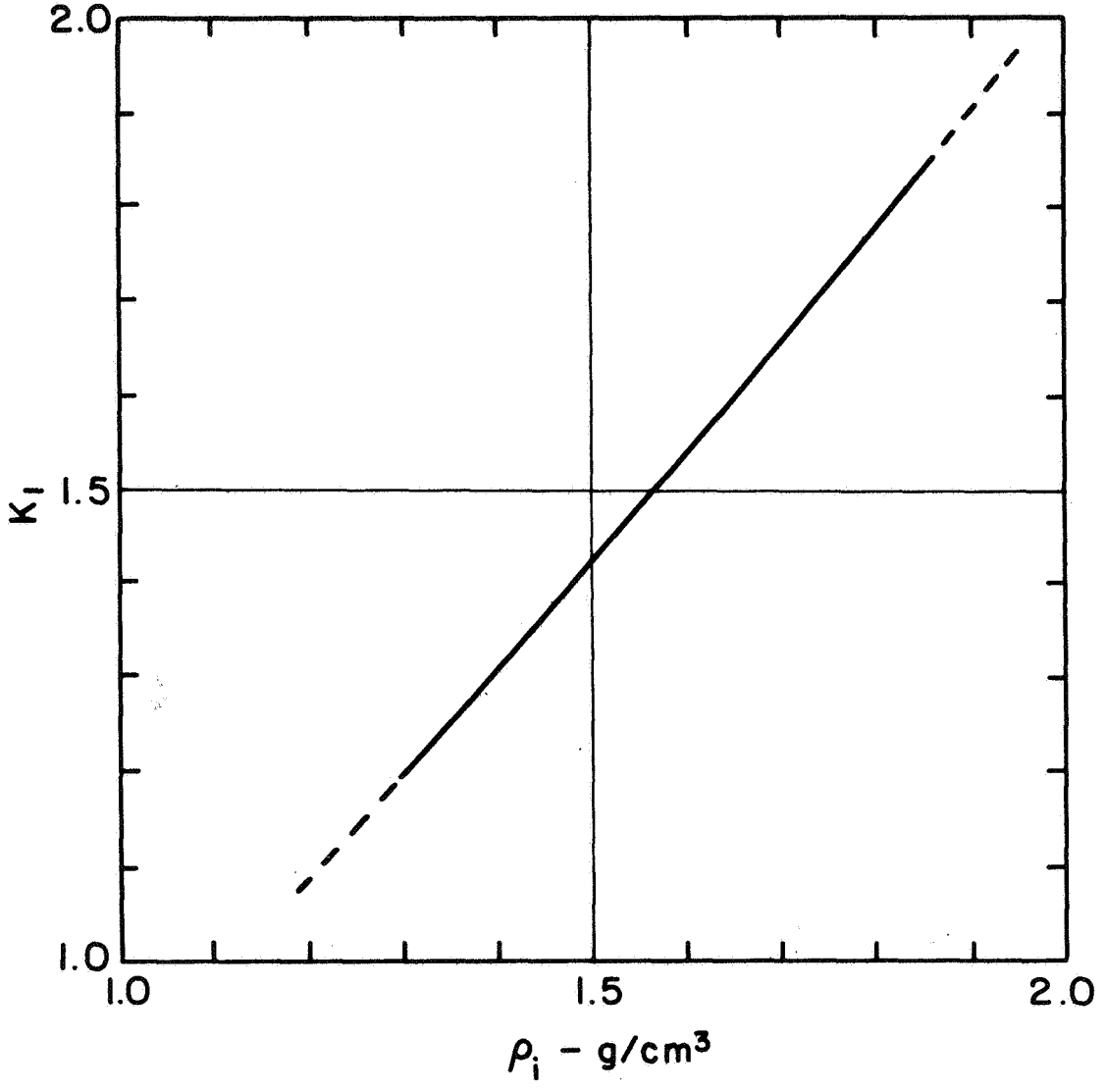

FIGURE 1-12 RELATIONSHIPS BETWEEN ρ_i and K_1 FOR LUNAR SOIL SIMULANT — TERRESTRIAL ENVIRONMENT

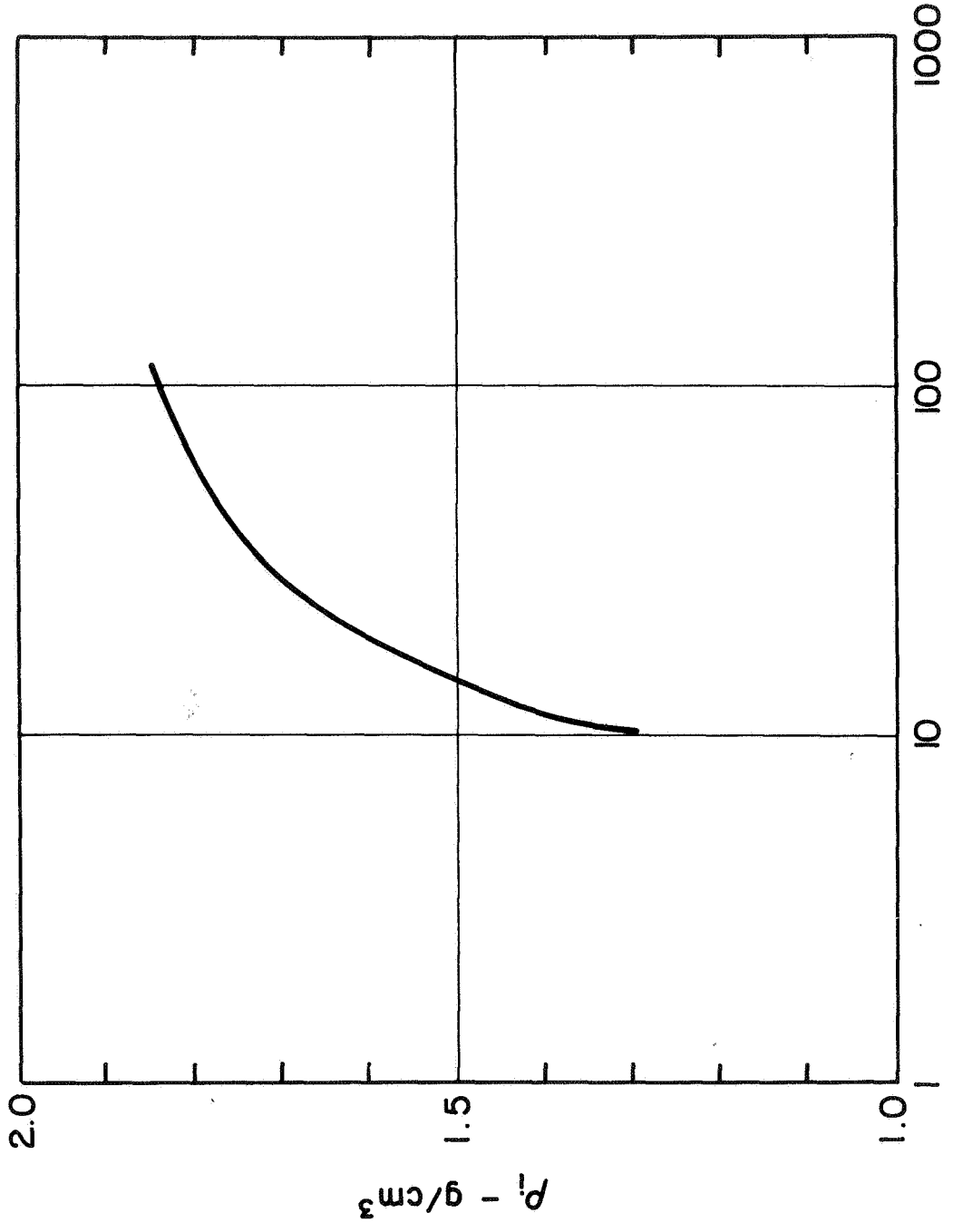

FIGURE 1-13 RELATIONSHIP BETWEEN ρ_i AND K_3 FOR LUNAR SOIL SIMULANT — TERRESTRIAL ENVIRONMENT

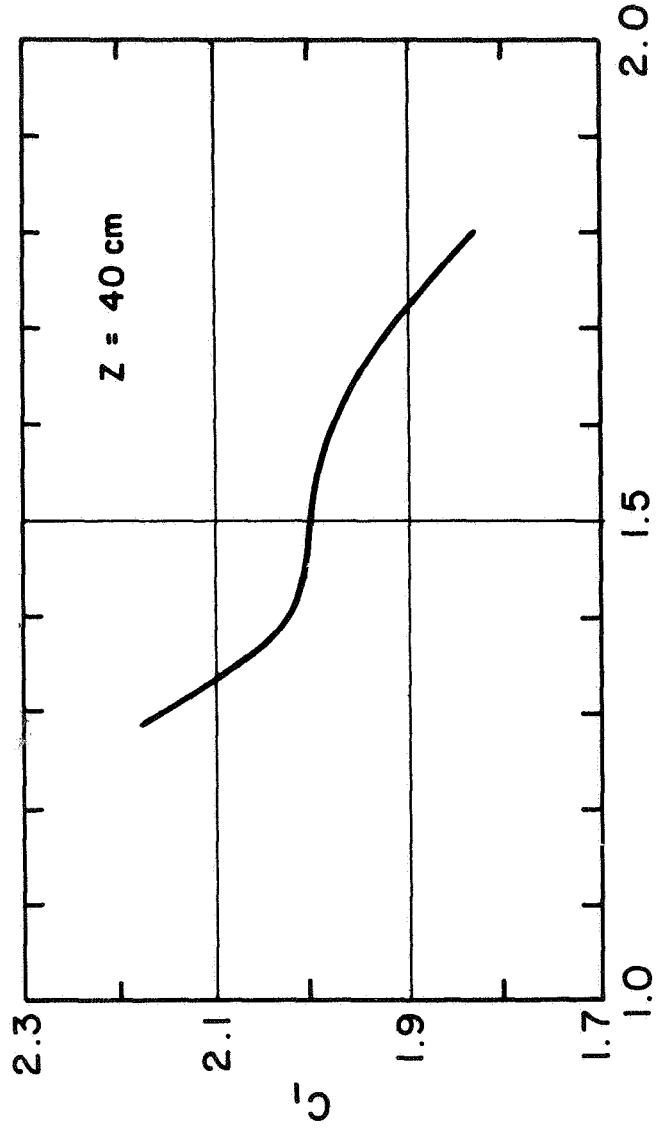

FIGURE 1-14 RELATIONSHIP BETWEEN ρ_i and constant of integration, C_1, FOR LUNAR SOIL SIMULANT — TERRESTRIAL ENVIRONMENT

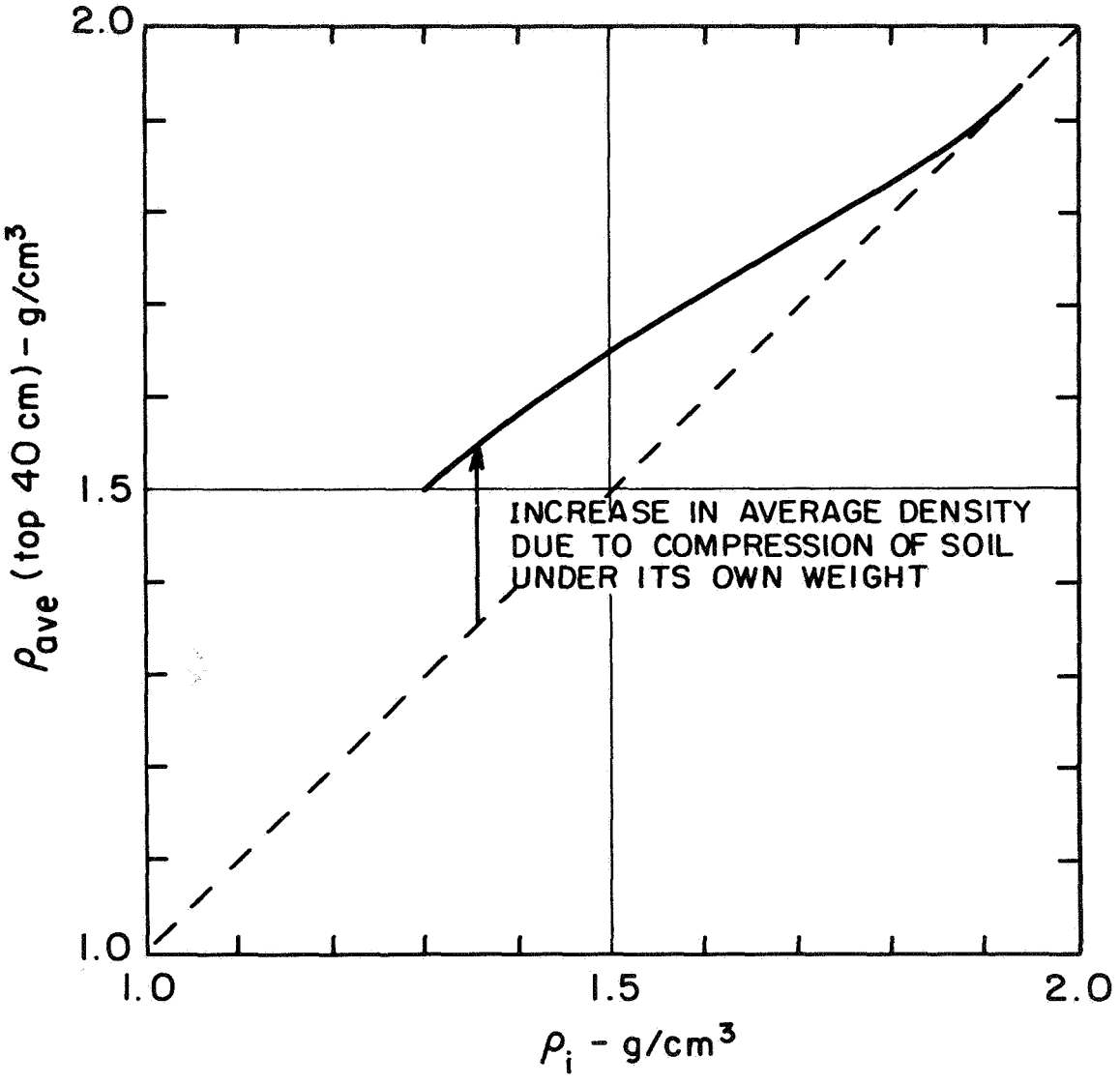

FIGURE 1-15 COMPUTED RELATIONSHIP BETWEEN ρ_i AND ρ_{ave} (TOP 40 cm) FOR LUNAR SOIL SIMULANT — TERRESTRIAL ENVIRONMENT

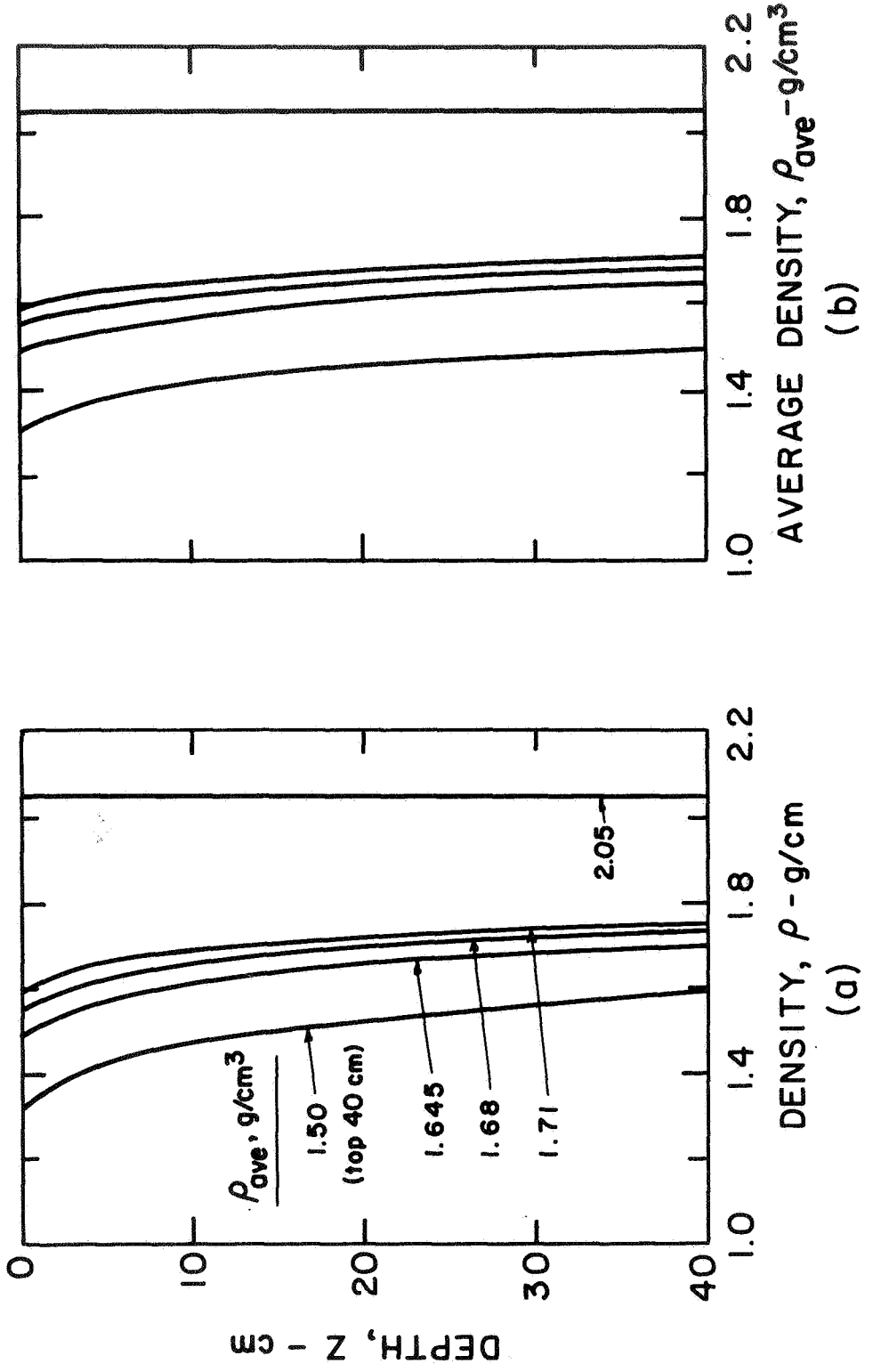

FIGURE 1-16 VARIATION OF ρ AND ρ_{ave} WITH DEPTH FOR VARIOUS VALUES OF ρ_{ave} AT z = 40 cm — LUNAR SOIL SIMULANT IN TERRESTRIAL ENVIRONMENT

shows the variation of ρ and ρ_{ave} with depth for values of ρ_{ave} (top 40 cm) ranging from 1.50 to 2.05 g/cm^3.

X. DETERMINATION OF PROBABLE DENSITY, VERTICAL STRESS, AND SHEAR STRENGTH VARIATIONS WITH DEPTH FOR ACTUAL LUNAR SURFACE (REDUCED GRAVITY)

An analysis similar to that described in the last section was made to determine the probable variation of density, vertical stress, and shear strength with depth for the actual lunar surface under conditions of reduced gravity. It was assumed that thin layers of lunar soil were deposited on the surface as a result of the scattering action of crater formation through meteor bombardment. As for the terrestrial soil, it was necessary first to determine a compression curve relating density and stress. The position of this curve was determined by further assuming that the lunar soil fits the compressibility pattern established in Figure 1-9. For the first set of calculations, a value of ρ_{ave} = 1.50 g/cm^3 for the top 40 cm was used. The position of the corresponding compressibility curve was found by making a trial-and-error solution for K_1, K_3, and ρ_i. The curve is shown in Figure 1-9 marked "L" to signify its applicability to the lunar soil under reduced gravity.

Before discussing the trial-and-error solution, a preliminary observation can be made which shows that the curve "L" of Figure 1-9 must be appreciably flatter than curve "T." If ρ_{ave} for the top 40 cm is 1.50 g/cm^3, then the vertical compressive stress due to gravity at this depth must be:

$$\sigma_{(z = 40\ cm)} = (1.50)(40)(1/6) \simeq 10\ g/cm^2$$

since the gravity-induced stress is only 1/6 of the value for the same soil on the earth's surface.* In order that ρ_{ave} be equal to 1.50 g/cm^3 for the top 40 cm, it is necessary that the value of ρ at a depth of 40 cm be

*Although stresses are, by definition, expressed in dynes/cm^2 in the metric system, units of grams/cm^2 are used herein for both terrestrial and lunar applications because of the better "feel" for behavior that is obtained with these units. For computation of lunar gravitational forces, a density equal to 1/6 of the mass density is used.

appreciably greater than 1.50 g/cm^3. The preceding observation shows that the value of ρ = 1.56 g/cm^3 for ρ = 10 g/cm^2 shown by Curve L is a reasonable value. The value of ρ_i for the actual lunar surface should be greater than ρ_i for the terrestrial soil profile prepared in the test bin if both sections have the same value of ρ_{ave}, because the increase in density with increase in depth is smaller for the lunar soil due to reduced gravity stresses.

Modifications in the derivations of expressions for ρ and ρ_{ave} to account for reduced gravity consist simply of substituting $\rho_i/6$ for ρ_i in cases where gravity stresses are being calculated. Thus, the expression for $d\sigma$, the incremental stress increase due to the weight of a small additional surface layer, as given by Equation (1-3) becomes:

$$d\sigma = (\rho_i/6)\, dz \tag{1-3a}$$

and the desired relationships between ρ, ρ_{ave}, and depth are:

$$\rho = \frac{\ln[(\rho_i/6)\ (z + c_1)]}{K_3} + K_1 \tag{1-7a}$$

and

$$\rho_{ave} = \frac{1}{K_3}\left\{\left(1 + \frac{c_1}{z}\right)\left(\ln[(\rho_i/6)(z + c_1)] - 1\right) - \frac{c_1}{z}\left(\ln\frac{\rho_i c_1}{6} - 1\right)\right\} + K_1 \tag{1-8a}$$

However, the boundary condition that $\rho = \rho_i$ for $z = 0$ holds for the lunar soil section as it did for the terrestrial soil section; therefore the expression for the constant of integration, c_1, is:

$$c_1 = 6/\rho_i\ e^{K_3(\rho_i - K_1)} \tag{1-6a}$$

Solutions of Equations (1-7a) and (1-8a) give the best agreement between the computed stress-density relationship and the confined compression curve when K_3 = 13.55, K_1 = 1.39, and ρ_i = 1.37 g/cm^3. Using these values the

distributions shown in Figure 1-17(a) were determined. The variations of vertical stress, cohesion, and shear strength with depth shown in Figure 1-17(b,c) were obtained by combining data from Figures 1-17(a), 1-4, and 1-6 (w/c = 1.8%).

Under conditions of lunar gravity, the cohesion constitutes a very significant percentage of the total shear strength on a horizontal plane, s_h, as shown by Figure 1-17(c). However, the importance of the cohesion component is likely to be much less in the case of shear induced by surface loading, because of the additional confinement provided by applied direct stresses. For example, although it is difficult to estimate the minimum contact pressure to be exerted by the wheels of lunar roving vehicles at this point in time, it seems likely that this pressure will be greater than 0.75 psi (0.517 N/cm^2). This contact stress will, of course, both dissipate with depth and cause some densification. Assuming that most of the deformation occurs within the top 15 to 20 cm of material, it is reasonable to assume that the average normal stress within most of this zone is at least 0.45 psi (about 30 g/cm^2). This value of normal stress would cause densification of the lunar soil to about 1.64 g/cm^3 for which cohesion, $c \simeq 5$ g/cm^2 and $s_h \simeq 28.5$ g/cm^2 (0.28N/cm^2). Therefore a conservative estimate of the percentage contribution of cohesion to the shear strength is about 18% for this case.

Using the same procedures as described in the preceding section, it was possible to relate ρ_i to K_1, K_3, and ρ_{ave} (top 40 cm) for a range of values of ρ_{ave} for the actual lunar soil (reduced gravity). These relationships are shown in Figures 1-18 through 1-21. The compression curve labeled $\rho_{ave} = 1.50$ g/cm^3 in Figure 1-18 is the same as curve "L" in Figure 1-9. The curve relating ρ_i and ρ_{ave} for the terrestrial soil is repeated in Figure 1-21 for comparison. The relationships in Figures 1-18 through 1-21 were used in the computations of footprint depths, described in the following section.

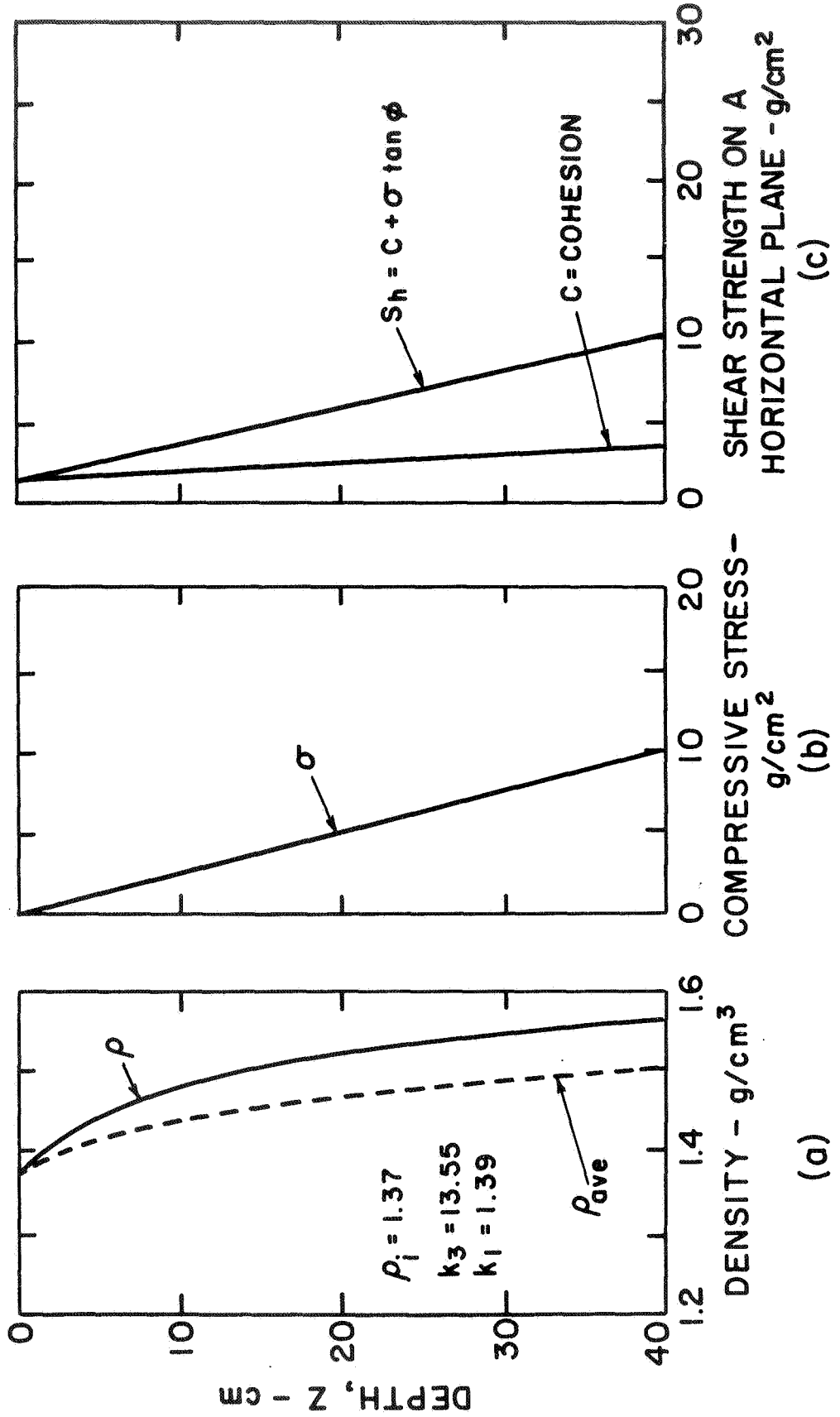

FIGURE 1-17 ESTIMATED VARIATION OF DENSITY, VERTICAL STRESS, AND SHEAR STRENGTH WITH DEPTH FOR ACTUAL LUNAR SOIL (REDUCED GRAVITY FIELD)

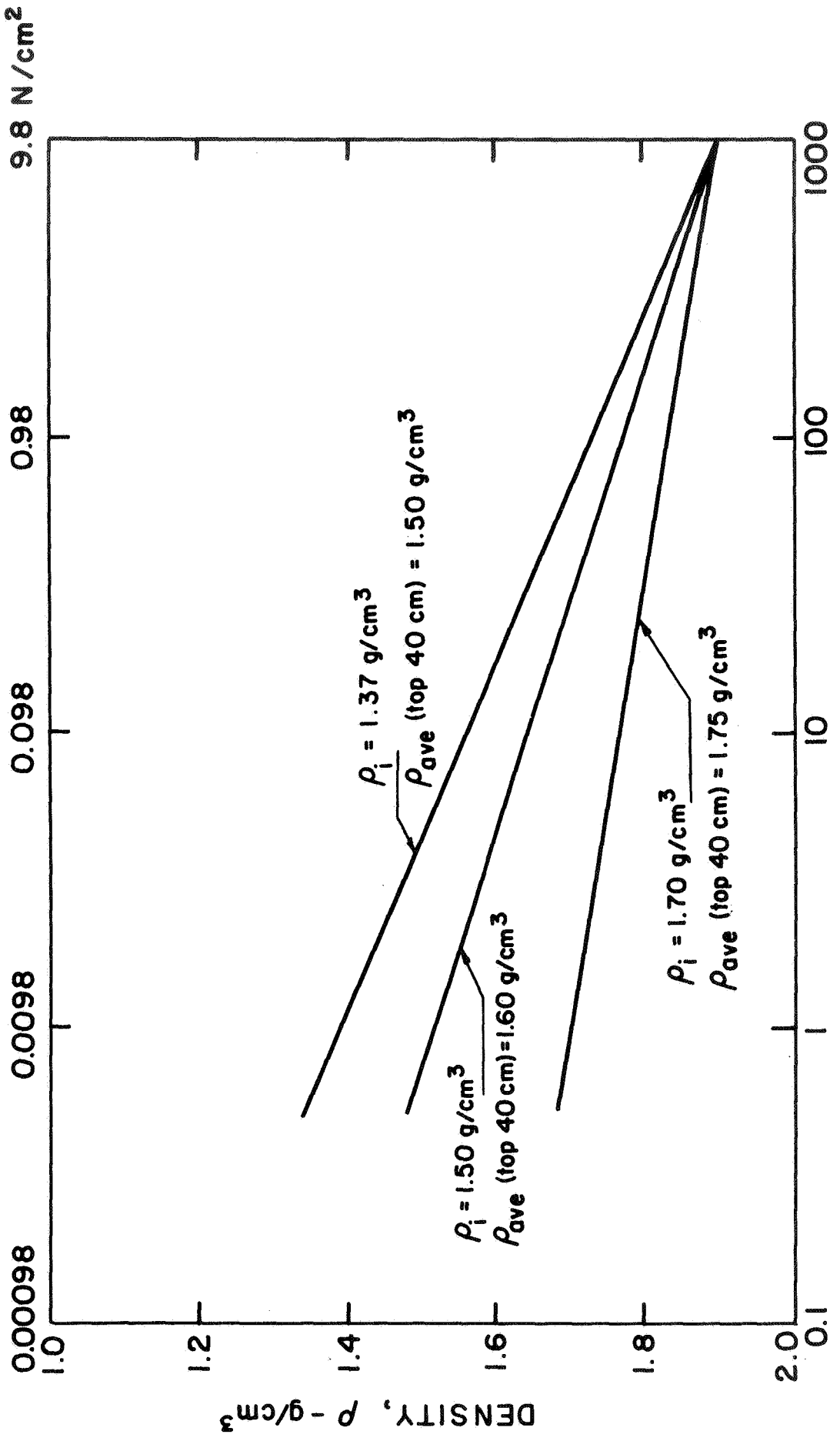

FIGURE 1-18 TYPICAL COMPRESSION CURVES FOR LUNAR ENVIRONMENT

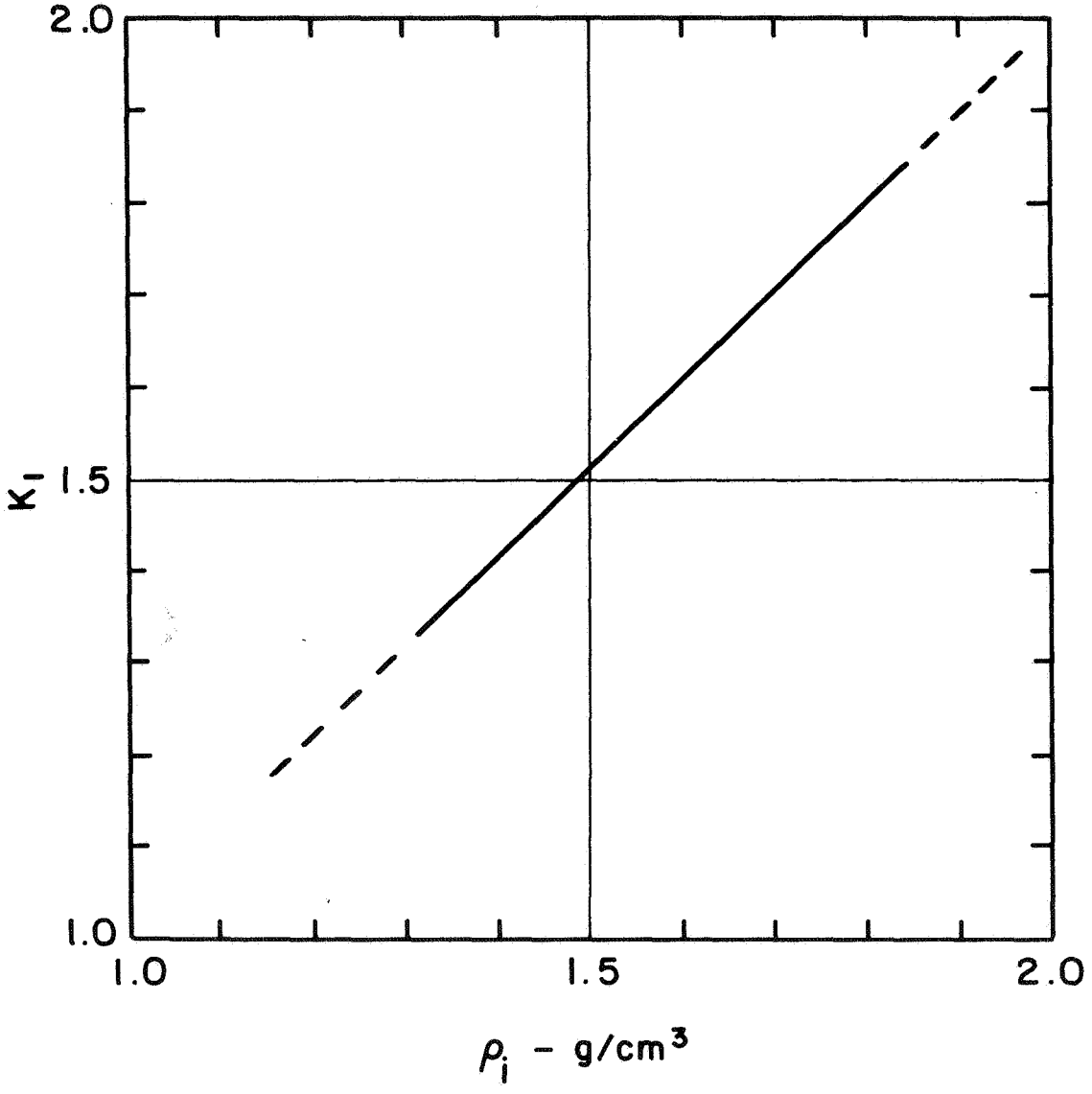

FIGURE 1-19 RELATIONSHIP BETWEEN ρ_i AND K_1
FOR LUNAR ENVIRONMENT

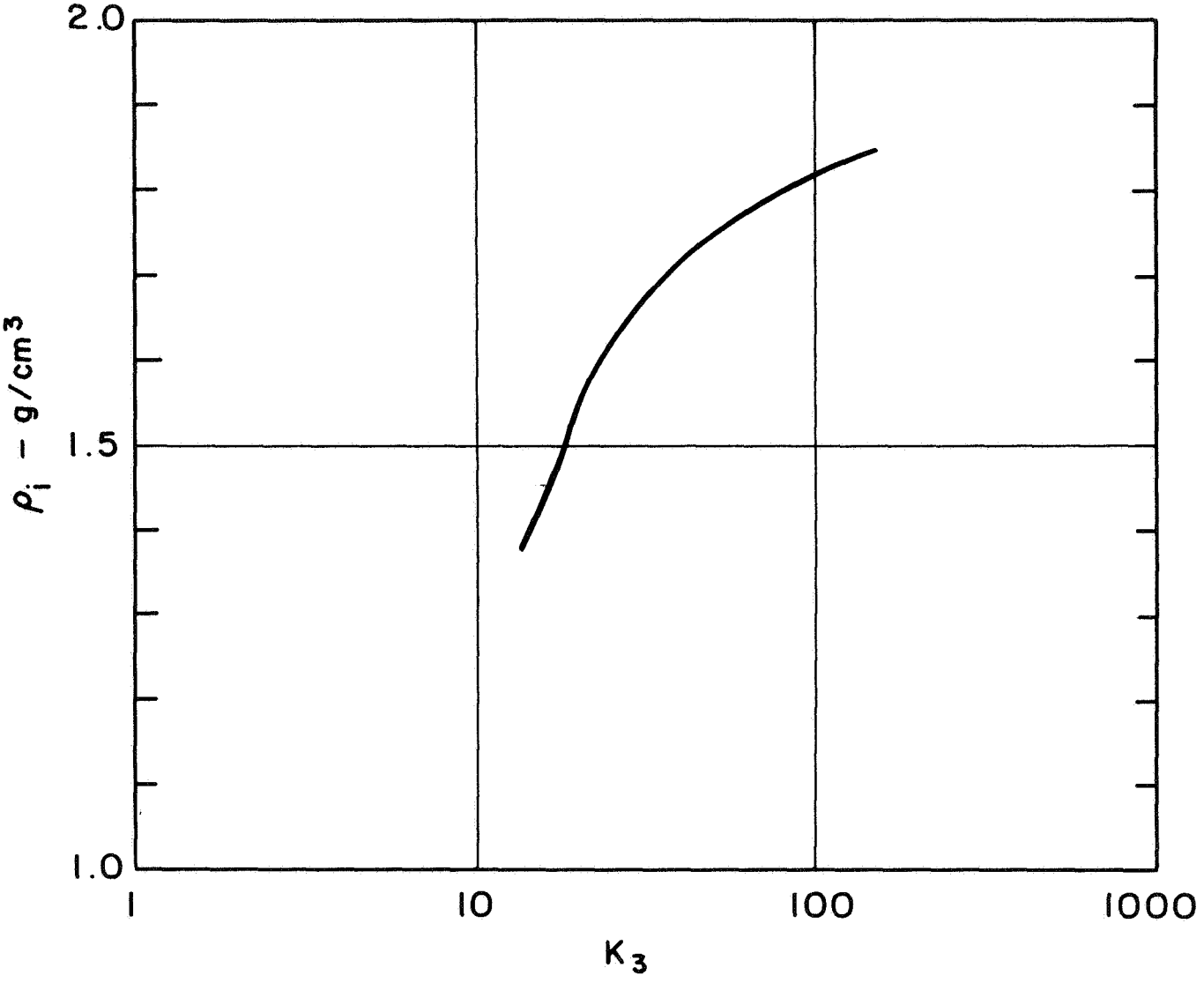

FIGURE 1-20 RELATIONSHIP BETWEEN ρ_i AND K_3
FOR LUNAR ENVIRONMENT

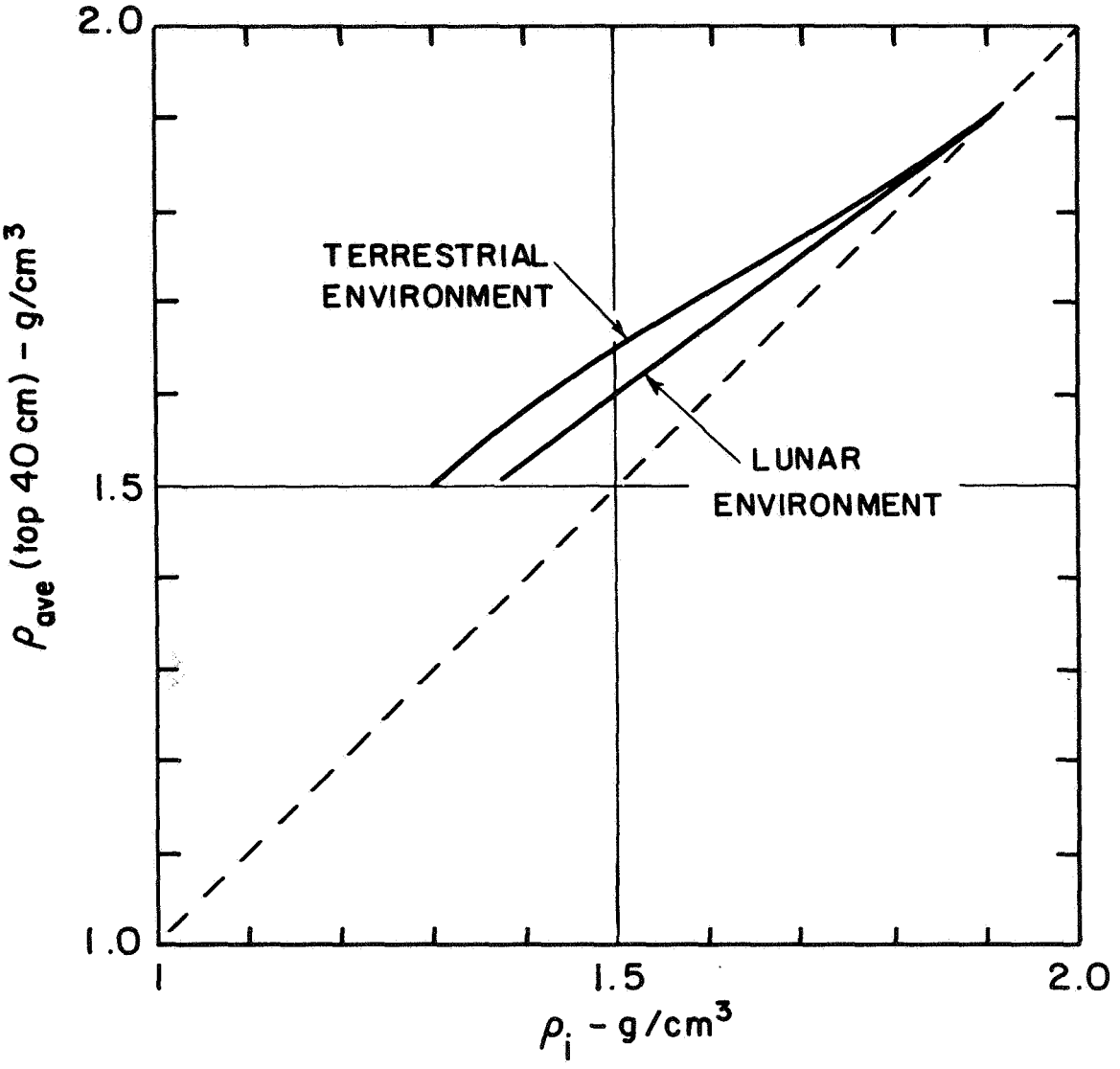

FIGURE 1-21 COMPUTED RELATIONSHIP BETWEEN ρ_i AND ρ_{ave} (TOP 40 cm) FOR LUNAR ENVIRONMENT

XI. ANALYSIS OF FOOTPRINTS IN LUNAR SOIL

Footprints made by astronauts during Apollo missions are likely to be plentiful and photographs of these "load-sinkage" tests may be useful for deduction of lunar soil properties. Therefore, considerable effort has been devoted to the study of footprints formed in the lunar soil simulant.

A series of boot imprint tests were performed on 40-cm layers of the lunar soil simulant, placed in a 2' x 2' x 2' test bin, at various values of ρ_{ave}. Because the size of the boot was appreciable relative to the test bin dimensions, boundary effects undoubtedly had some influence on the absolute values of settlements observed. However, most of the studies thus far have been for comparative purposes, thus boundary effects tend to cancel. A 3.5' x 7' x 3.5' deep test bin with teflon-lined sides is currently being constructed for use in future model tests. Boundary effects are expected to be minor in this bin, and the results of tests conducted therein can be used to judge the extent of the influence of boundaries in the smaller bin.

Figures 1-22 and 1-23 show photographs and sketches of a boot imprint made by stepping down on the surface of the simulated soil with a weight of 180 pounds on one foot. The profile of the simulated soil for this test is represented in Figure 1-10. The dimensioned sketch of the boot used (see Figure 1-23) shows that the bearing area is about 45 sq. in. Although the stress distribution under the boot was not expected to be precisely uniform, the average stress was 4 psi. The observed maximum depth of the footprint was 3.5 inches, and the average depth was 3.2 inches.

Other footprints were made by applying static loads in increments to the boot by means of a steel rod attached to a dummy foot inside the boot. Figure 1-24 shows a typical load-settlement curve for such a test. This curve

FIGURE 1-22 FOOTPRINT IN SIMULATED LUNAR SOIL

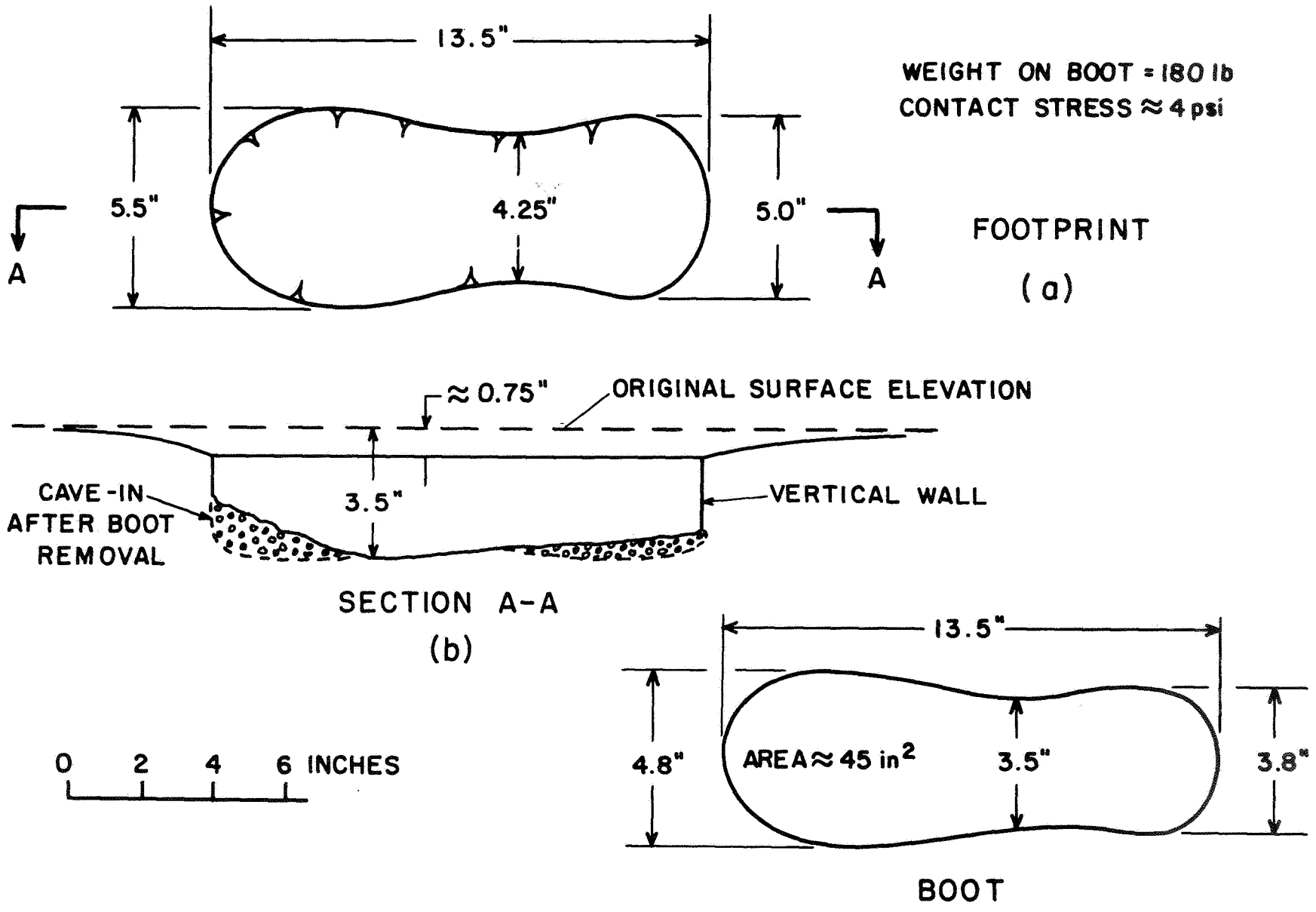

FIGURE 1-23 FOOTPRINT DETAILS

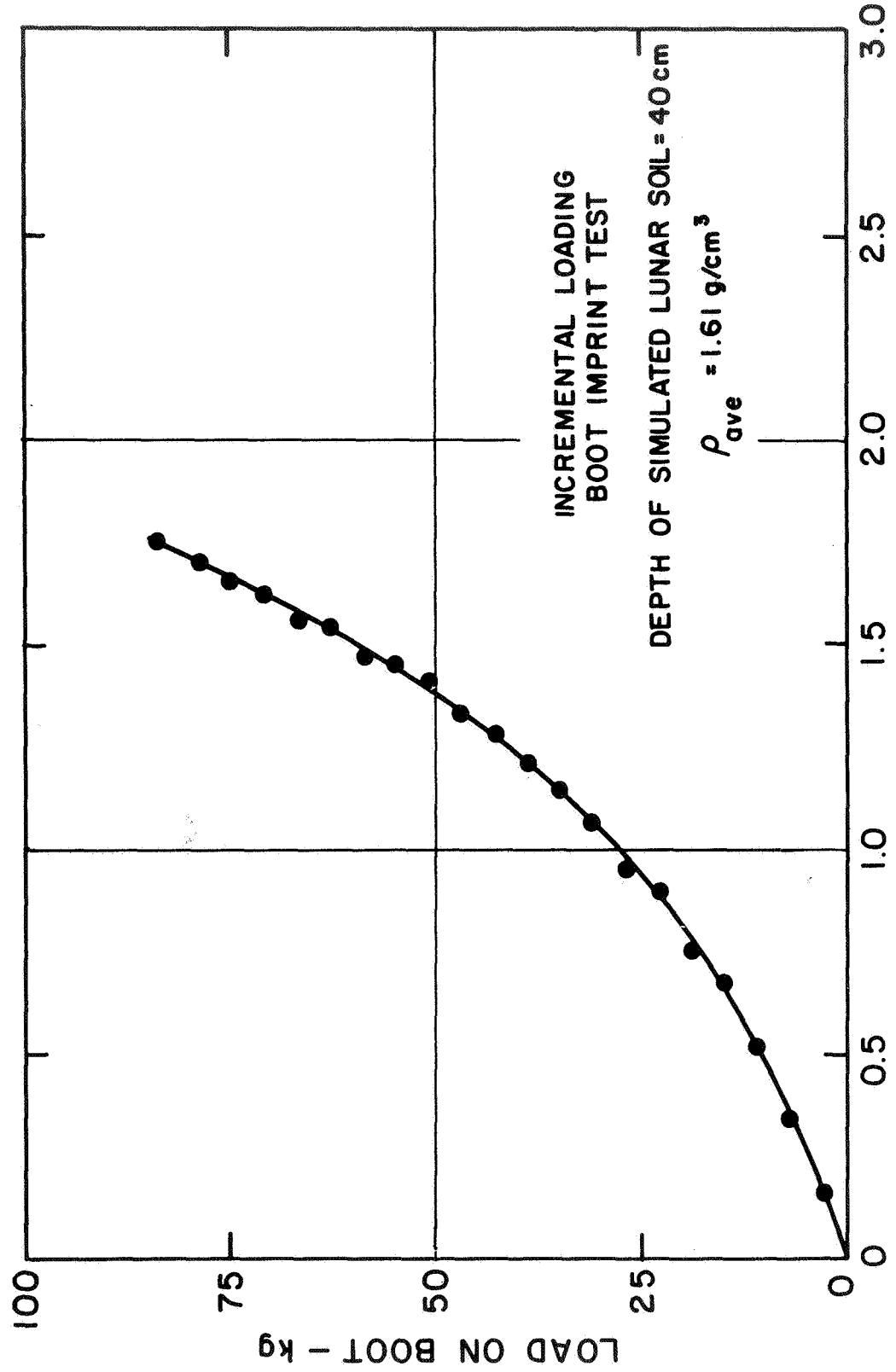

FIGURE 1-24 LOAD SETTLEMENT CURVE FOR BOOT IMPRINT TEST

is somewhat similar in shape to the compression curves shown in Figure 1-8, indicating that compression plays a significant role in the observed deformations.

A number of footprint test results are shown in Figure 1-25. The footprints made by a man stepping on the soil (labeled "quick loading" in Figure 1-25) were made in a period of about 10 seconds. Footprints made by stepping down on the soil in about one second were significantly deeper and were accompanied by the escape of air from around the boot, as evidenced by small puffs of dust. The deeper footprint for this very rapid loading were apparently caused by induced pore air pressures. Comparison of the data points for the 10-second loadings and the incremental loadings shown in Figure 1-25 indicate, however, that pore air pressures were not a significant factor.

In general, the settlement of the boot under any given load is due partly to compression (volume decrease) of the soil under the boot and partly to shear deformation. A series of computations of the compression component of the settlement were made. Various loads and initial densities for both the terrestrial lunar soil simulant and the actual lunar soil were assumed.

For the purpose of computing the stress distribution beneath the boot, a rectangular contact area of 4 by 11.25 inches were assumed (same contact areas as for the boot), and a contact stress of 4 psi (180-lb load) was used. Vertical stress distributions for a rectangular uniformly loaded area on a compressible layer underlain by a rigid base are given by Burmister (1956). The variations of the initial vertical gravity stress and the total vertical stress including surface load with depth for ρ_{ave} = 1.50 g/cm^3 are shown in Figure 1-26(a). The appropriate compression curve from Figure 1-11 was used to determine the variation of final density with depth as shown in Figure 1-26(b). The vertical strain, ε_v, was calculated at various depths by

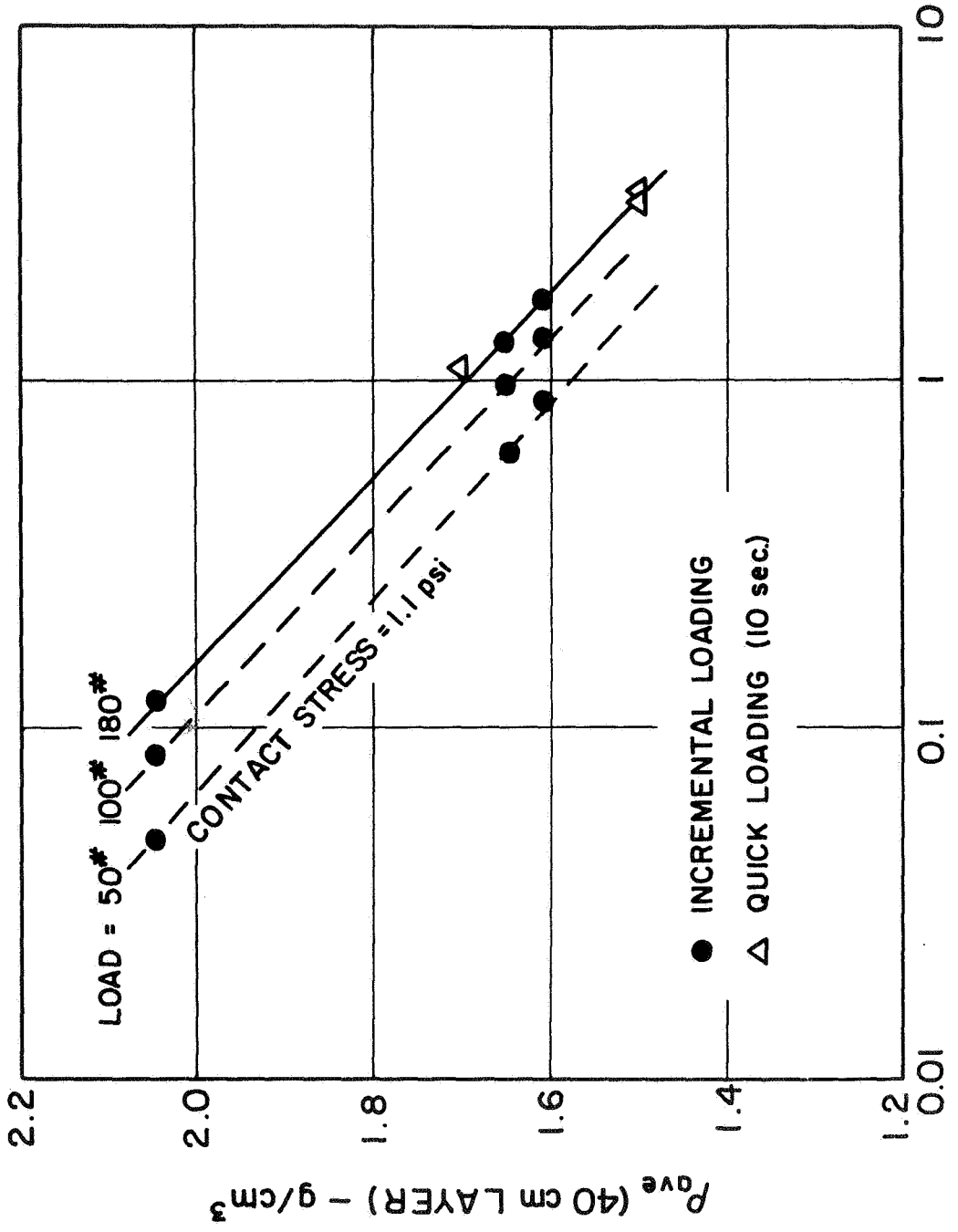

FIGURE 1-25 VARIATION OF MEASURED TOTAL AVERAGE DEPTH OF FOOTPRINT WITH ρ_{ave} FOR VARIOUS MAGNITUDES OF LOAD

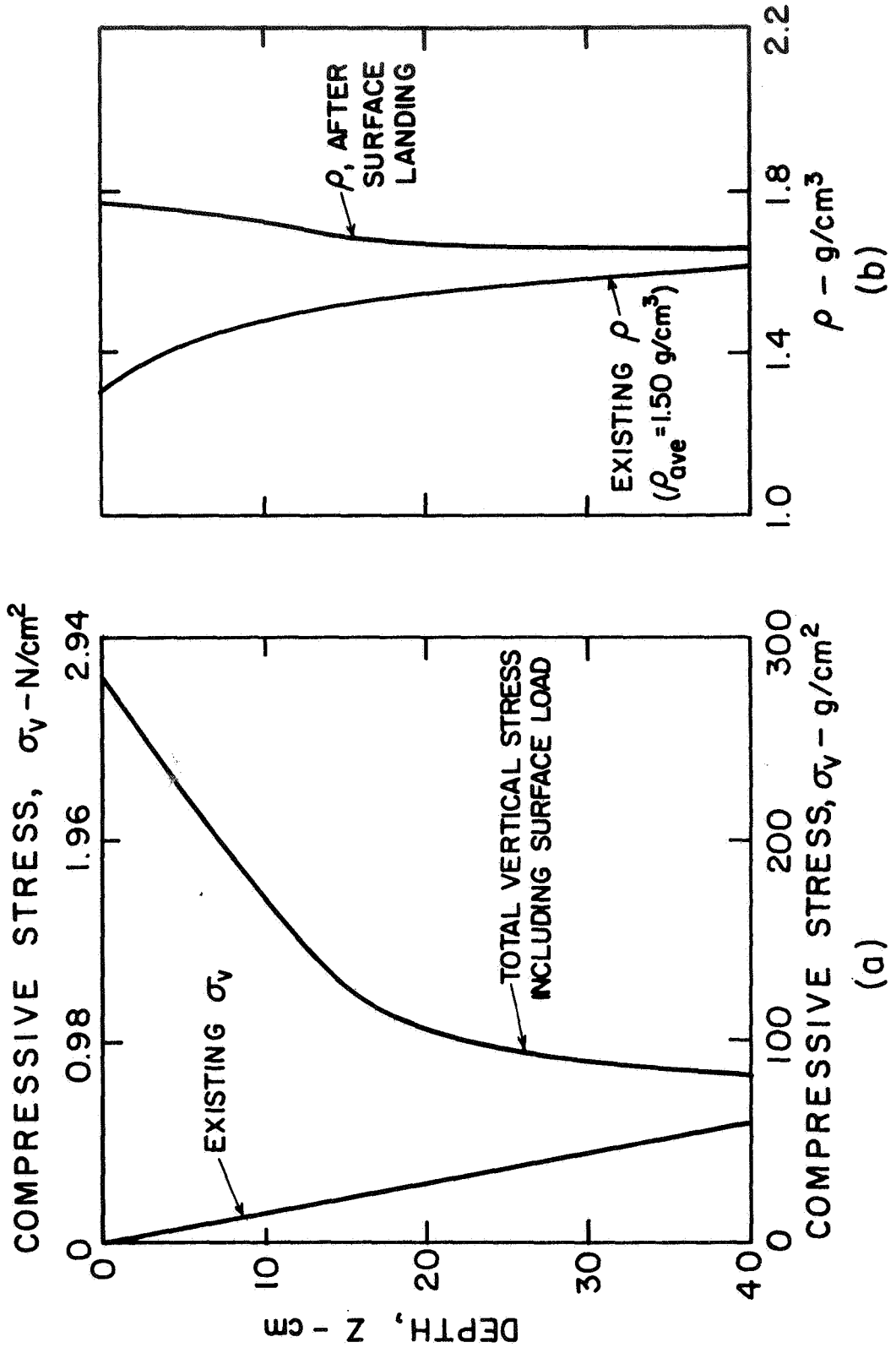

FIGURE 1-26 VARIATION OF VERTICAL STRESS AND DENSITY BEFORE AND AFTER LOADING SURFACE WITH BOOT FOR LUNAR SOIL SIMULANT

$$\varepsilon_v = 1 - \frac{\rho_1}{\rho_2} \qquad (1\text{-}10)$$

where ρ_1 = original density

ρ_2 = final density

and plotted in Figure 1-27. The area to the left of the curve gives the predicted depth of footprint, 1.50 inches. Similar computations were made for loads of 100 lbs and 50 lbs and for values of ρ_{ave} = 1.60 and 1.75 g/cm^3. The results are shown in Figure 1-28. Computations of compression settlements for a 50-lb load on the actual lunar surface were also made for average densities of 1.50, 1.60, and 1.75 g/cm^3. These values are also plotted in Figure 1-28 as single points. Small extrapolations (or interpolations) were made as needed to obtain the compression settlements for 40- and 60-lb loads on the lunar surface. For the case of compression on the lunar surface, a depth of 100 cm of material and a Boussinesq solution for stresses beneath a uniformly loaded rectangular area were used.*

In Table 1-1 a comparison is made between the total observed settlements (Δ_{total}), taken from Figure 1-25, and the computed compression settlement ($\Delta_{compr.}$), taken from Figure 1-28. The shear component of each settlement value, obtained by subtracting the compression component from the total observed settlement, is also shown in Table 1-1. The data in Table 1-1 show that the ratio of compression settlement to total settlement, $\Delta_{compr.}/\Delta_{total}$, decreases with increasing load and with decreasing density. Decreasing $\Delta_{compr}/\Delta_{total}$ with increasing load is reasonable because shear strains would

---

*For comparison, these assumptions were made for one case of the lunar soil simulant. The compression was found to be negligibly larger because the stresses dissipate less rapidly with depth for the case of a rigid base underlying the compressible layer.

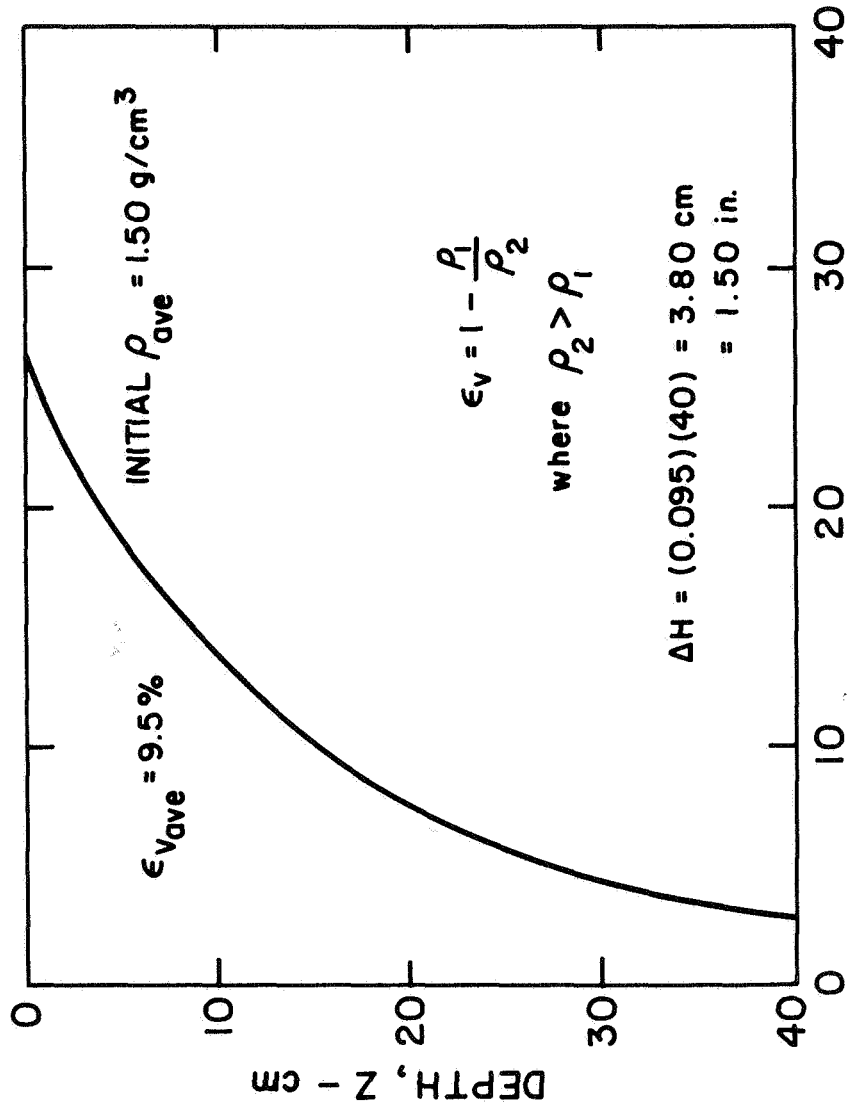

FIGURE 1-27 VARIATION OF VERTICAL STRAIN WITH DEPTH FOR LOAD ON BOOT = 180 LB

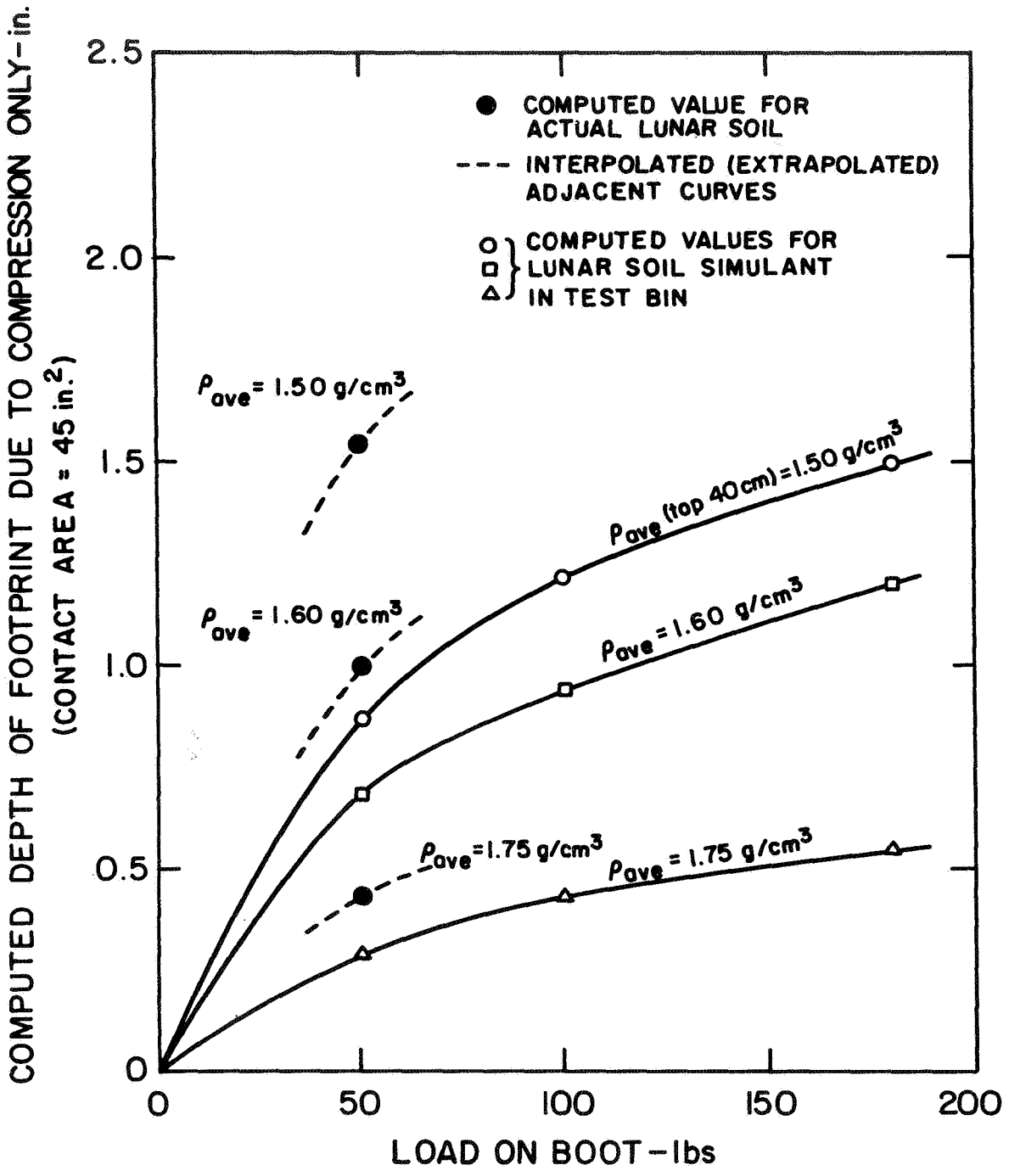

FIGURE 1-28 COMPRESSION SETTLEMENT VS LOAD ON BOOT

TABLE 1-1

COMPARISON OF TOTAL SETTLEMENTS AND

COMPRESSION SETTLEMENTS FOR LUNAR SOIL SIMULANT

ρ_{ave} (g/cm^3)	Load (lb)	Stress (psi)	Δ_{total} (in.)	$\Delta_{compr.}$ (in.)	$\frac{\Delta_{compr.}}{\Delta_{total}}$	Δ_{shear}
1.50	50	1.11	1.62	0.87	0.54	0.75
1.50	100	2.22	2.45	1.22	0.50	1.23
1.50	180	4.0	3.2	1.50	0.47	1.70
1.60	50	1.11	0.85	0.68	0.80	0.17
1.60	100	2.22	1.32	0.94	0.71	0.38
1.60	180	4.0	1.75	1.20	0.685	0.55
1.75	50	1.11	0.32	0.29	0.90	0.03
1.75	100	2.22	0.52	0.43	0.83	0.09
1.75	180	4.0	0.70	0.55	0.785	0.15

be expected to predominate near the failure condition and compression strains would be expected to predominate for low stress levels. (Note: Stress level is defined as the contact stress divided by the ultimate bearing capacity.) The same reasoning applies for the decrease of $\Delta_{compr.}/\Delta_{total}$ with decreasing density for the same load. The bearing capacity decreases with the density. Therefore, the applied loads represent higher stress levels for low densities.

Probable values for the compression settlement of a 50-lb load on the actual lunar surface are given in Figure 1-28. (A load of 50 lbs was chosen because this represents the lunar weight of a suited astronaut if his earth weight is 300 lb.) However, in order to estimate the variation of total depth of footprint with density for the lunar surface, it was necessary to obtain estimates for the shear component of settlement. Because the ratio $\Delta_{compr.}/\Delta_{total}$ is obviously a function of stress level and density, it was assumed that, for a given value of ρ_{ave} and stress level, the value of $\Delta_{compr.}/\Delta_{total}$ will be the same for the lunar surface as for the lunar soil simulant. Because the bearing capacity (and therefore the stress level for a given contact stress) is affected by the reduced gravity on the lunar surface, consideration is given to the effect of reduced gravity in making a projection of this type.

To establish an equivalence of stress level for the lunar soil simulant (terrestrial environment) and the actual lunar soil (reduced gravity), it was necessary to compute the variation of bearing capacity and average density for both cases.

Equation (1-11) was used to obtain values of the ultimate bearing capacity, q_{ult}.

$$q_{ult} = \frac{b\gamma}{2} N_\gamma s_\gamma + cN_c s_c + q'N_q s_q \qquad (1\text{-}11)$$

where q_{ult} = unit ultimate bearing capacity

γ = soil unit weight

b = width of loaded area

c = soil cohesion

q' = surcharge, $d\gamma$

s_γ = shape factor (1 - 0.3 b/L)

s_c = shape factor (1 + 0.2 b/L)

s_q = shape factor (1 + 0.2 b/L)

N_γ, N_c, N_q = bearing capacity factors, dependent on the soil friction angle, ϕ

d = depth of loaded area

L = length of loaded area

Meyerhof's (1951) charts were used for the bearing capacity factors. To enter Meyerhof's charts, the parameter β is used. Beta is defined as the angle between the horizontal and a line connecting the bottom of the footing and the point of emergence of the slip surface. Average values of d = 1 in. and $\beta = 5°$ were used for all calculations. Deformations for this rectangular footing are between triaxial and plane strain conditions, but probably closer to plane strain. Therefore ϕ for plane strain ($\phi_{p.s.}$) was used to enter the bearing capacity charts.

The results of the bearing capacity computations for the lunar soil simulant and the actual lunar soil are summarized in Tables 1-2 and 1-3 The data in Tables 1-1 and 1-2 are plotted in Figure 1-29. The stress levels for 40-,50-,and 60-lb loads on the actual lunar soil given in Table 1-3 were used to enter Figure 1-29 to obtain the corresponding values of $\Delta_{compr.}/\Delta_{total}$. These values of $\Delta_{compr.}/\Delta_{total}$ were applied to the computed values of $\Delta_{compr.}$

TABLE 1-2

BEARING CAPACITIES FOR LUNAR SOIL SIMULANT

ρ_{ave} (g/cm^3)	$\phi_{p.s.}$ (deg.)	c (psi)	q_{ult} (psi)	Stress Levels in %		
				50-lb load 1.11 psi	100-lb load 2.22 psi	180-lb load 4.0 psi
1.50	33	0.032	7.96 (5.48 N/cm^2)	14	28	50
1.60	36.5	0.058	15.3 (10.5 N/cm^2)	7.2	14.5	26
1.75	43	0.136	59.6 (41.2 N/cm^2)	1.85	3.7	6.7

TABLE 1-3

BEARING CAPACITIES FOR ACTUAL LUNAR SURFACE (REDUCED GRAVITY)

ρ_{ave} (g/cm^3)	$\phi_{p.s.}$ (deg.)	c (psi)	q_{ult} (psi)	Stress Level in %		
				40-lb load	50-lb load	60-lb load
1.50	33	0.032	2.67 (1.84 N/cm^2)	33	41.5	50
1.60	36.5	0.058	5.82 (4.0 N/cm^2)	15	19	23
1.70	43	0.136	28.1 (19.4 N/cm^2)	3.15	3.95	47.5

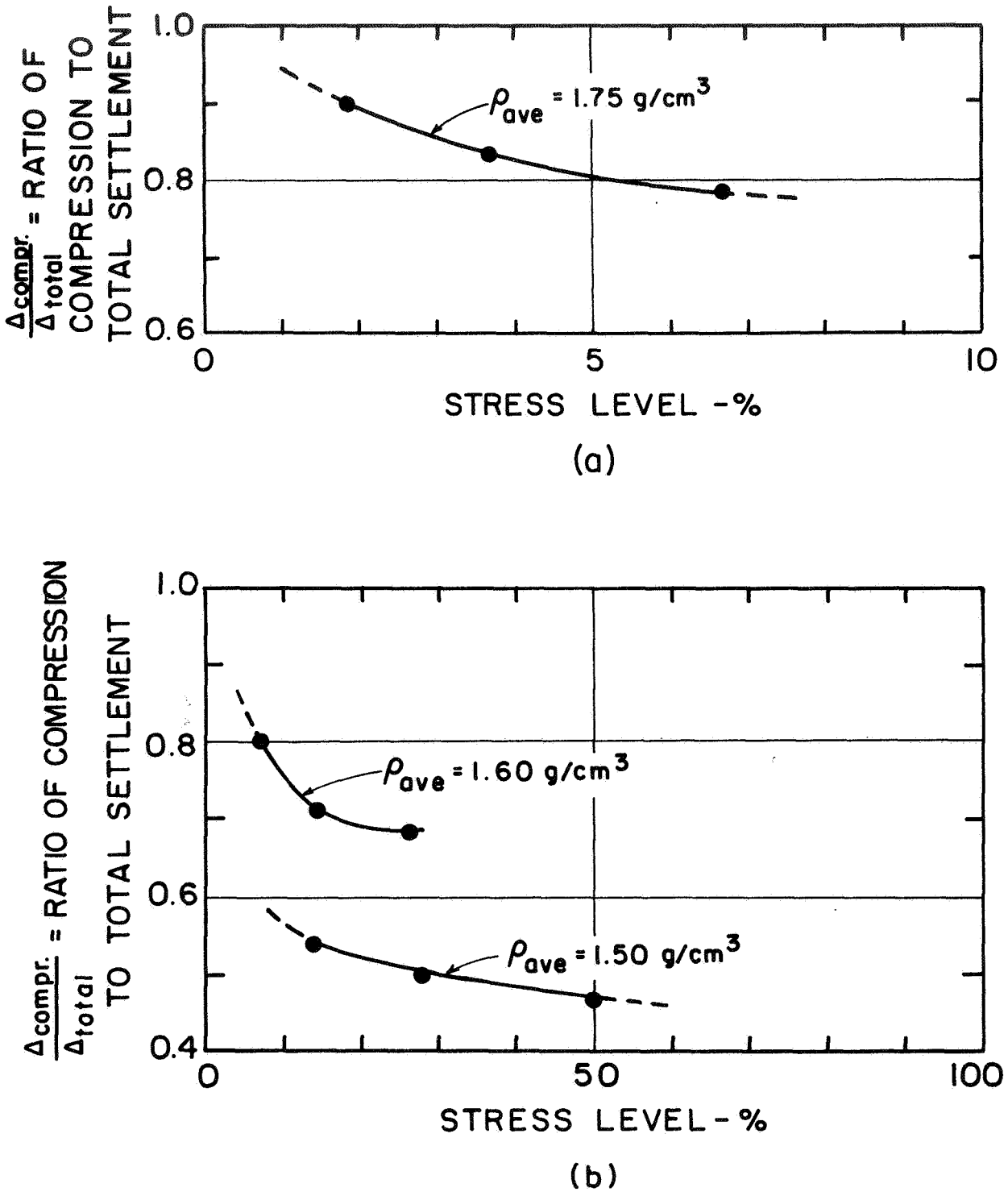

FIGURE 1-29 RELATIONSHIPS BETWEEN ρ_{AVE}, STRESS LEVEL, AND RATIO OF COMPRESSION TO TOTAL SETTLEMENT

to obtain values of Δ_{total} for the actual lunar surface. The results are summarized in Table 1-4 and plotted in Figure 1-30 to facilitate interpolation. The curves plotted in Figure 1-30 represent the desired relationships between probable total depth of footprint and ρ_{ave} for the top 40 cm of lunar material. Assuming a terrestrial weight of a suited astronaut of 300 lbs and a boot area of 45 $in.^2$, the curve for a 50-lb load would be appropriate. Slightly different astronaut weights and boot sizes may be considered by interpolation.

XII. PENETRATION RESISTANCE TESTS

Penetration resistance measurements are being considered as a means by which astronauts may gather data leading to the assessment of lunar surface soil properties. Approximate values of resistance are needed for design of penetrometers that may be utilized on Apollo missions. An important application of penetration resistance data may be for the design of lunar roving vehicles. The Corps of Engineers utilizes cone penetrometer data for cohesionless soils in trafficability analysis by obtaining the slope, G, of the penetration resistance (in psi) versus depth of penetration (in inches). Although the lunar soil is not considered to be completely cohesionless, it may still be possible to utilize such a modulus.

A series of penetration resistance tests was performed with the following objectives:

(1) To develop suitable penetration test techniques and to try out trial penetrometer models.

(2) To test the sensitivity of G values to density.

(3) To establish, if possible, probable values of G for the actual lunar surface.

TABLE 1-4

FOOTPRINT DEPTHS FOR LUNAR MATERIAL OF VARIOUS DENSITIES

ρ_{ave} (g/cm^3)	Load (lb)	Stress psi	$\frac{\Delta_{compr.}}{\Delta_{total}}$	$\Delta_{compr.}$	Δ_{total}
1.50	40	0.89	0.492	1.40	2.85
1.50	50	1.11	0.48	1.55	3.23
1.50	60	1.33	0.47	1.65	3.51
1.60	40	0.89	0.705	0.86	1.22
1.60	50	1.11	0.69	1.0	1.45
1.60	60	1.33	0.685	1.08	1.58
1.75	40	0.89	0.842	0.37	0.44
1.75	50	1.11	0.82	0.435	0.53
1.75	60	1.33	0.81	0.48	0.59

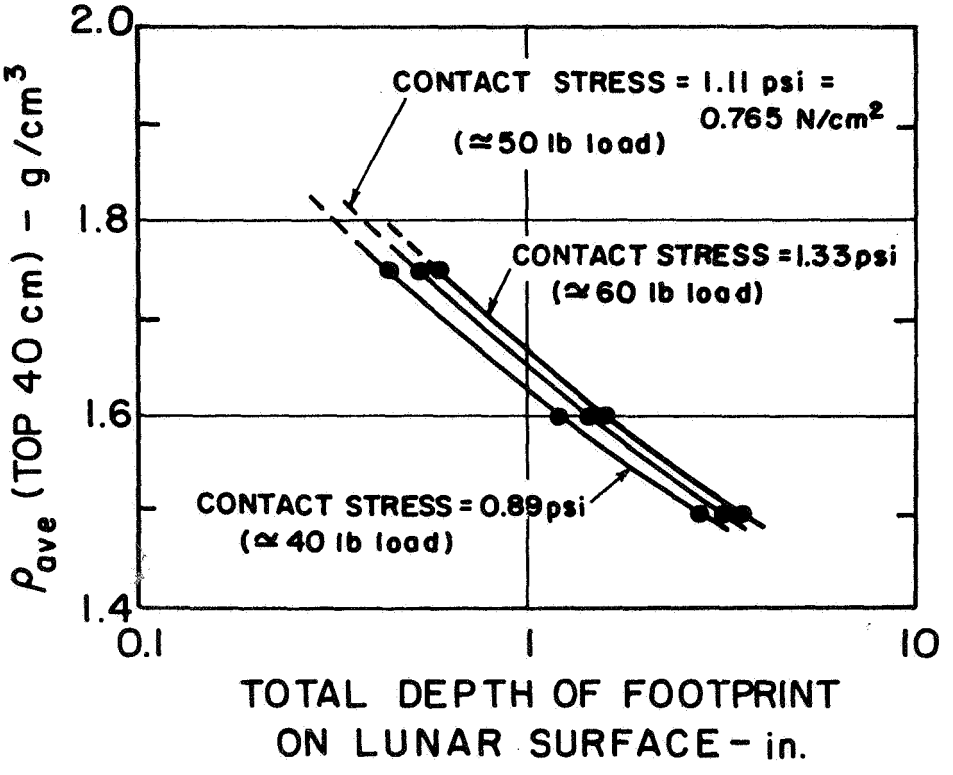

FIGURE 1-30 RELATIONSHIPS BETWEEN TOTAL DEPTH OF FOOTPRINT AND ρ_{ave} FOR A COMPRESSIBLE LUNAR SURFACE LAYER 40-cm THICK

The initial penetration resistance tests were performed by applying static (incremental) loads to a 1-inch-diameter, flat-ended, constant-diameter rod. Later tests were performed using a Waterways Experiment Station (WES) type cone penetrometer. This cone penetrometer has a 30° angle at the point (15° measured from the axis of the cone), a cone base area of 0.5 $in.^2$ (diameter = 0.798 in.) and a shaft diameter of 0.625 in. Comparison tests showed that this cone gives G values which are about 2/3 of the values obtained with the 1-inch-diameter, flat-ended rod. This difference in G values is probably due chiefly to differences in deformation mechanisms and partly to differences in shaft friction.

A typical cone penetration resistance curve is given in Figure 1-31. This curve shows that after a certain critical depth is exceeded, the penetration resistance increases only slightly with depth. This behavior is typical of penetration into granular materials. Vesic (1967) cited numerous cases in which a break in the load-penetration curve occurred at about 20-penetrometer diameters for very dense sand and about 10 diameters for very loose sand. This break in the curve occurred at 5 to 10 cone diameters for the lunar soil simulant, with an average value of about 8 diameters. This result indicates that, if the WES cone penetrometer is used on the lunar surface, the G values obtained may be representative of only the top 6 in. or so. However, it will probably be desirable to penetrate to greater depths to determine the degree of homogeneity in the soil profile.

Some of the first penetration tests were performed without a man standing on the soil adjacent to the penetrometer. Because an astronaut would be standing on the lunar surface soil during testing and because stresses due to the loads from his feet affect the results, additional tests were performed with a man standing in place. Comparative test results for the lunar soil

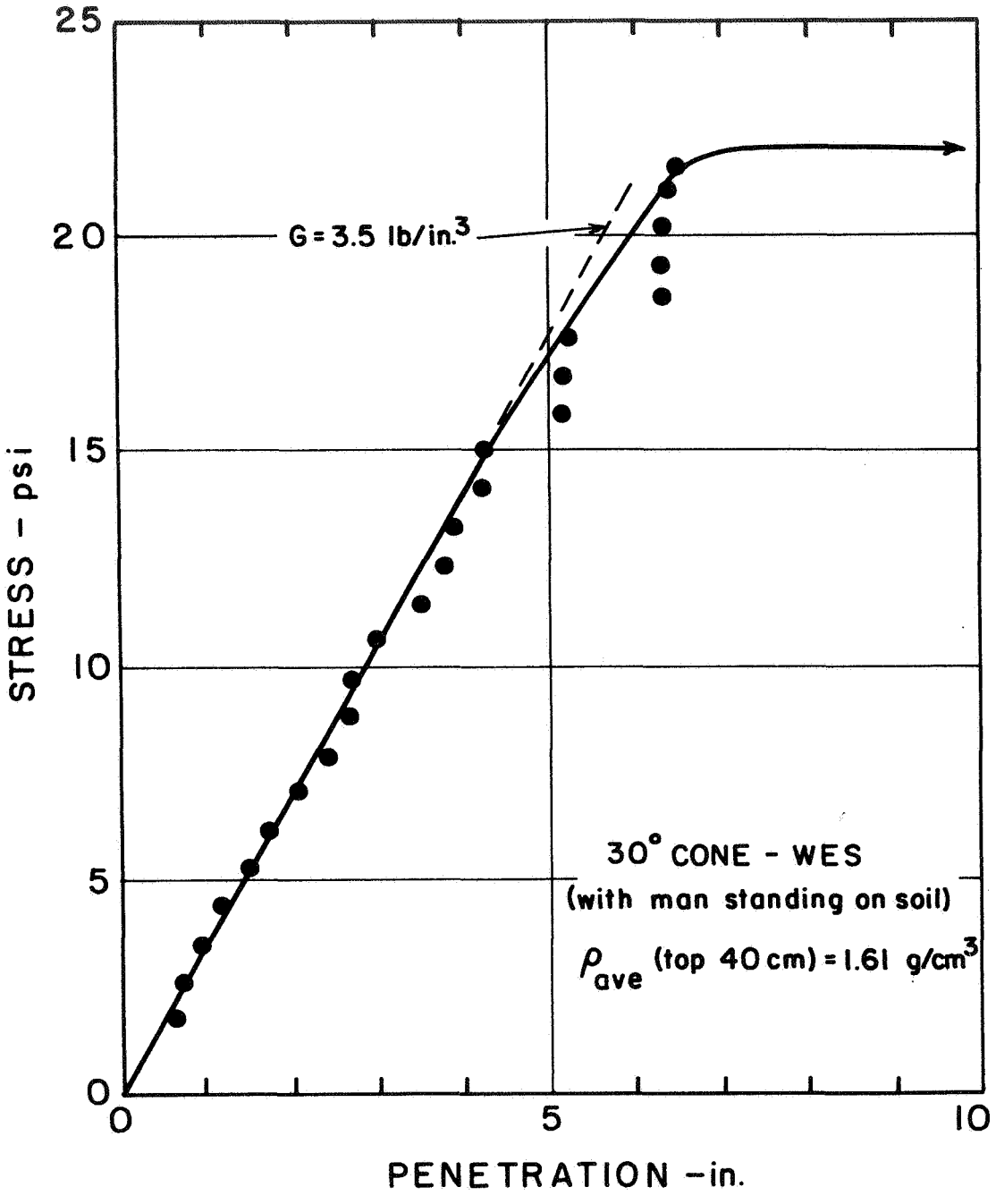

FIGURE 1-31 PENETRATION TEST RESULTS FOR 30° CONE

simulant are shown in Figure 1-32. The data indicate that the G value is about 40 percent less when a man is not standing adjacent to the penetrometer. It was also found that the position of the feet and the position of the penetrometer with respect to the feet affected the G value.

As a standard procedure for these tests, the feet were placed with 6 in. clear space between them; and the penetrometer was placed 2 in. in front of the toes, as shown by the sketch in Figure 1-32. For one case in which the penetrometer was placed directly in between the feet, equidistant from toe and heel, the G value was found to be about 50 percent higher. Thus it appears highly desirable to establish a standard testing position to be adopted for gathering penetrometer data. The position used in this study may well not be the most desirable. For example, if the feet were placed at a spacing of about 10 in. and the penetrometer placed 4 in. in front of the toes the existing stresses would probably be affected only slightly by the loads applied by the feet, for depths less than 5 or 6 in.

Values of G for the medium coarse basalt sand (see Figure 1-1 for gradation curve) are also plotted in Figure 1-32. These values of G were obtained without a man standing adjacent to the penetrometer, and they indicate that the differences in the gradation of the lunar soil simulant and the medium coarse basalt sand do not appreciably affect the G values.

Although it was known that the mechanism of penetrometer deformation involved both shear and compression deformations, initial analyses were made assuming only shear occurred. Thus the G values were related to the rate of increase in shear strength with depth. However, more recent test results have indicated that compression may play a significant role in the deformation mechanism.

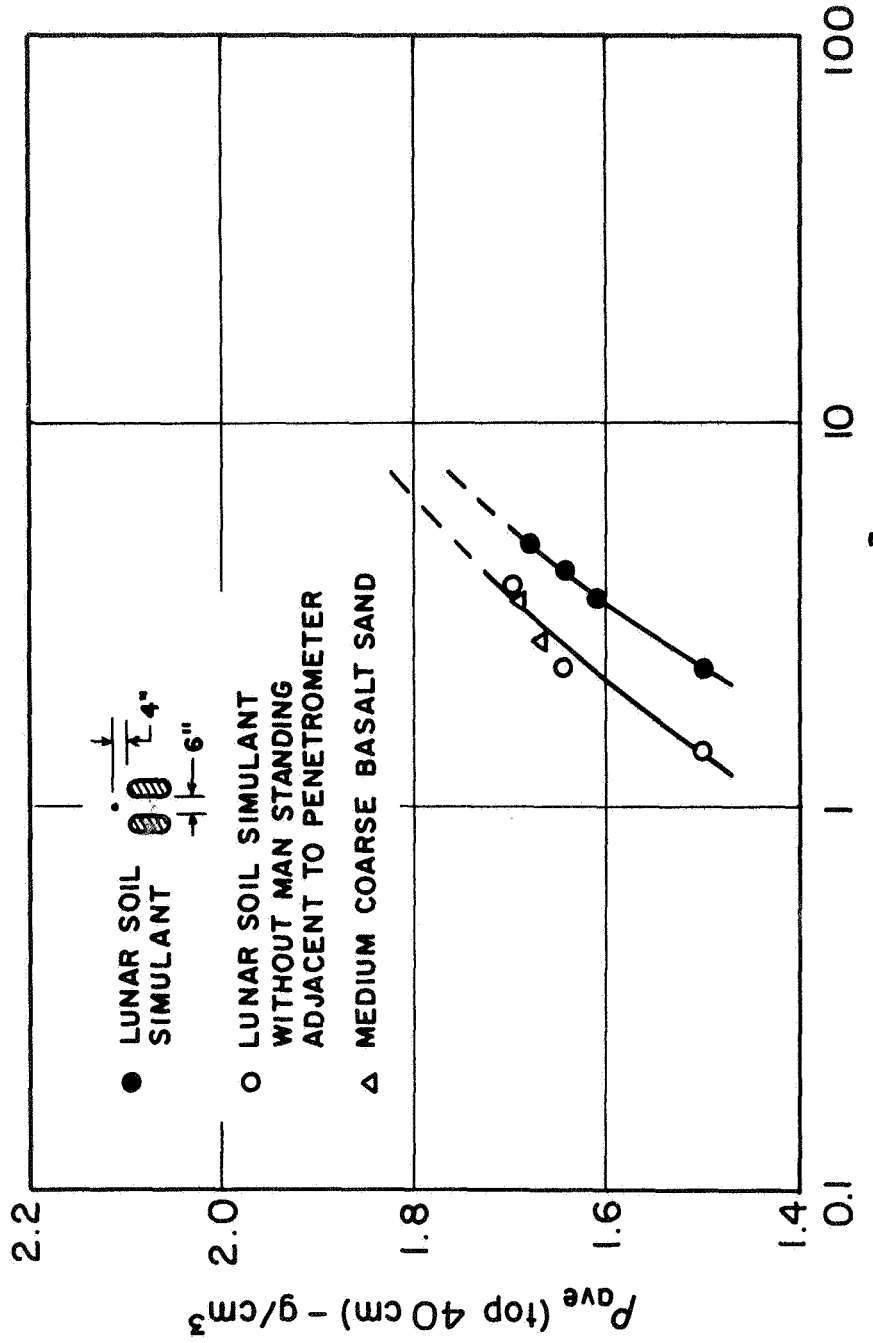

FIGURE 1-32 VARIATION OF G WITH ρ_{AVE} FOR TOP 40 cm OF LUNAR SOIL SIMULANT

First, some penetration tests on Monterey No. 20 sand (a clean medium sand) were performed and these data were combined with data available from the literature to obtain the curve labeled "clean sand" shown in Figure 1-33. The data show that the G values are much greater for the clean sand than for the lunar soil simulant, even though the shear strength is only slightly higher for the clean sand at equivalent density. This result seems much more plausible, however, when it is realized that the lunar soil simulant is many times more compressible than the clean sand, at equivalent densities.

Secondly, a number of penetration tests were performed on layers of soil submerged in water in an effort to simulate a reduction in gravity. One test result each for the lunar soil simulant, medium coarse basalt sand, and Monterey No. 20 sand tested after submergance are shown in Figure 1-33. The data show that the G values for the submerged soil layers were substantially less than would have been expected for dry soil layers of the same density. These reductions in G value were undoubtedly due to the reduction in "effective unit weight" caused by the bouyant effect of the water, with an accompanying reduction in deformation modulus. Similar reductions in "equivalent unit weight," with corresponding reductions in modulus and shearing resistance, were made for dry soil layers by simply reducing the dry density. In these latter cases, however, the corresponding reduction in G value was much greater than for the submerged soil layers. This comparison indicates that the reduction in G value with reduction in density is due not only to the decrease in shearing resistance, but also in part to the increase in compressibility. Thus it appears that compression plays a significant role in the soil penetration mechanism.

The major problem involved in projecting the G value-soil density relationship determined for the lunar soil simulant to the lunar surface is

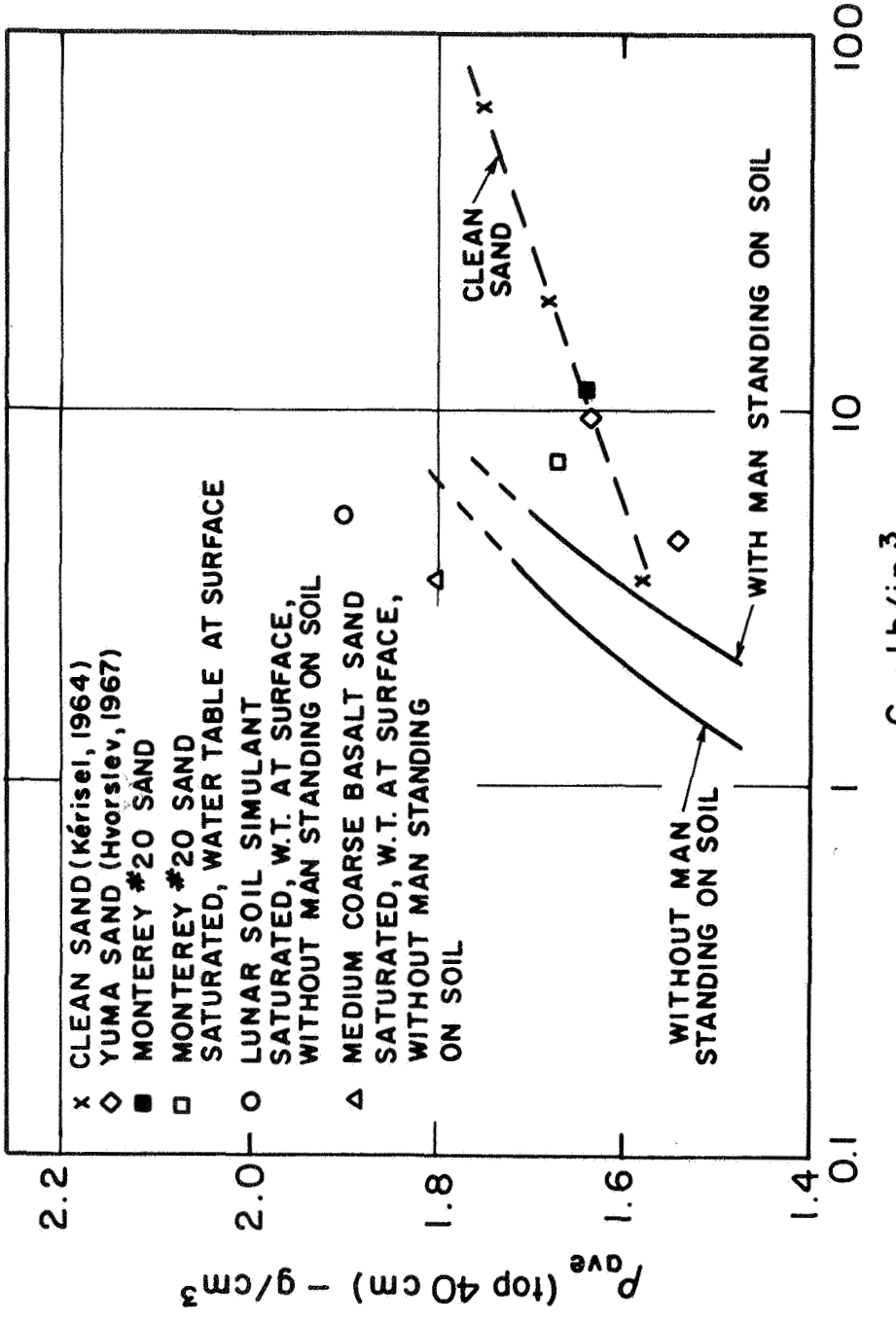

FIGURE 1-33 VARIATION OF G VALUE WITH ρ_{ave} FPR TOP 40 cm FOR CLEAN SAND AND SUBMERGED SOIL LAYERS

that of accounting for the effect of reduced gravity. Reduced gravity will result in a reduction of G due both to the reduction in shearing resistance and deformation modulus (smaller "effective unit weight") and to the increase in compressibility. On the other hand the compressibility should be only slightly influenced by the strength of the gravitational field.

The most promising experimental approach to this problem may be that of performing penetration tests on layers of lunar soil simulant submerged in liquids of various densities, including some liquids which produce an effective soil unit weight essentially equivalent to that of the lunar surface. In this way the effect of reduced gravity can be ascertained and the relative influence of shear and compression can be evaluated.

However, a number of problems must be overcome in using this technique. First, it may be very difficult to deposit saturated soil layers at low densities. In preparation for the test on the simulated lunar soil layer submerged in water (described in preceding paragraphs) an attempt was made to deposit the soil as loosely as possible by sedimenting it through about 1 inch of water. Nevertheless, the resulting average dry density was about 1.90 g/cm^3. Secondly, the influence of the pore fluid on the shear strength parameters must be assessed before penetration data can be analyzed. In the case of submergence in water, it is expected that the cohesion is essentially destroyed for the lunar soil simulant (which may account for the high density obtained under water). The effect of water on the friction angle, ϕ, has not yet been determined, but it is expected to be very small. The effect of other liquids on ϕ may be very pronounced, however. Thirdly, the loading of the saturated soil layers must be very slow to avoid build up of pore fluid pressures.

The most promising theoretical approach to the problem of reduced gravity may be the application of the finite element method to the penetration resistance test. Reduced gravity may be accounted for by simply assigning initial stresses to each element which are consistent with the effective soil unit weight. One of the difficulties in the application of this method is the determination of appropriate stress-strain parameters for the low densities and very low confining pressures appropriate for the lunar surface. Another problem is the proper incorporation of the rather complex boundary conditions associated with the cone penetrometer. Modification of an existing finite element computer program for analysis of this problem is in progress.

A third method, which may be described as semi-empirical, for assessing the influence of lunar gravity on G values is that of utilizing the results of the footprint depth studies described in the preceding section. This method can be applied immediately because data which have already been presented are used in making the projection.

Data in Tables 1-1 and 1-4 show that, for ρ_{ave} = 1.50 g/cm^3 and contact stress = 1.11 psi, the depth of footprint for the lunar soil simulant is 1.62 in. and for the actual lunar soil it is 3.23 in. Thus according to these calcualtions, the net effect of the reduced gravity for the lunar surface was to double the boot penetration, for the same load and the same value of ρ_{ave}. Although the G values obtained by considering the boot to be a large penetrometer are not the same as for the cone penetrometer due to scale effects, the above data suggest that the G value would be cut about in half for the same value of ρ_{ave} in the lunar environment. This factor can be applied to the measured G values (with the cone penetrometer) for the simulated lunar soil to obtain an estimate of the cone penetrometer G value for the lunar surface. Repeating these comparisons for other values of ρ_{ave} yields the results in Table 1-5.

TABLE 1-5

G VALUES ADJUSTED FOR EFFECT OF GRAVITY

ρ_{ave} (g/cm^3)	Lunar Soil Simulant Δ_{total} for 50-lb load (in)	Actual Lunar Soil Δ_{total} for 50-lb load (in)	$\frac{\Delta_{total} \text{ for Lunar Soil Simulant}}{\Delta_{total} \text{ for actual lunar soil}}$	G value for Lunar Soil Simulant—with man standing ($\#/in.^3$)	Adjusted G Value for Lunar Surface ($\#/in.^3$)
1.50	1.62	3.23	0.50	2.3	1.15
1.60	0.85	1.45	0.585	3.4	2.0
1.75	0.32	0.53	0.605	7.0	4.2

The G values in Table 1-5 are plotted in Figure 1-34 for convenience in interpolation. Note that these values should be reduced by about 40 percent if the astronaut places the penetrometer far enough from his feet to eliminate their influence.

Figure 1-34 shows that the probable variation in G with ρ_{ave} is pronounced, indicating that measured G values may provide a reasonable indication of lunar soil density and shear strength.

XIII. DISCUSSION OF LUNAR SURFACE SOIL DENSITY

If it is assumed that the soil density--friction angle and the soil density--bearing capacity--compressibility relationships are governed primarily by the grain size, shape, and gradation, and if it is further assumed that the lunar soil simulant matches the actual lunar soil with respect to these properties, soil simulation studies can be used to modify and perhaps improve estimates of lunar soil density.

Considerable attention has been devoted to the estimation of the lunar soil friction angle from surveyor test results, and confidence in the 35°-37° range reported is quite high. Property relationships for the lunar soil simulant (see Figure 1-4) indicate that the corresponding average value of soil density is about 1.60 g/cm^3.

Estimated bearing capacities for the actual lunar surface (based on soil simulation studies) given in Table 1-3 indicate that for an average density of 1.60 g/cm^3 the bearing capacity is about 6 psi for a 4-inch-wide loaded area. Estimates of lunar soil bearing capacity from Surveyor data indicate that the value is at least as great as 6 psi, from which it may be inferred that the average density is as great as 1.60 g/cm^3.

Thus a combination of Surveyor test results and soil simulation studies indicate that a reasonable value of the average density for the top 40 cm

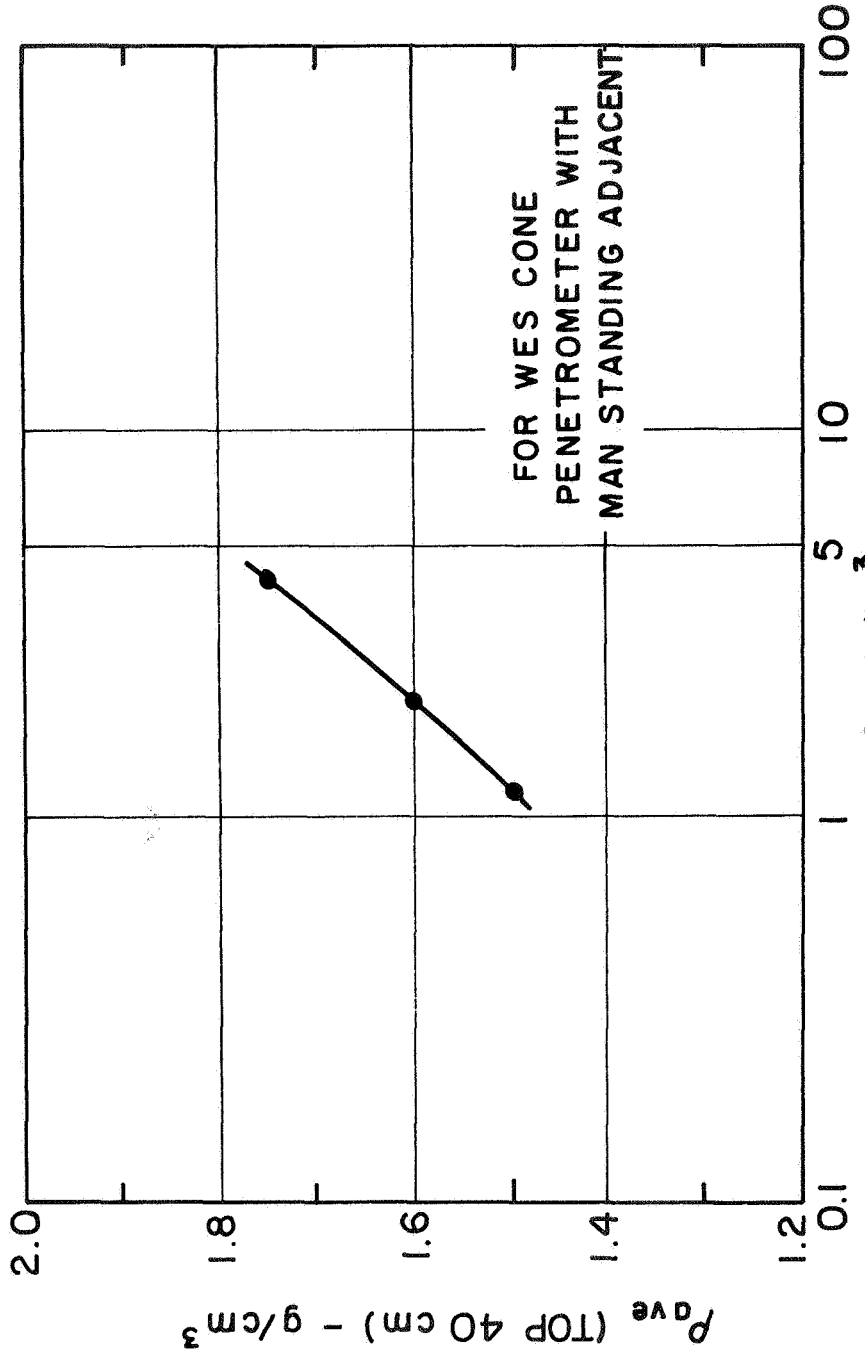

FIGURE 1-34 PROBABLE VARIATION OF G WITH ρ_{AVE} FOR LUNAR SOIL

of lunar soil may be about 1.60 g/cm^3. This corresponds to an average density of about 1.54 g/cm^3 for the top 5 cm. Of course local variations in the degree of densification due to vibrations (meteor impact and seismic activity) are likely to cause some variation in the average density for the top 40 cm. Secondly, some density variations are likely as a result of variations in soil gradation. Although the Surveyor sites were surprisingly similar in appearance and properties, some small differences in gradation were observed. For example, the material at the Surveyor VII site is somewhat coarser than at other sites. Due to these sources in density variation, it seems likely that the average density of the top 40 cm may range from about 1.55 g/cm^3 to 1.65 g/cm^3 for those parts of the lunar surface which may properly be called soil.

XIV. CONCLUSIONS

1. It has been possible to prepare a lunar soil simulant whose composition, gradation, density, and shear strength parameters are sufficiently close to those values estimated for actual lunar soil to allow meaningful correlations.

2. Lunar soil simulant density has been correlated with (a) height of drop during placement (sprinkling), (b) friction angle, (c) cohesion, (d) permeability, and (e) compressibility. These correlations are presented in Figures 1-2, 1-4, 1-6, 1-7 and 1-9, respectively.

3. A combination of theoretical and experimental analyses were used to develop probable correlations between average soil density and depth of footprints on the lunar surface and G values for lunar surface materials. These correlations are presented in Figures 1-30 and 1-34, respectively. With the possible exception of height of drop during placement, all of these

properties appear to be a sensitive function of soil density. Therefore, it is likely that, if the average soil density can be determined, most all other properties of interest can be estimated.

4. Results of the lunar soil simulation studies described herein indicate that the average density for the top 40 cm of lunar soil may be slightly higher than the value 1.50 g/cm^3 suggested in the final Surveyor report. In addition, consideration of probable variations in degree of initial densification due to vibration on the lunar surface has led to the conclusion that the lunar soil density probably varies somewhat from one location to another. On this basis an estimated range of 1.55 to 1.65 g/cm^3 for the average density of the top 40 cm was established.

5. As indicated in Figure 1-30, the estimated range in depth of footprint (with contact stress = 1.1 psi) for the lunar surface is 1.0 in. to 2.1 in. for a corresponding range in soil density of 1.65 g/cm^3 to 1.55 g/cm^3 (average value for top 40 cm).

6. As indicated in Figure 1-34, the estimated range in G value for the lunar surface is 1.5 lb/in.^{3} to 2.5 lb/in.^{3} for a corresponding range in average soil density of 1.55 g/cm^3 to 1.65 g/cm^3. Test data show that the G values are influenced by both the type of penetrometer used and the positioning of the penetrometer with respect to the feet of the man performing the test. The estimated G values given above are applicable to the WES 30-degree cone penetrometer placed 2 in. in front of the toes with 6 in. clear space between the feet. If a flat-ended rod penetrometer of about 1-in. diameter were used, it is expected that the G values would be about 50 percent higher. If the penetrometer were placed entirely outside the influence of the man's feet, it is expected that the G values would be about 40 percent lower.

7. Experience obtained with the lunar soil simulant indicates that in-place density measurements on the lunar surface will be very difficult, though perhaps possible. Success during attempts to remove a "cake-like" block of the lunar soil simulant by excavating around it was only marginal, but lower gravity-induced shear stresses during excavation on the lunar surface may be enough to make the difference.

8. If in-place density measurements prove impossible, the correlation between density and footprint depth given in Figure 1-30 can be used to estimate lunar soil density. If direct density measurements are obtained, these values can be used to check and modify, if necessary, the correlation given in Figure 1-30 . In either case, one or two in-situ density measurements is the most that can be hoped for in early missions, but footprints will be abundant wherever the astronauts go and will serve as a prime source of data.

XV. RECOMMENDATIONS

1. Good measurements of in-place density of lunar surface soil should be made during early Apollo missions if possible. The results of lunar soil simulations indicate that most soil properties of interest may be estimated through correlation with density. Therefore, in-place density measurements are highly desirable. It appears that the most promising method for density determination is the excavation of an undisturbed block of lunar soil, as described in the Geotechnical Investigations Section of the Definitive Experiment Plan for the Apollo Lunar Field Geology Experiment.

2. If attempts to measure the in-place density of the lunar surface materials are successful, the density and the depth of astronaut footprint should be correlated and these data should be used to check and modity.

if necessary, the relationship between density and depth of footprint presented in Figure 1-30. If attempts to measure in-place density are unsuccessful, the relationship presented in Figure 1-30 may be used as an indicator of lunar soil density.

3. Penetration resistance tests should be performed during early Apollo missions. Measurement of the penetration resistance, in terms of the slope of the stress-penetration curve, G, serves at least three purposes. First, the G values obtained may be used in design of lunar roving vehicles. Second, the measured G values may be used to estimate soil density and other important properties through correlations. Third, the penetrometer serves as a probe in determining the homogeneity of the soil profile.

4. If possible, the G values should be measured with a WES cone penetrometer, since vehicle design studies using this penetrometer are currently being made. Of course G values may be obtained with other penetrometers and the G value which would have been obtained with the WES cone can be estimated through correlations. However, some accuracy is lost in using an intermediate correlation.

5. A standard procedure (especially with respect to the relative position of the man's feet and the penetrometer) for performance of penetration resistance tests should be adopted and publicized. Although it differs somewhat from the procedure adopted for the tests reported herein, in retrospect it appears that placement of the penetrometer about 4 in. in front of the toes (centered) with about 10 in. between the feet may be the best arrangement. With this arrangement the G value for the first 5 or 6 in. of penetration will probably not be significantly affected by the presence of the man's feet. Secondly, for tests performed in the

terrestrial environment, the rate of penetration should be sufficiently low to allow dissipation of pore air pressures.

6. Additional laboratory and model tests on the lunar soil simulant should be conducted to expand and verify the correlations between soil properties and footprint depth and G value reported herein. Special attention should be given to the determination of stress-strain parameters appropriate for very low densities and very low pressures. Also, at least one additional lunar soil simulant with a coarser gradation should be studied to further explore the influence of gradation on other properties. Penetration tests under conditions of reduced gravity should be simulated by using soil layers submerged in various heavy liquids.

7. Theoretical analyses using the finite-element approach should be performed in an effort to assess the influence of reduced gravity on deformations. These analyses, including both plane-strain and axisymmetric loading conditions, should be correlated with corresponding model test results as a check.

References

1. Meyerhof, G. G., "The Ultimate Bearing Capacity of Foundations," Geotechnique, Vol. II, 1951, p. 301.

2. Burmister, D. M., "Stress and Displacement Characteristics of a Two-Layer Rigid Base Soil System: Influence Diagrams and Practical Applications," Proc. Highway Research Board, Vol. XXXV, 1956, p. 773.

3. Vesic, A. S., "Ultimate Loads and Settlement of Deep Foundations in Sand," Proc. Symposium on Bearing Capacity and Settlement of Foundations, Duke University, Durham, N.C., 1967, p. 53.

4. Kerisel, J., "Deep Foundations, Basic Experimental Facts," Proc. Deep Foundations Conference, Mexico, 1964.

5. Hvorslev, M. J., Panel Discussion Session II Shallow Foundations, Proc. Symposium on Bearing Capacity and Settlement of Foundations, Duke University, Durham, N.C., 1967, p. 93.

CHAPTER 2

LUNAR SURFACE TRAFFICABILITY STUDIES

(J. B. Thompson and J. K. Mitchell)

I. INTRODUCTION

The current state of the art of vehicle mobility and trafficability prediction as related to the design and operation of lunar roving vehicles was reviewed and evaluated under contract NSR 05-003-189 and summarized by Mitchell et al. (1969). It was noted that there is at present no method which is completely suitable for the reliable prediction of needed trafficability and soil-vehicle interaction parameters. Recommendations were made that intensive studies of both an experimental and theoretical nature be initiated in order to develop the information necessary for design and performance prediction of lunar roving vehicles.

To these ends experimental studies are now underway at the U. S. Army Engineer Waterways Experiment Station, Vicksburg, Mississippi, for the purposes of 1) establishing the performance parameters of wheels of a type proposed for lunar vehicles and 2) answering basic performance questions such as the maximum slope that may be negotiated on the lunar surface and the nature of soil-wheel interaction for very lightly loaded wheels. The results of experimental studies of this type may also be useful for the establishment of similitude relationships for lunar trafficability analysis once reliable cone index values for lunar soils are available. The essential elements of this method are described by Mitchell et al.(1969). Preliminary estimates of cone index values for lunar soil have been made based on the results of tests on simulated lunar soil conducted both in our laboratory (see Volume I, Chapter 1) and at MSFC.

Our group has concerned itself during the past year with some analytical aspects of lunar trafficability. Initially, attention was directed at the question, "How much difference is a variation in soil conditions likely to make on the performance parameters of a lunar roving vehicle?" In order to gain insight into this question, a parameter study was made using the Bekker "Soil Value System" method of analysis. That the theoretical basis for the Soil Value System relationships is open to serious question is well recognized. Nonetheless, it is the only quasi-theoretical method available at the present time, and a considerable body of previous trafficability work for lunar exploration purposes has been done using this method.

It would have been desirable to develop the analysis using the WES similitude method; however, work described by Mitchell et al. (1969) has shown that the existing relationships between performance parameters and combined wheel-soil parameters are not valid for wheels and loading conditions proposed for lunar roving vehicles.

The accuracy of the Bekker method as applied to wheels of a type proposed for lunar vehicles was then evaluated by comparing the theory to existing test results. Because the Soil Value System provides only for the evaluation of two extreme wheel-soil configurations, rigid wheel and track, a technique for predicting the performance of a deformable wheel such as might be used on a lunar roving vehicle was developed. Finally the crucial problem of vehicle mobility on slopes was examined.

II. PARAMETER STUDY

The following parameter study was conducted to determine the effect of possible variations in soil conditions on the performance parameters

of a lunar roving vehicle. The Bekker Soil Value System vehicle performance parameters were used as indicators.

A. Basic Relationships of the "Soil Value System"

The key relationships that are developed in the Soil Value System are for the performance parameters thrust, motion resistance, and drawbar pull (Bekker, 1960). The merits and limitations of the theory underlying these relationships and the test methods used for the determination of needed soil parameters have been discussed at length in the literature and are summarized by Mitchell et al.(1969).

The appropriate relationships are as follows:

Wheel on Track Thrust -

$$H = (\ell bc + w\tan\phi)\left[1 - \frac{K}{i_o \ell}\left(1-e^{-i_o \ell/K}\right)\right] \qquad (2\text{-}1)$$

The above equation is applicable for a soil exhibiting a stress-deformation curve in which stress continuously increases with deformation. For a soil which exhibits a stress-deformation curve in which stress falls off after a certain deformation is reached, another expression in terms of two parameters, K_1 and K_2, can be written for thrust. Because little information is available on the stress-deformation properties of the lunar soil, it will be assumed that the soil is of the first type. If the results of the Bevameter annular shear test are plotted as the ratio of the recorded shear stress to the soil shear strength versus the deformation, K is equal to the inverse of the slope of the curve at zero deformation. In other words the magnitude of the stress-deformation parameter indicates the steepness of the stress-deformation curve.*

---

*It has been suggested (Costes, personal communication, 1969) that K may not be independent of i_o and ℓ. If so, the usefulness of both K as a meaningful soil parameter and Equation (2-1) may be questioned.

Motion Resistance

Rigid Wheel -

$$R = [b(\frac{k_1}{b} + k_2)]^{\frac{-1}{2n+1}} \frac{1}{n+1} (\frac{3w}{3-n})^{\frac{2n+2}{2n+1}} D^{\frac{-n-1}{2n+1}} \quad (2\text{-}2)$$

Track -

$$R = [b(\frac{k_1}{b} + k_2)]^{-\frac{1}{n}} \frac{1}{n+1} (\frac{w}{\ell})^{\frac{n+1}{n}} \quad (2\text{-}3)$$

Drawbar Pull -

$$DP = H - R \quad (2\text{-}4)$$

where:

ℓ - wheel or track contact length

b - wheel or track contact width

D - wheel diameter

w - wheel or track load

i_o - slip of wheel or track

K - soil stress deformation parameter

c, ϕ - soil strength constants

k_1, k_2, n - soil sinkage parameters .

B. Wheel and Soil Parameters Utilized

The wheel dimensions and load-deformation characteristics adopted for this study were taken from the results of a metal wheel test program conducted by AC Electronics (1967). The wheels used in this test program were 40 inches in diameter and 10 inches in width across the contact surface. Because the contact length was not measured during testing, it was estimated from the load- deformation characteristics of the wheels.

For the purpose of this study the following wheel loads and corresponding contact lengths were used:

TABLE 2-1

w (lbf.)	ℓ (in.)
50	14.7
75	16.5
100	18.2
150	20.6

From a consideration of the deformation characteristics of the wheels studied it might be anticipated that the motion resistance characteristics would fall between those of a track and a rigid wheel. Therefore, Equations (2-2) and (2-3) should theoretically envelope the measured motion resistance values. This hypothesis is examined in Section 2-III.

Values assumed for soil cohesion (c) and angle of internal friction (ϕ) were as follows, based on data available from the Surveyor program.

$$c = 0.05 \text{ to } 0.15 \text{ psi}$$

$$\phi = 37° \pm 4$$

The soil sinkage parameters k_1, k_2, and n are less certain. Scott (1968)* reported values for n of 1.0 and 0.7 determined from load-sinkage tests using the Surveyor Surface Sampler with the scoop closed and open, respectively. For the purpose of this study, k_1 and k_2 were combined into a single parameter, $k = \frac{k_1}{b} + k_2$, and the following ranges of values for k and n were assumed for this study:

---

*Verbal communication as stated at the Lunar Soil Wheel Interaction Meeting at the Jet Propulsion Laboratory, November 15, 1968.

$$k = \frac{k_1}{b} + k_2 = 0.5 \text{ to } 6.0$$

$$n = 0.75 \text{ to } 1.25$$

Estimates of the soil stress-deformation parameter K can be based only on terrestrial experience as appropriate tests have as yet not been conducted on the lunar surface. Based on a compilation of terrestrial values by Mitchell et al. (1969), the range assumed was:

$$K = 0.5 \text{ to } 1.5.$$

C. Results of the Parameter Study

Using the values stated above for the various wheel and soil parameters, the performance indicators wheel thrust, motion resistance (for both rigid wheel and track), and drawbar pull (for both rigid wheel and track) were calculated. The results are presented in Figures 2-1 through 2-5. The sensitivity of each of these performance indicators to each of the assumed soil parameters is discussed below.

i. Influence of K, Soil Stress-Deformation Parameter - K affects the calculated thrust as shown in Figure 2-1, and consequently drawbar pull as indicated in Figures 2-4 and 2-5. The influence is greatest for low values of K and for high wheel loads. For example, at a slip of 10 percent and a wheel load of 150 pounds, the variation in the calculated thrust over the range of K assumed in this study is 38.5 pounds. For any given wheel load, the influence of K decreases appreciably with increasing slip.

ii. Influence of Soil Sinkage Parameters - The assumed values of the soil sinkage constants, k and n, affect the calculated motion resistance (Figures 2-2 and 2-3) and consequently drawbar pull (Figures 2-4 and 2-5). The effect of each is discussed separately below.

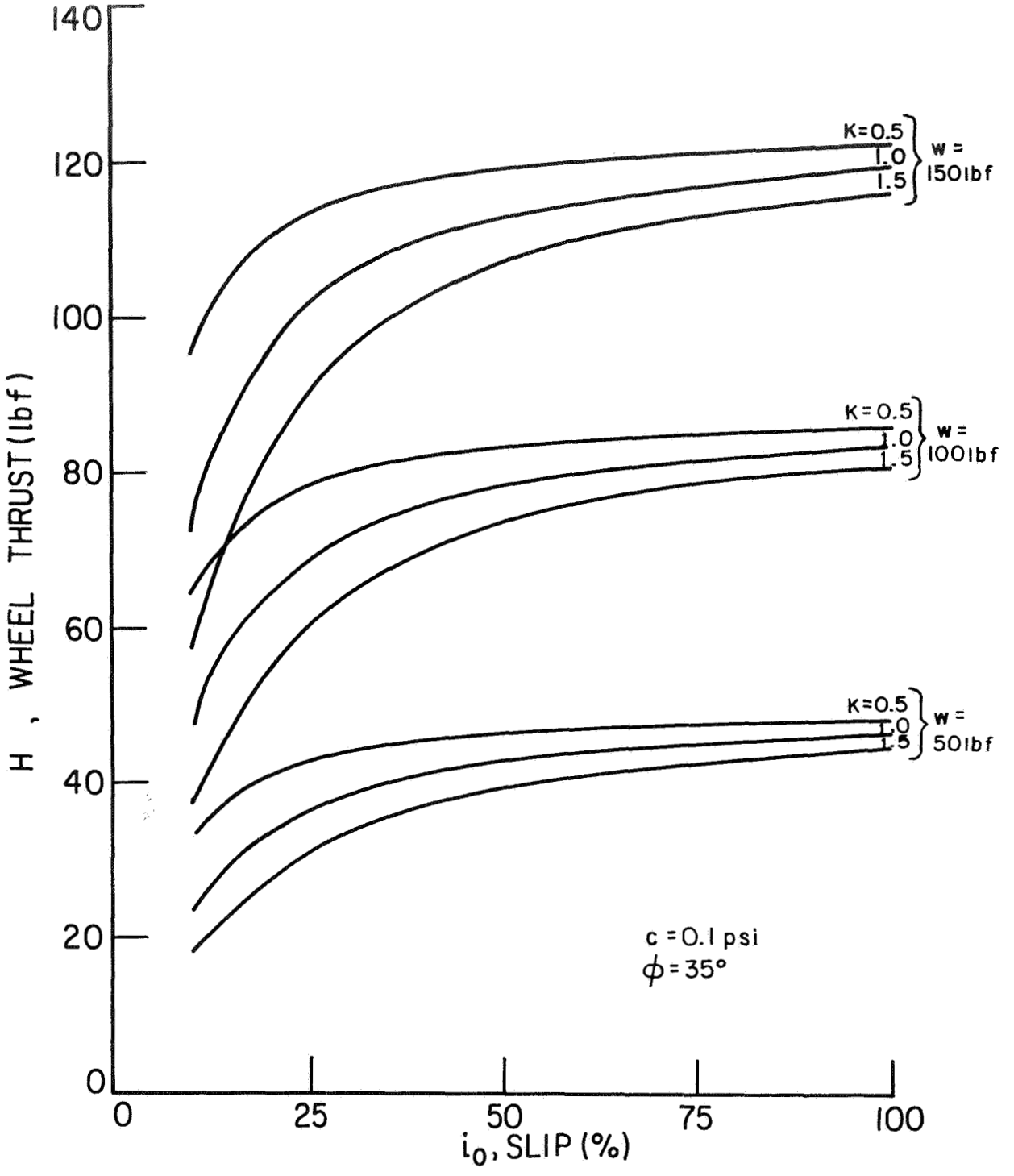

FIGURE 2-1 WHEEL THRUST VS SLIP

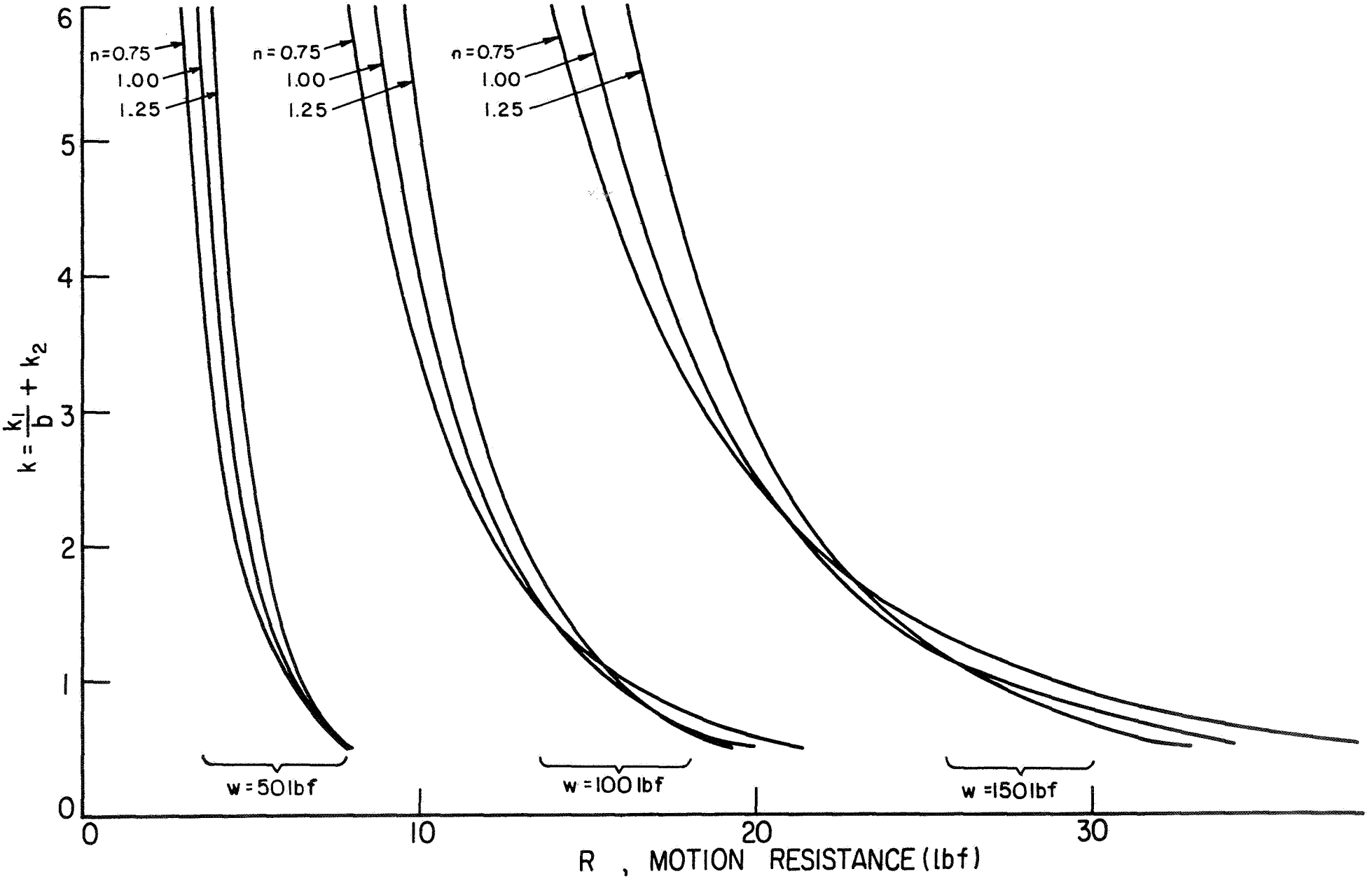

FIGURE 2-2 MOTION RESISTANCE VS $\left(\frac{k_1}{b} + k_2\right)$ FOR A RIGID WHEEL

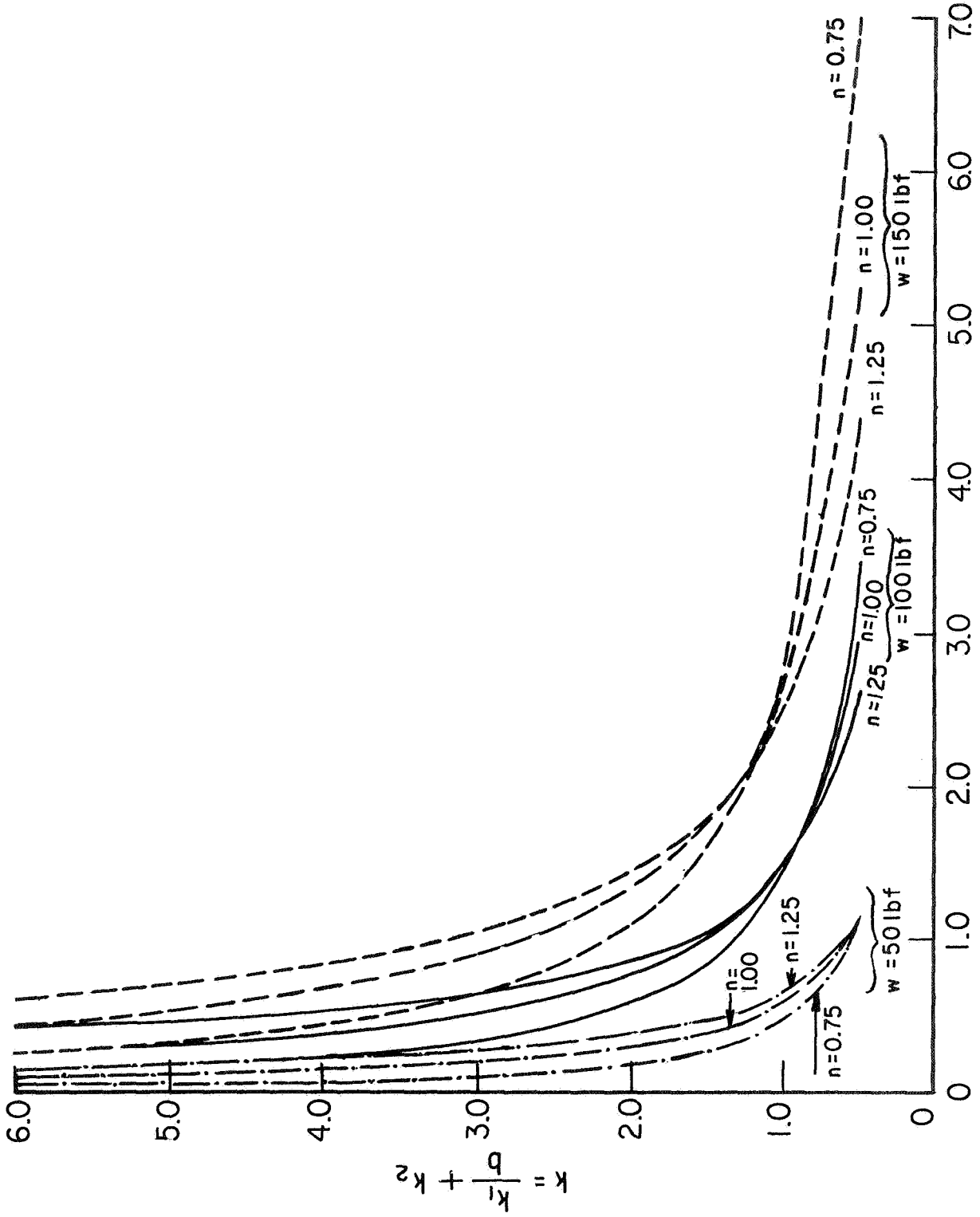

FIGURE 2-3 MOTION RESISTANCE VS $\left(\frac{k_1}{b} + k_2\right)$ FOR A TRACK

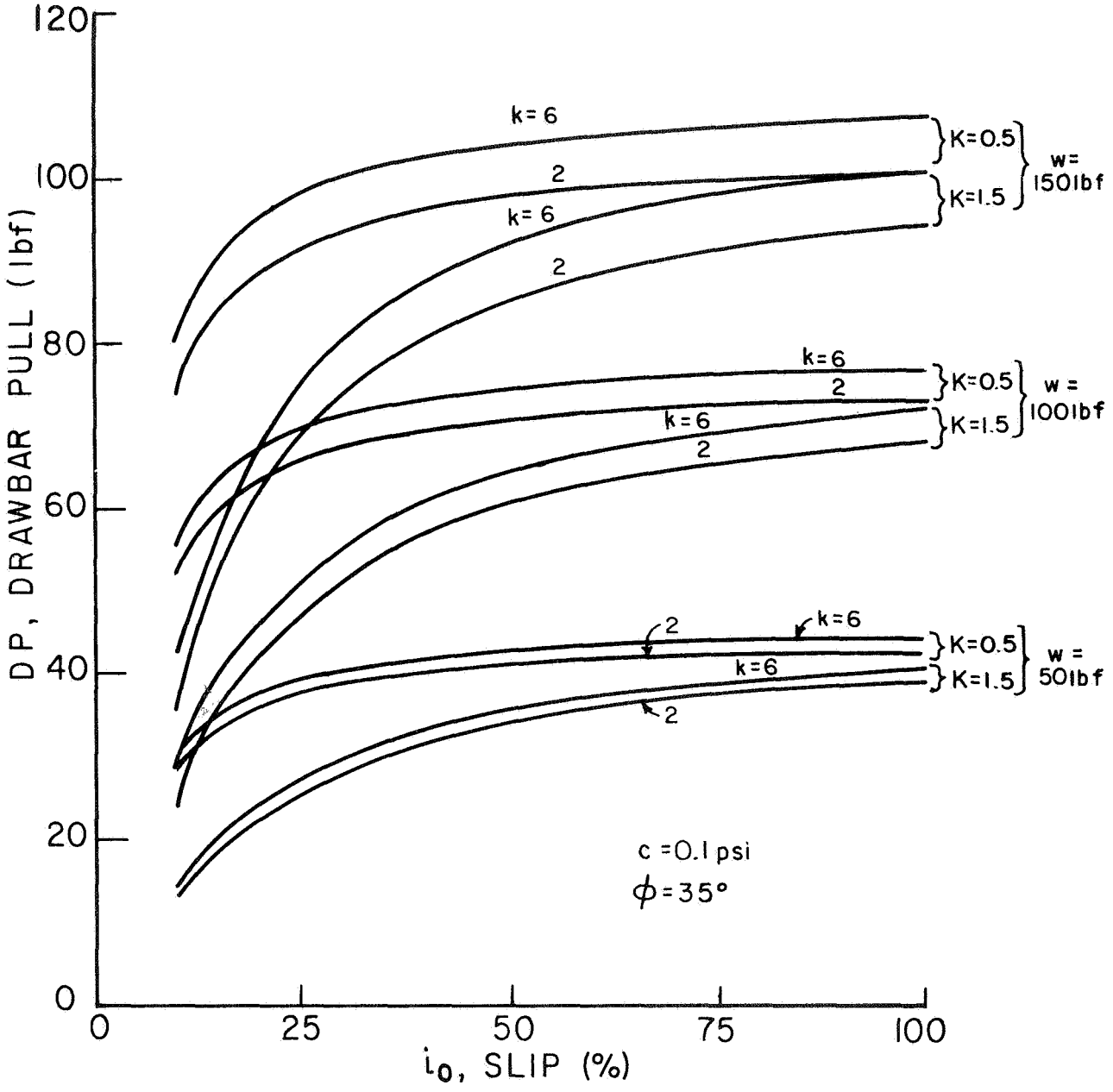

FIGURE 2-4 DRAWBAR PULL VS SLIP FOR A RIGID WHEEL

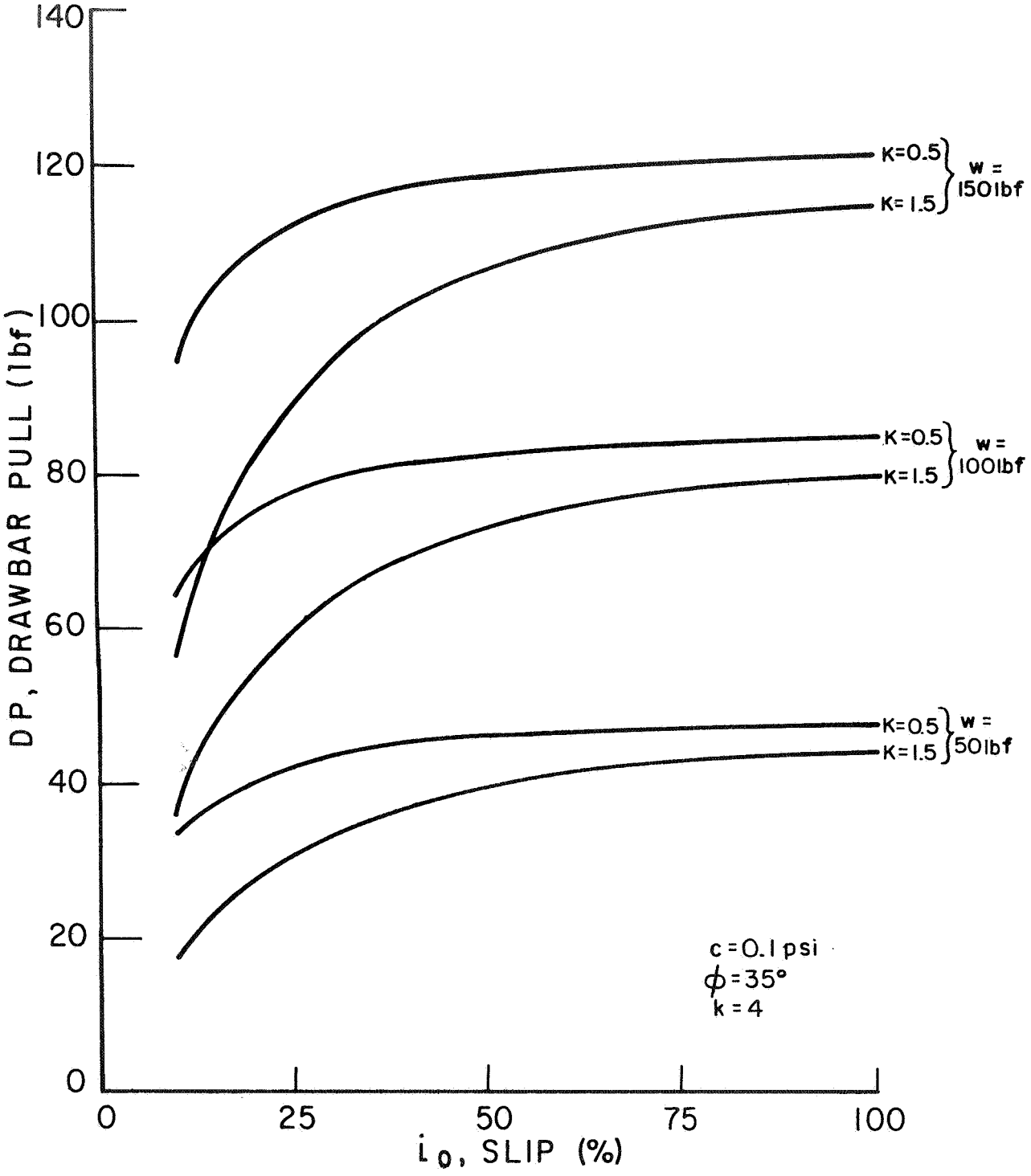

FIGURE 2-5 DRAWBAR PULL VS SLIP FOR A TRACK

a) n - Within the range of k generally considered applicable to lunar soil (i.e., 2.5 or greater), the effect of the assumed value of n on the calculated motion resistance is seen to be small in the range of wheel loads studied. This is true whether the metal wheel is assumed to behave as a rigid wheel or track. The variation in the calculated motion resistance with n increases with increasing wheel load and value of k and is largest in the case of the rigid wheel assumption. For a wheel load of 150 pounds and a value of k of 6, the variation in the calculated motion resistance of a rigid wheel is only 2.2 pounds for the range of n values studied. Therefore, wheel performance does not appear to be sensitive to variation in values of n.

An interesting observation from Figures 2-2 and 2-3 is that, according to the Bekker Theory, larger values of n result in larger values of motion resistance in the applicable range of k values. Therefore, a consistently conservative design should recognize this fact.

b) k or $\frac{k_1}{b} + k_2$ - The effect of k on the motion resistance increases with a decrease in the value of the parameter and an increase in the wheel load and is greatest for the rigid wheel assumption. For a wheel load of 150 pounds, the difference between the motion resistance of the rigid wheel at values for k of 2 and 6 is 7.7 pounds. The effect of k on the motion resistance of a track is negligible within the applicable range of the parameter, and a value of k = 4 was used in calculating the drawbar pull of a track.

iii. Influence of Soil Strength Constants - In Figures 2-1 through 2-5, the wheel performance indicators were calculated with assumed soil strength values of c = 0.1 psi and ϕ = 35 degrees.* These two parameters also affect the calculated wheel thrust and consequently drawbar pull. The influence of the assumed values of c and ϕ can be seen most easily by examining the thrust equation, Equation (2-1). For given values of K, ℓ, and i_o the term in brackets has a fixed value which is multiplied by values of ℓ, b, c, w, and ϕ. Therefore, for a given wheel load, and consequently contact length, and for the wheel width specified above, it is possible to express in percent the effect of deviations in values of c and ϕ, from 0.1 psi and 35 degrees, respectively, on the calculated value of thrust.

The percent change in the calculated value of thrust as a function of the assumed values of c and ϕ is shown in Figure 2-6. Over the range of c and ϕ values of probable significance, that is 0.05 psi < c < 0.15 psi and 33° < ϕ < 41°, and over the range of wheel loads studied, the maximum variations in the calculated thrust are theoretically 30 and 26 percent due to deviations in c and ϕ, respectively. Therefore, the assumed soil strength parameters may be expected to have a significant effect on the vehicle performance. It is noteworthy that the additional effect of the wheel load on the percent change in the calculated value of thrust shown in Figure 2-6 is the result of the load-deformation characteristics of the wheel. If the wheel load-contact length relationship for the wheel were linear, the percent change shown in Figure 2-6 would be independent of the wheel load.

---

*As determined by Bevameter (ring shear). Corresponding values of ϕ determined by triaxial test are generally higher.

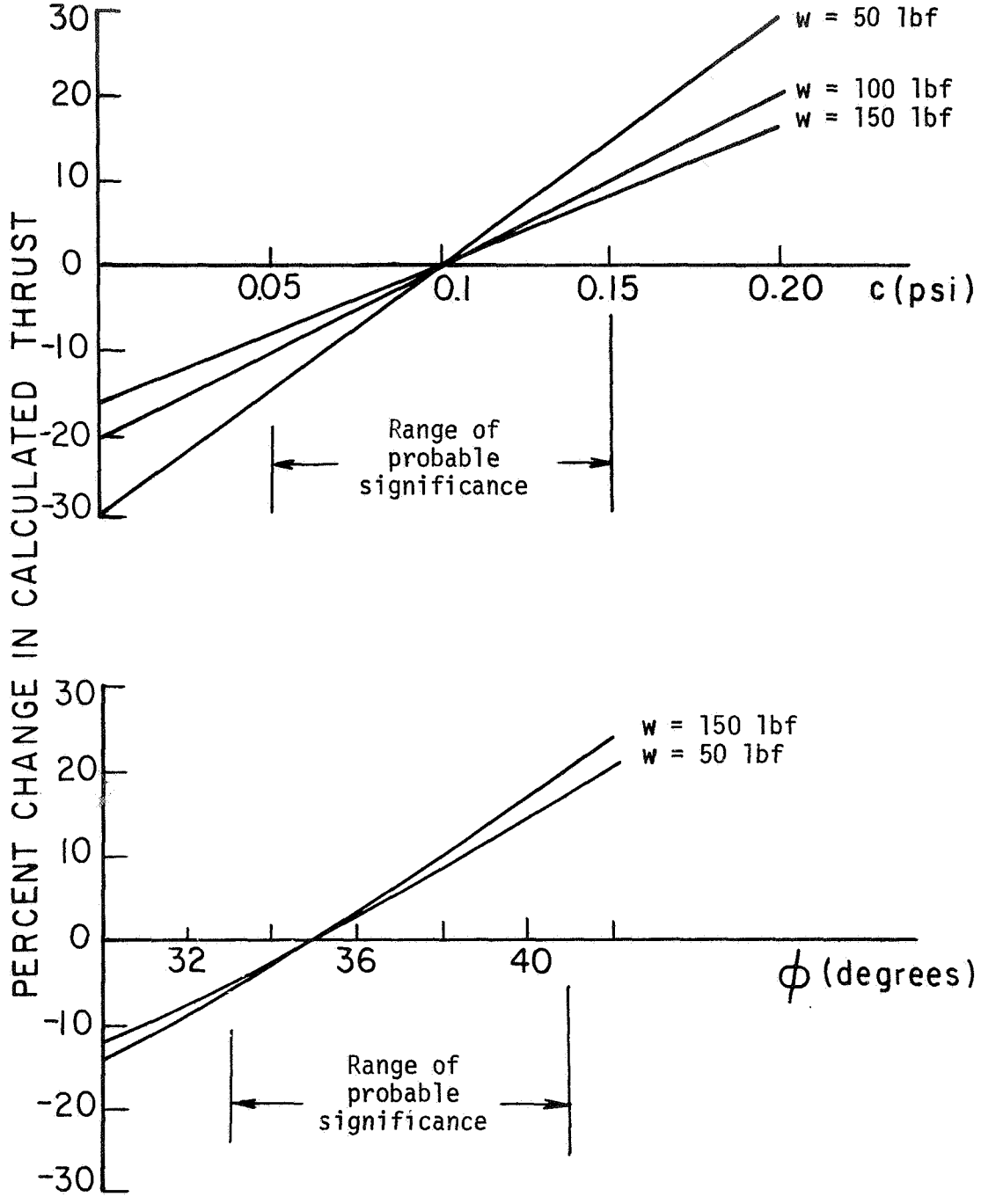

FIGURE 2-6 PERCENT CHANGE IN CALCULATED THRUST VS c AND ϕ

Figure 2-6 can be used to adjust values of thrust for one assumed set of strength parameters to another. For example, if a given wheel at a given wheel load is to be tested on several different soils, one would only need to calculate the performance indicators based on c = 0.1 psi and $\phi = 35°$ and then enter Figures 2-6(a) and (b) at the revised parameter values. read the percent change, and adjust the performance indicators accordingly. This approach assumes, of course, that for each wheel load, there is a corresponding contact length independent of the test soil.

iv. Discussion - The effects of the wheel load, wheel diameter, contact length, and contact width on the wheel drawbar pull have not been presented in the preceding graphs. However, study of Equations (2-1), (2-2), and (2-3) shows that the wheel diameter, contact length, and contact width should be maximized to maximize drawbar pull. With the exception of the motion resistance of the track, in the applicable range of k, the wheel load has a significant effect on the performance indicators (Figures 2-1 through 2-5). An increase in wheel load results in an increase in the calculated thrust, motion resistance, and drawbar pull.

An important problem in lunar trafficability investigations is likely to be the mobility of a rover on slopes. Bekker (1960) stated that the maximum slope a vehicle can climb is given by the drawbar pull to weight ratio. Although this conclusion does not consider such important factors as the general stability of the soil mass, it will be used here as a first order measure of the slope climbing capability of a vehicle. Calculated

drawbar pull to weight ratios are shown in Figures 2-7 and 2-8. These plots indicate that in spite of the fact that the heavier wheel loads result in larger values of drawbar pull, the increase in wheel load is not matched by an increase in hypothetical slope climbing ability. It appears therefore that for values of slip greater than approximately 10 percent, the axle load should be minimized in order to maximize the slope climbing ability of a vehicle.

D. Conclusions from Parameter Study

The following conclusions may be derived from the study of the influence of soil conditions and vehicle characteristics on vehicle performance parameters using the Soil Value System. The validity of these conclusions is, of course, entirely dependent on the validity of Equations (2-1), (2-2), (2-3), and (2-4).

1) The effect of variations of the soil stress-deformation parameter, K, on the calculated value of thrust is greatest at low values of slip and increases with increasing wheel load. Because efficient use of available energy may require the operation of the lunar rover at low values of slip, an accurate estimate of this parameter may be required for adequate prediction of vehicle performance.

2) The effect of variations of the soil sinkage constant, n, on the calculated motion resistance is relatively small in the applicable range of values of k. Therefore, an accurate estimate of this parameter would not be required to adequately predict vehicle performance, assuming, of course, that performance is predicted correctly by the relationships used. However, a consistently conservative design should adopt the maximum value of n in the range considered applicable.

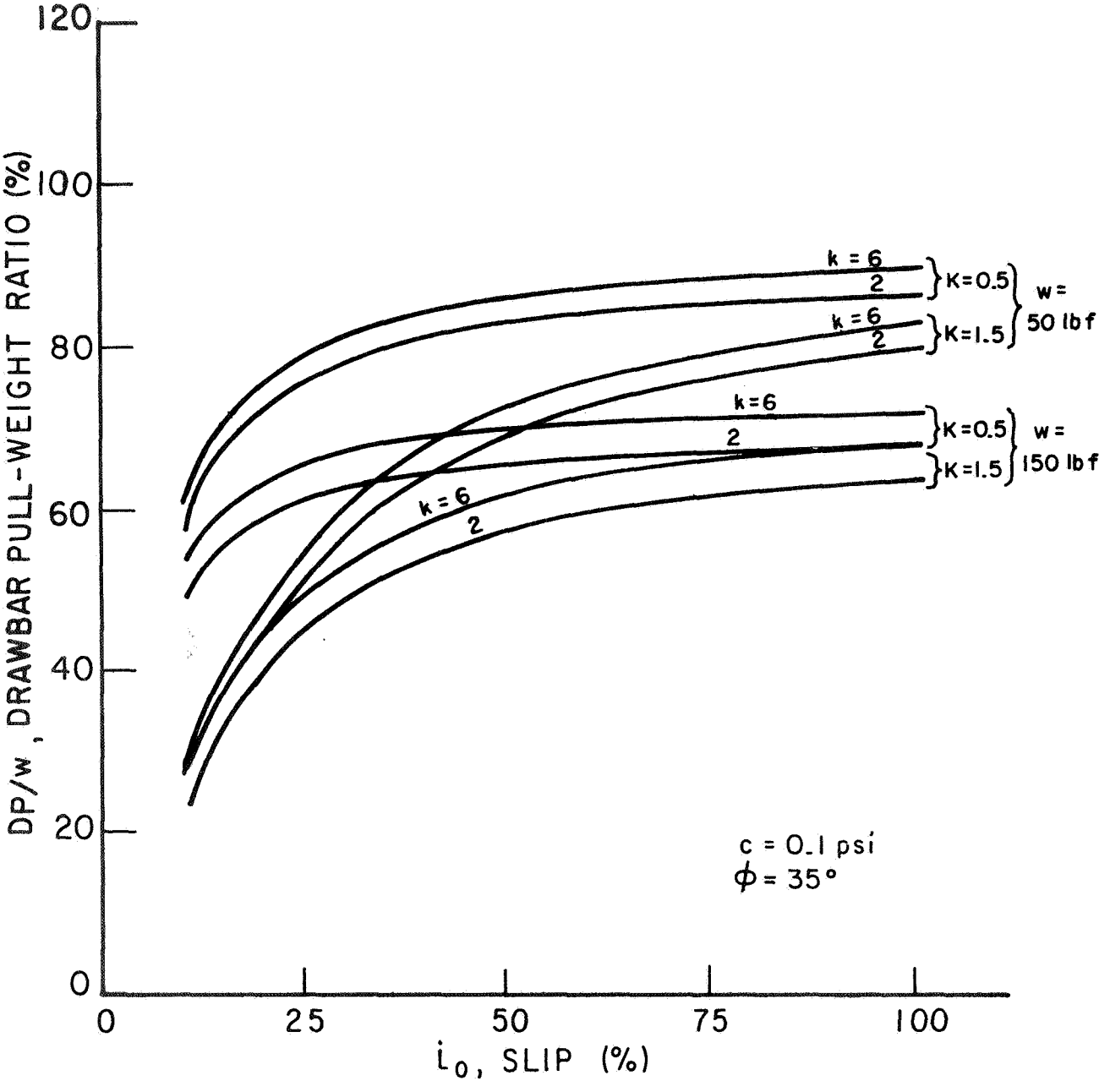

FIGURE 2-7 $\frac{DP}{W}$, DRAWBAR PULL-WEIGHT RATIO FOR A RIGID WHEEL

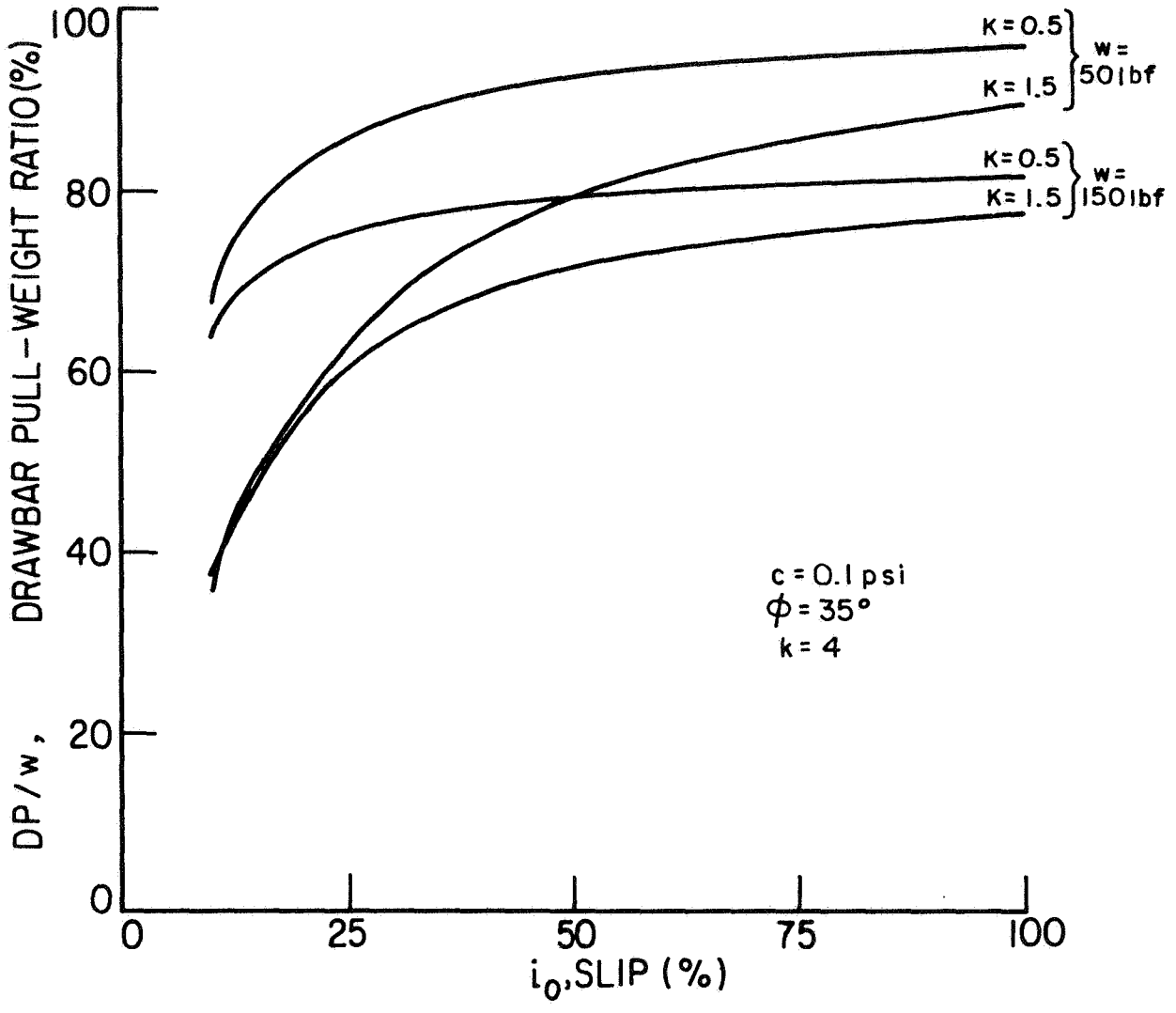

FIGURE 2-8 $\frac{DP}{w}$, DRAWBAR PULL-WEIGHT RATIO VS SLIP FOR A TRACK

3) The effect of variations of the soil sinkage constant, k, on the calculated motion resistance increases with an increase in wheel load and is only significant in the case of the rigid wheel assumption. The required accuracy in the estimation of this parameter will depend to a great extent on the anticipated wheel load and wheel deflection characteristics. For the wheels investigated in this study, an accurate prediction of this parameter will not be required if wheel loads on the order of 100 pounds force are anticipated as the maximum error in motion resistance prediction would only be approximately 4 pounds.

4) The effect of variations of the soil strength parameters, c and ϕ, on the calculated value of thrust is significant, and accurate prediction of these parameters is required if the vehicle performance is to be adequately evaluated.

5) An increase in the wheel load leads to an increase in the calculated thrust, motion resistance, and drawbar pull. However by taking the drawbar pull to weight ratio as an indicator of the slope climbing ability of a vehicle, the lighter the wheel load the steeper a slope the vehicle should be able to climb.

6) The characteristic wheel dimensions of contact width, contact length, and diameter should be maximized from a trafficability viewpoint.

III. COMPARISON OF THEORY WITH EXISTING TEST RESULTS

The conclusions reached in the above parameter study are only significant if the Soil Value System method adequately evaluates the mobility of any proposed lunar vehicle. Very limited metal wheel test results that may be used for an evaluation of the accuracy of the method

were reported by AC Electronics (1967). Mobility tests on both wire mesh and metal elastic wheels were conducted. Because the performance of both wheel types was nearly identical, average values of the measured performance indicators are used in this discussion.

The soil used in this wheel test program was a dry sand with the following parameter values.

$$c = 0.035 \text{ psi}$$

$$\phi = 31°$$

$$\left.\begin{aligned} k_1 &= 0 \\ k_2 &= 6 \end{aligned}\right\} \quad k = 6$$

$$n = 1$$

$$K = \text{(not measured)}.$$

Tests were performed using wheel loads of 50, 75, 100, and 150 pounds force. The test wheel dimensions and load-deformation characteristics were the same as those used in conducting the parameter study. Therefore, the various values of the performance indicators calculated for the parameter study can be compared directly to the measured values except that the calculated thrust and drawbar pull values must be corrected to the values of c and ϕ exhibited by the soil used in this test program. From Figure 2-6 the following percent corrections of the calculated thrust are required for each wheel load.

Table 2-2

w (lbf)	Percent Change in Thrust
50	-29.2
75	-27.0
100	-24.1
150	-22.6

Plots of the predicted and measured wheel thrust, motion resistance, and drawbar pull are shown in Figures 2-9 through 2-11 and are discussed below.

A. Thrust

Unfortunately, the soil stress-deformation parameter, K, was apparently not measured in this test program. Therefore a value of K of 0.5 was assumed since it resulted in the best fit between the predicted and measured values of thrust as shown in Figure 2-9. For the wheel loads of 50 and 75 pounds force, the predicted and measured values of thrust are quite close. However for the wheel loads of 100 and 150 pounds force the predicted values of thrust are increasingly larger than the measured values. The explanation for this difference offered by AC Electronics was that slip between the wheel and the soil occurred and therefore the optimum soil strength was not mobilized. Although this explanation seems plausible, it is possible that the Soil Value System method of analysis is not an adequate method of analysis. However, it is encouraging that the general shape of the predicted and measured thrust plots correspond quite well.

The apparent slip between the wheel and the soil noticed in this test program points out an important problem in terrestrial wheel testing. Since terrestrial wheel-soil friction and adhesion may differ from those on the moon, lunar conditions may have to be artificially duplicated in order to accurately model the wheel-soil interaction.

B. Motion Resistance

Because the Soil Value System method provides only for the calculation of the motion resistance due to the force exerted on the wheel by the soil, a correction must be made for the inherent resistance

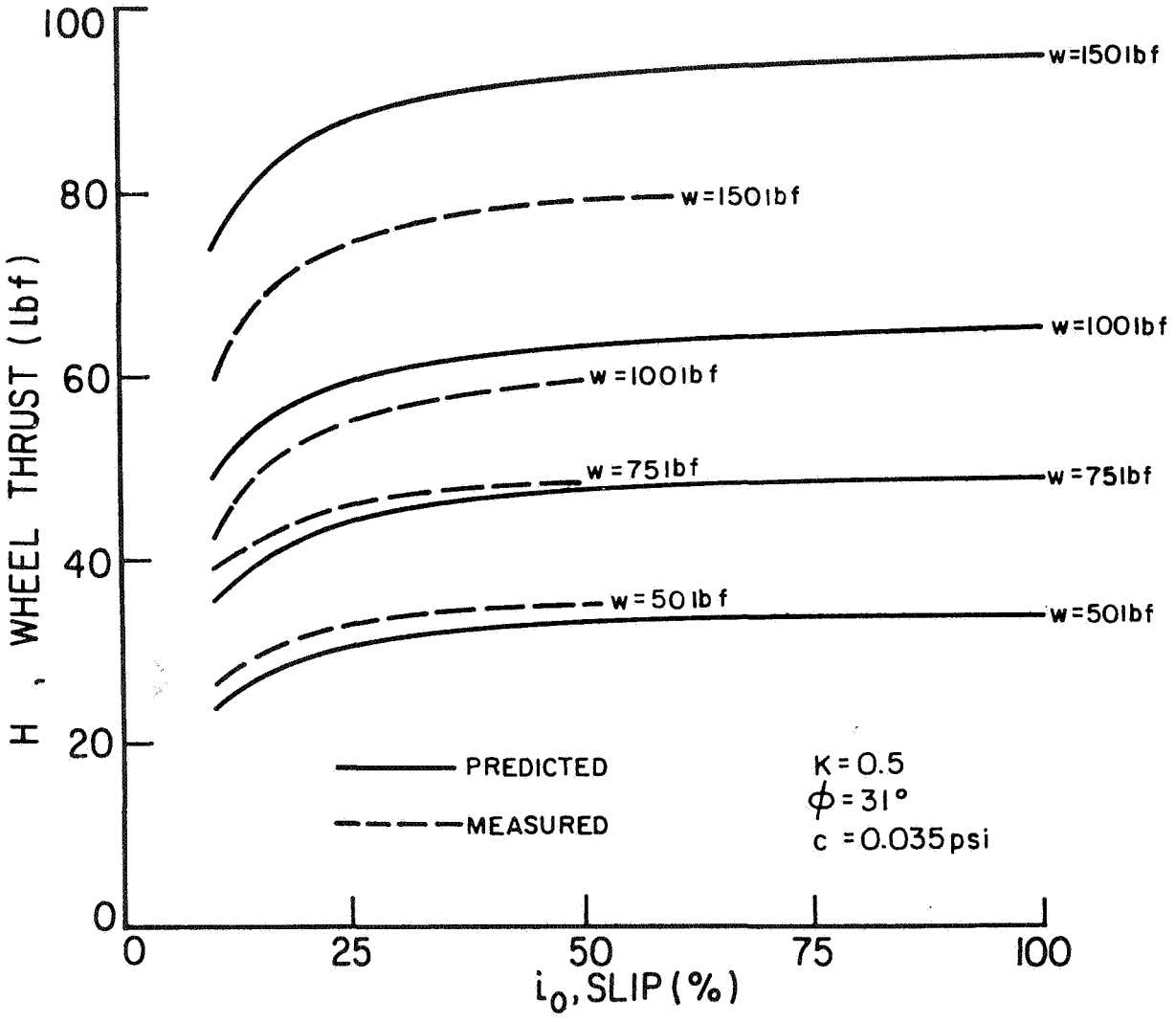

FIGURE 2-9 COMPARISON BETWEEN PREDICTED AND ACTUAL WHEEL THRUST VS SLIP

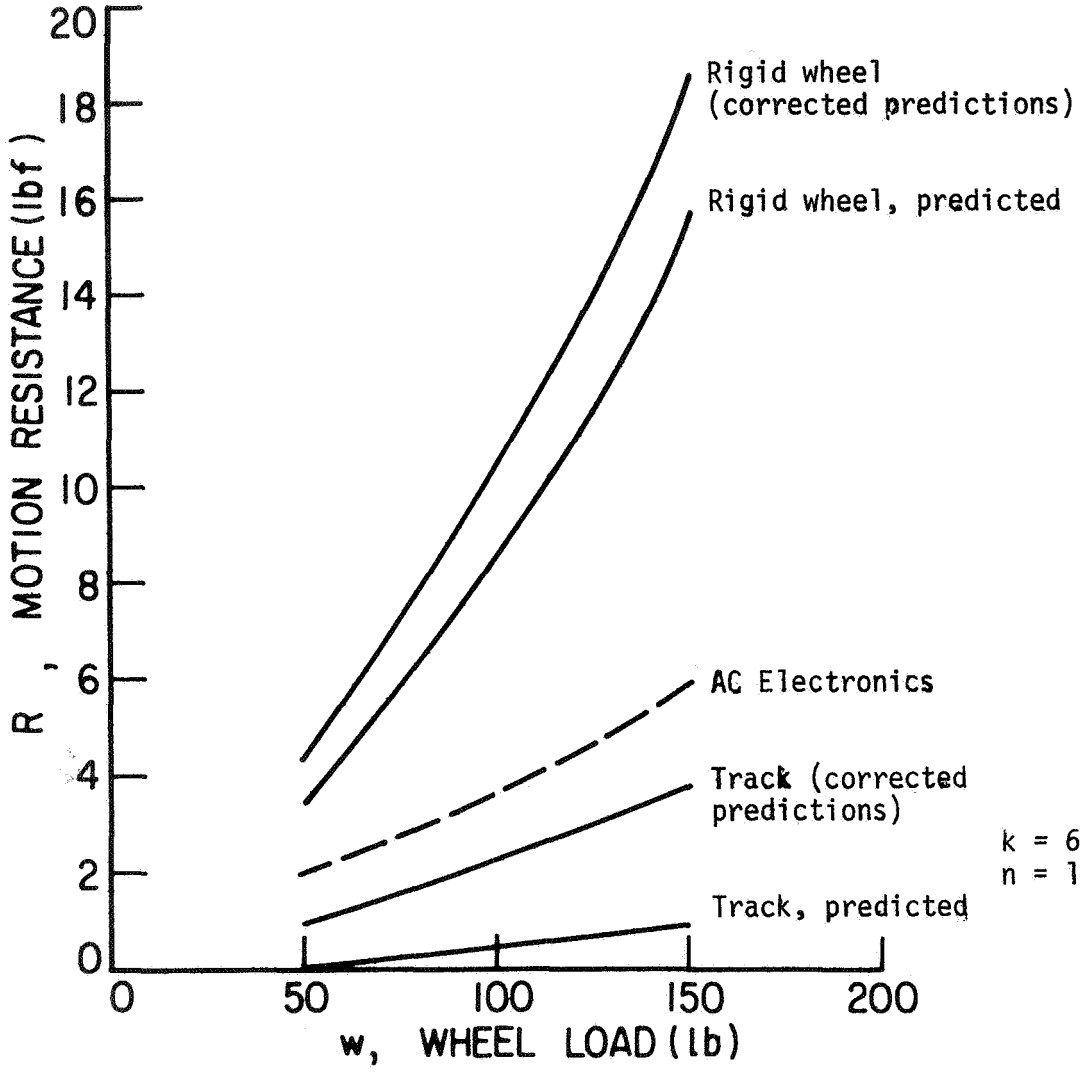

FIGURE 2-10 COMPARISON BETWEEN PREDICTED AND ACTUAL MOTION RESISTANCE VS WHEEL LOAD

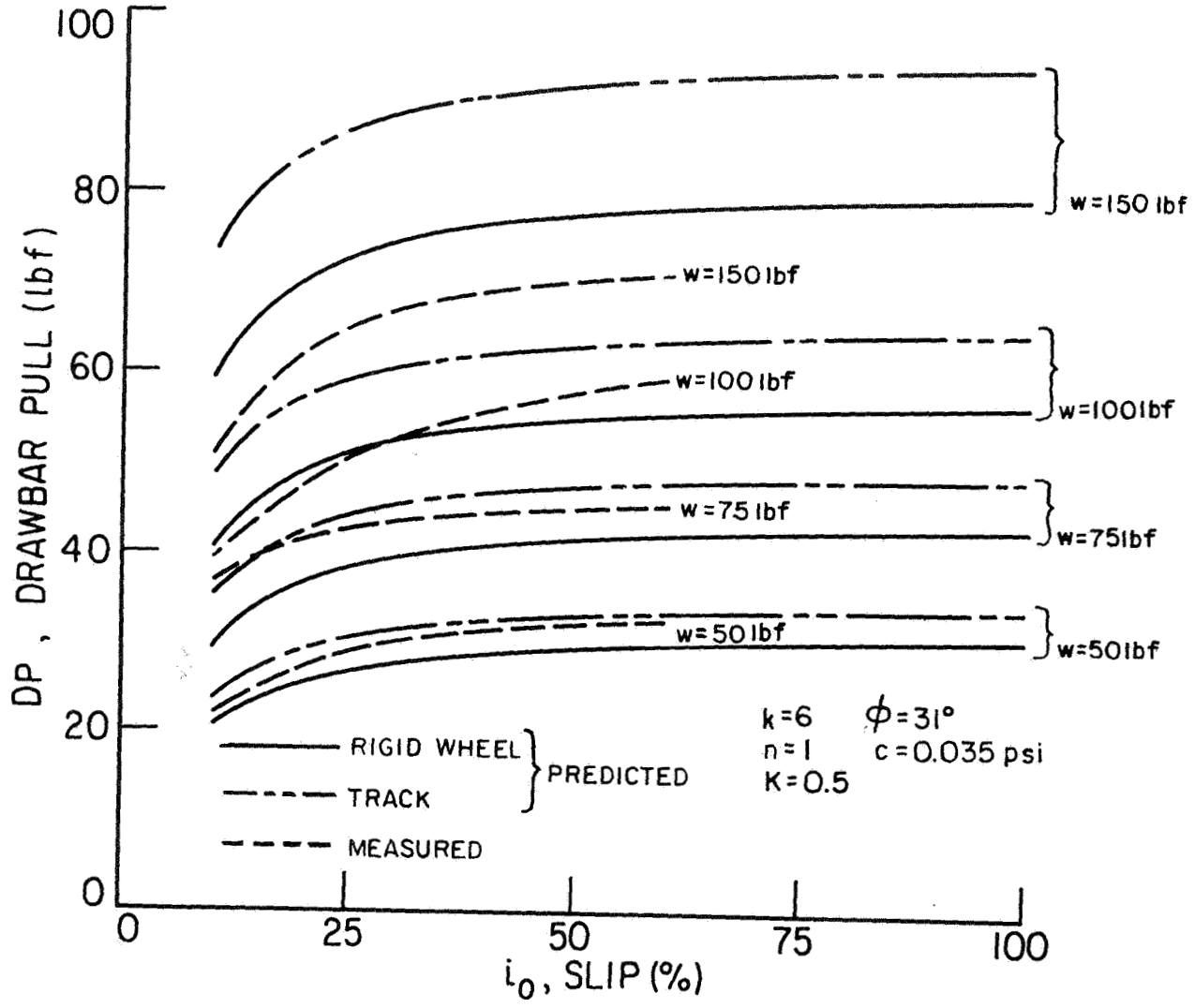

FIGURE 2-11 COMPARISON BETWEEN PREDICTED AND ACTUAL DRAWBAR PULL VS SLIP

of a given wheel to motion. One way of approaching this problem is to measure the motion resistance of the wheel on a hard flat surface at specified wheel loads. Values of the inherent wheel motion resistance were measured by AC Electronics using this method, and the appropriate corrections have been applied to the predicted values of motion resistance. The measured, predicted, and corrected predicted values of motion resistance are plotted in Figure 2-10.

As predicted in Section 2-II, the rigid wheel and track motion resistance assumptions do envelope the measured values of motion resistance. The measured values of motion resistance are small and the test wheels appear to behave more like a track than a rigid wheel. This is of course what one would expect considering that 1) the reported sinkage was on the order of 1 in., and 2) the contact length, ℓ, was on the order of 15 to 20 in.

C. Drawbar Pull

The predicted and measured values of drawbar pull are plotted in Figure 2-11. The predicted and measured values of drawbar pull correspond quite well for the wheel loads of 50 and 75 pounds force, but for the wheels loads of 100 and 150 pounds force the predicted values are increasingly greater than the measured values.

D. Conclusions from Comparison of Theory with Existing Test Results

The comparison of the predicted metal wheel performance indicators to those measured by AC Electronics results in the following conclusions.

1) For those wheels tested, the predicted and measured values of thrust compared quite well at the low wheel loads. However, the deviation between the predicted and measured values was considerable for the larger wheel loads.

2) The measured values of the motion resistance of the wheel were enveloped by the two assumptions, a) the wheel behaved as a rigid wheel, and b) the wheel behaved as a track. The wheels tested exhibited values of motion resistance which suggest that this type of wheel behaves more like a track than a rigid wheel.

3) Even though deviations between predicted and measured values of the performance parameters were evident, the general shape of the predicted and measured thrust, motion resistance, and drawbar pull plots were similar.

IV. PREDICTING THE PERFORMANCE OF A LRV DEFORMABLE WHEEL

The thrust, motion resistance, and drawbar pull trafficability equations [Equations(2-1) through(2-4)] of the soil value system cannot be used directly for predicting the performance of a deformable wheel such as might be used on a lunar roving vehicle (e.g., metal-elastic or wire wheel), because the wheel-soil contact configuration corresponds to neither a track nor a rigid wheel. The load-deformation characteristics of the wheel must be considered in order to predict contact configurations and stresses.

For any general configuration, the forces acting on a driven deformable wheel are shown in Figure 2-12a where:

D = undeformed wheel diameter

T = driving torque

w = wheel load

z = wheel or plate sinkage

θ = radial angle

τ = tangential wheel-soil interaction stress

σ = normal wheel-soil interaction stress

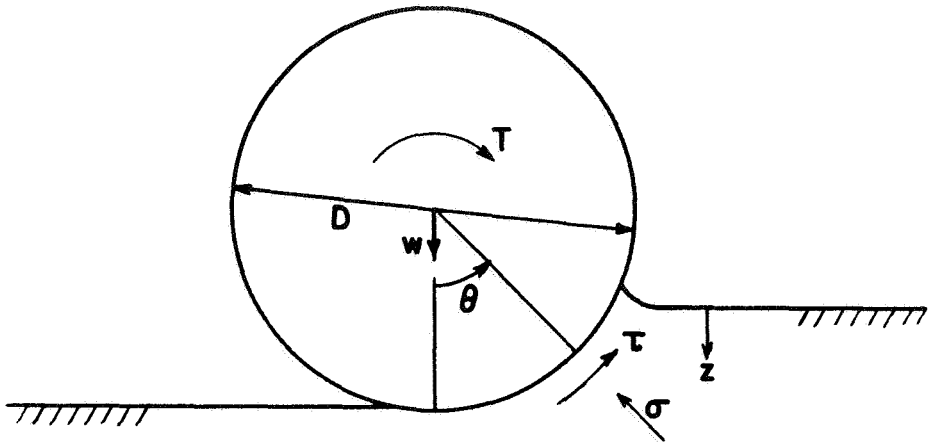

(a)

Forces acting on a driven deformable wheel

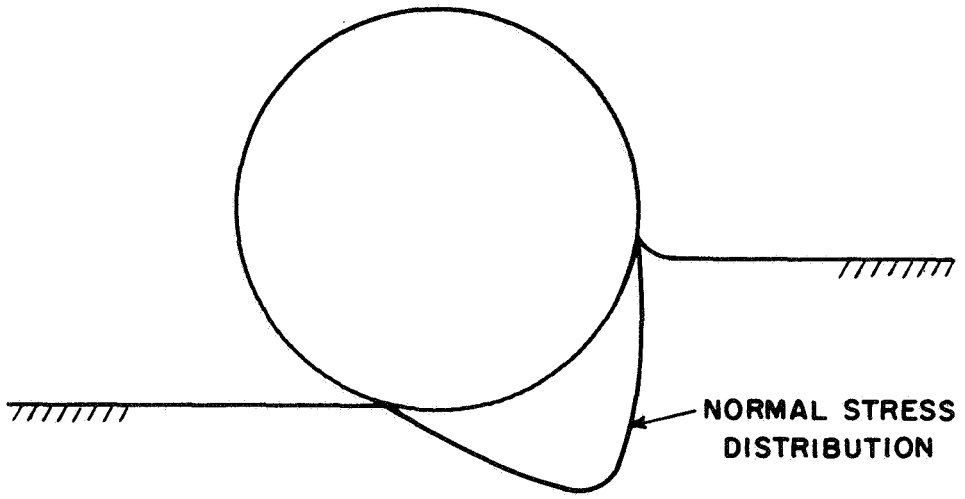

(b)

Normal stress distribution for a driven rigid wheel in sand (after Wong and Reece, 1967)

FIGURE 2-12

The two unknowns needed to predict the performance of the wheel are the normal and tangential wheel-soil interaction stress distributions. If these soil stresses can be related to appropriate soil parameters and the wheel-soil contact configuration, then the stress distributions can be evaluated for any assumed contact configuration. A correct solution will give (1) compatibility between the assumed stresses and deformations in the soil, (2) compatibility between the stresses and deformations in the wheel, and (3) compatibility between the soil and wheel deformations. A possible technique for predicting the performance of deformable wheels is outlined in detail below following a discussion of the normal and tangential soil stress distributions and the problem of determining the expected deformed configuration of a wheel.

The normal stress, σ, and tangential stress, τ, vary both perpendicular, to and in the plane of Figure 2-12a. For purposes of this discussion σ and τ are considered to be the average normal and tangential stresses acting on the wheel at any angle, θ. As with the Soil Value System the normal stress at any point along the contact surface might be considered to be equal to that pressure required to cause a plate of the same width as the wheel to sink to the same depth. Several equations have been proposed to describe the plate load-sinkage behavior of soils. Bekker (1960) derived as part of the original Soil Value System the following expression.

$$P = \left(\frac{k_1}{b} + k_2\, z^n\right) \tag{2-5}$$

where b = plate width

p = plate pressure

k_1, k_2, n = soil sinkage parameters

z = plate sinkage.

Contrary to common soil mechanics knowledge the above expression when applied to granular soils yields a load-sinkage relationship which is independent of the plate width, b, as $\frac{k_1}{b}$ is small compared to k_2. Wong and Reece (1967) presented the following expression as a result of plate load tests on sand.

$$p=\left(\frac{k_1}{b}+k_2\right)\left(\frac{z}{b}\right)^n \qquad (2\text{-}6)$$

Wong and Reece also recognized that the maximum normal stress for a wheel in sand does not occur at the point of maximum sinkage as Equations (2-5) and (2-6) would predict, since, in fact, the normal stress approaches zero at the point of maximum sinkage if rut recovery is negligible. These authors concluded that for a rigid wheel operating in sands under a condition of purely soil-soil slip the location of the maximum normal stress is a function only of the wheel slip. If the normal stress distribution for a deformable wheel in lunar soil is found to be significantly non-uniform, an experimental wheel test program will be required to predict the maximum normal stress location.

As a first approximation one could adopt a normal stress distribution similar to that measured by Wong and Reece for a driven rigid wheel in sand as shown in Figure 2-12b. However, the normal stress distribution will likely be more uniform for a deformable wheel operating in lunar soil than for a rigid wheel operating in sand because of the flexibility of the wheel and the cohesion exhibited by the lunar soil. Therefore, an experimental investigation of the normal stress distribution for a deformable wheel operating in soil similar to lunar soil will probably be required.

The tangential stress, τ, at any angle θ is primarily a function of the normal stress, the soil strength parameters, the soil deformation, and one or more soil stress strain parameters. Since soil deformation at all points along the wheel-soil contact is probably sufficient to cause plastic yield,* the magnitude of τ can be evaluated from the Mohr-Coulomb failure theory relating τ to the normal stress, σ, as follows.

$$\tau = c + \sigma \tan \phi \qquad (2\text{-}7)$$

where c = soil cohesion

ϕ = soil angle of internal friction.

The deformed configuration of a wheel might be estimated by using either an empirical equation such as that derived by Shuring and Howell (1967) or by employing the finite element method. Shuring and Howell's expression, Equation (2-8), considers only the normal wheel-soil interaction stress and probably will not be sufficiently general for direct application.

$$p(\theta) = \lambda_f \left|\frac{df}{d\theta}\right| + \lambda_L f \qquad (2\text{-}8)$$

where λ_f, λ_L = wheel deformation constants

f = radial penetration of contact surface

θ = radial angle.

The finite element method might be applied most readily to the metal elastic wheel, but it would be very difficult to adopt for the wire mesh wheel. For the metal elastic wheel, the nature of the connections and the effects of the three-dimensional geometry of the wheel would

*Such an assumption is probably very reasonable and in practice it will probably be satisfied for wheel slips greater than about 20%. Its use in the Bekker method would simplify Equation (2-1) to $H = (\ell bc + w \tan \phi)$.

have to be evaluated carefully. Developing an empirical equation for the load-deformation characteristics of a deformable wheel or the application of the finite element method would require considerable knowledge of the load-deformation behavior of the wheel.

Assuming that the relationship between the normal stress distribution, soil parameters, and wheel-soil contact configuration is known, the normal and tangential soil stresses could be evaluated for any assumed contact configuration. If these stresses are applied to an undeformed wheel, a predicted wheel-soil contact configuration could be obtained. If the assumed contact configuration agreed with the predicted contact configuration determined by applying these stresses to an undeformed wheel, one point on the standard wheel performance curves will have been determined. If not, the process would be repeated until the assumed and expected contact configurations agree. After a satisfactory contact configuration has been determined the corresponding wheel load, applied torque, wheel thrust, and wheel motion resistance, could be evaluated from appropriate graphical integrations of the calculated normal and tangential soil stresses. The process would then be repeated for several wheel loads in order to fully predict the performance of a given wheel.

Application of the technique described above would require detailed knowledge of both the stresses induced in the soil by the rotating deformable wheel and the load-deformation characteristics of the wheel. Acquisition of this knowledge may prove to be a difficult task, involving at least a considerable number of experimental wheel tests. It is recommended that future development of this technique, if it proves desirable, be performed by an organization possessing wheel test capabilities.

Unfortunately, it is not likely that a complete solution to the problem could be developed within the time limits established for design of a LRV. Thus, such an approach can best be considered a desirable long range goal. Meeting the short range objectives of LRV deformable wheel design and performance prediction will necessarily require the use of empirical approaches and possibly some aspects of the quasi-theoretical "Soil Value System" method.

V. VEHICLE MOBILITY ON SLOPES

Existing wheel-soil interaction approaches, both quasi-theoretical and empirical, have been developed for vehicles traversing level ground. To apply these approaches to vehicles on slopes, one must assume that the deformation patterns of both the wheel and the soil are similar to those for a vehicle on level ground. Although it is possible that this may be the case for small slope angles, it is well known that the stability of a loaded soil mass decreases with the inclination of the slope. There are several possible factors which may cause a vehicle operating on a slope to become immobilized.

If the soil mass is stable, the Soil Value System approach predicts that the maximum slope the vehicle could climb is given by:

$$\text{Maximum Slope } (\%) = \frac{DP}{W} \qquad (2\text{-}9)$$

where DP = drawbar pull on level ground

W = vehicle weight.

In other words, the vehicle will continue to climb slopes of increasing steepness until the thrust minus the motion resistance is equal to the component of the vehicle weight down the slope. The implicit assumption

in the above simple relationship is that expressions for motion resistance and thrust derived for vehicle operation on a flat surface are also valid for a vehicle operating on a slope.

A second factor which may cause immobilization on a slope is failure of the soil mass in a manner similar to that of a footing on a slope. The analysis of this problem becomes very complex when the stress distribution induced in the soil by a rotating wheel and the wheel flexibility are considered in addition to the slope angle, wheel dimensions, and soil strength properties.

A third factor which may cause immobilization on a slope is the phenomenon of "slip sinkage." That is, the wheel may form a rut sufficiently deep that forces resisting motion are greater than forces causing motion. Slip sinkage cannot be evaluated theoretically at the present time.

The amount of information available regarding immobilization factors, wheel deformation patterns, and induced soil stresses observed in wheel tests on slopes is small. In view of the complexity of the problem, particularly in relation to the stability of the soil mass and possible slip sinkage, we believe that a solution to the problem of LRV mobility on slopes can best be achieved through a test program such as that being conducted by the U. S. Army Engineer Waterways Experiment Station for the Marshall Space Flight Center.

VI. CONCLUSIONS

The following conclusions have been drawn from studies of lunar soil trafficability thus far.

A. If the Bekker Soil Value System equations can be shown to give a reasonable measure of the performance characteristics of a lunar roving vehicle, then analysis based on reasonable assumptions for wheel dimensions, wheel loads, and soil properties shows that:

1. Thrust increases with slip up to values of about 30%. Further increase in slip does not lead to significant increases in thrust, but may result in wasted propulsion energy.

2. The value of the soil sinkage constant, n, has relatively little effect on motion resistance.

3. The value of the soil sinkage constant, $k = \frac{k_1}{b} + k_2$, has little effect on motion resistance. Unfortunately, the form of the pressure-sinkage relationship developed on the basis of this parameter is not realistic.

4. Variations of soil cohesion and friction over ranges considered to be reasonable for lunar soils; i.e., $0.05 < c < 0.20$ psi and $33° < \phi < 41°$, may lead to variations in predicted thrust of up to $\pm 35\%$ from the values calculated for $c = 0.10$ psi and $\phi = 35°$. Thus, accurate knowledge of lunar strength will be important if precise predictions of performance, fuel consumption, etc.,are to be made.

5. According to the Soil Value System, the maximum slope that a vehicle can climb is given by the drawbar pull to weight ratio. On this basis, wheel loads should be minimized if slope climbing ability is to be maximized. Unfortunately, the

prediction of the slope climbing ability must also take into account slip sinkage and gross soil failure. Furthermore the suitability of the Soil Value System equations for thrust and motion resistance when applied to wheels on slopes has yet to be demonstrated. Thus, the question of vehicle slope climbing ability and stability of vehicles on slopes remain largely unanswered.

6. The Soil Value System predicts that performance parameters should improve with increasing wheel width and diameter and increasing wheel-soil contact length. Clearly, however, there are other factors which will limit the size and deformability of the wheels that are used.

B. In spite of the limitations of the Soil Value System method of analysis, a comparison between predicted behavior and that exhibited by the wire mesh and metal-elastic wheels tested by AC Electronics (1967) was reasonably good, particularly at low wheel loads. The metal wheels gave a performance intermediate between that to be expected for a rigid wheel and a track.

C. Proper solution of the lunar soil trafficability problem will depend ultimately on the solution of the basic wheel-soil interaction problem. An approach to this problem, which has been suggested herein, is based on consideration of the stresses and deformations in the soil and wheel and their mutual compatibility. Such a method will require the detailed knowledge of the soil and wheel load-deformation characteristics, and will probably require the use of iterative computational methods.

D. The stability of vehicles on slopes remains largely unknown.

VII. RECOMMENDATIONS

As a result of the trafficability studies conducted on this project, as well as the work done previously and reported by Mitchell et al. (1969), the following recommendations for continued work are made.

A. Although the analyses reported herein based on the Soil Value System of analysis give some indication of the possible behavior of vehicles on the lunar surface, they were intended mainly to develop a feel for the relative importance of soil conditions on wheel performance. More detailed information is needed concerning the actual influences of wheel load, wheel size, wheel slip, soil conditions, and slope inclination on performance. The experimental investigations now underway by the Mobility Research Branch of the U. S. Army Engineer Waterways Experiment Station should provide tentative answers to many of these questions. Determination of the soil constants to be employed in the Soil Value System method of analysis can not readily be performed during Apollo missions. On the other hand, simple tests such as the cone penetration test can be easily conducted. Thus, every effort must be made to determine whether the similitude method can be extended to lunar conditions and the treatment of special wheel types likely to be associated with lunar roving vehicles.

B. Solution of the wheel-soil interaction problem following a procedure such as that suggested in Section 2-IV will be difficult and will involve full scale tests of wheels under a variety of

conditions. Our group does not possess the experimental capabilities to conduct these tests, but such a program should be encouraged elsewhere. Our studies of lunar rolling boulders (Vol. II, Chapter 1) are relevant to this effort and the theoretical analyses to be made, as well as the test results obtained during the summer of 1969, should provide valuable information.

C. As much information as possible must be obtained during early Apollo missions concerning the stress-deformation and strength characteristics of lunar surface soils. It is recognized that most data will not be in a form suitable for direct substitution into trafficability equations; however, these data in conjunction with test results obtained on simulated lunar soil should make the derivation of reasonable values for use in such analysis possible.

D. It is considered that the efforts of our group can be best directed to the following trafficability-related studies for the coming year:

1. Continued review of trafficability studies being made by other organizations.
2. Evaluation of the strength and stress-deformation characteristics of actual and simulated lunar soils and their significance in evaluating lunar roving vehicle trafficability.
3. Studies of gravity effects on lunar soil behavior and on the slope climbing ability of lunar vehicles.
4. Lunar slope stability analyses.

5. Development and testing of a cone penetrometer for gathering lunar soil data applicable to trafficability analysis.
6. Evaluation of other devices proposed for acquisition of lunar soil data.
7. Theoretical and experimental study of the interaction between rolling spheres and soil and extension of the findings to the assessment of probable wheel-soil interaction mechanisms.

LIST OF SYMBOLS

b	- Plate, wheel, or track width
c	- Soil cohesion
D	- Wheel diameter
DP	- Wheel or track drawbar pull on level ground
H	- Wheel or track thrust
i_o	- Slip of wheel or track
K	- Soil stress-deformation parameter
k	- Soil composite sinkage parameter
k_1, k_2, n	- Soil sinkage parameters
ℓ	- Wheel or track contact length
p	- Plate pressure
R	- Wheel or track motion resistance
T	- Driving torque
W	- Vehicle weight
w	- Wheel or track load
z	- Wheel or plate sinkage
θ	- Radial angle
τ	- Tangential wheel-soil interaction stress
σ	- Normal wheel-soil interaction stress
ϕ	- Soil angle of internal friction

REFERENCES

1. AC Electronics - Defense Research Laboratories (1967), "Lunar Wheel and Drive Experiment Test Program," 2 vols., Contract NASB-20267, June 1967.

2. Bekker, M. G. (1960), "Off-the-Road Locomotion," University of Michigan Press, Ann Arbor.

3. Mitchell, J. K. et al. (1969) "Materials Studies Related to Lunar Surface Exploration," Final Report, Vol. III, Chapter 1, Trafficability, prepared for Marshall Space Flight Center, Huntsville, Alabama, under Contract NSR 05-003-189, March 1969.

4. Shuring, D. and M. Howell, Jr. (1967), "A Contour-Adapting Wheel Model," AC Electronics, General Motors Corporation.

5. Wong, J. Y. and A. R. Reece (1967), "Prediction of Rigid Wheel Performance Based on Analysis of Soil-Wheel Stress, Part 1, Driven Rigid Wheel," Journal of Terramechanics, v. 4, N. 1, 1967.

CHAPTER 3

FOAMED PLASTIC CHEMICAL SYSTEMS FOR LUNAR SOIL STABILIZATION APPLICATIONS

(T. S. Vinson and J. K. Mitchell)

I. INTRODUCTION

It is now generally accepted that a fragmental surface layer exists on the moon that overlies blocky or coherent rock material. The depth of unconsolidated material appears to range from nearly zero to tens of meters. Improvement of the engineering properties of this layer as well as fractured rock zones, i.e. stabilization, may be desirable if not necessary in connection with exploration and future construction on the moon. Potential applications of suitable soil and rock stabilization techniques include the following:

1. Sealing of fissures and voids in otherwise intact soil and rock masses to enable utilization of lunar cavities as shelters, storage chambers, waste disposal chambers, etc.
2. Mixing of stabilizing agents with lunar soil or fragmental lunar rock for utilization as a construction material in insulation, shielding or launching facilities.
3. Protection and preservation of the structure of lunar surface material samples for earth-return.

Relative to lunar payload limitations, it is desirable to stabilize a large volume of soil per unit weight of stabilizing agent transported to the moon. Existing terrestrial chemical stabilizers do not change volume significantly when injected into a soil, and, therefore they give a relatively low ratio of stabilized soil volume to initial weight of

stabilizer. A more desirable material might be one that will expand when injected into a soil, thus stabilizing a greater amount of soil per unit weight of stabilizer transported; provided, of course, that the desired improvement of the engineering characteristics of the soil mass can be obtained.

Apart from the consideration of earth-to-moon transport of a stabilizer, desirable features of the stabilizer include (1) low viscosity prior to set so that relatively fine-grained materials can be treated, (2) control over setting times, (3) simple application, (4) ease in handling, (5) durability, (6) applicability over a wide range of temperature conditions and in vacuo, and (7) relative absence of toxicity or other hazards.

In view of these constraints attention has been directed at the potential applicability of foamed plastics. Foamed plastics are resinous materials, expanded or blown to form a cellular structure. The final volume can be as great as 50 times the volume before expansion. Expansion may be by chemical, physical, or mechanical methods. Basic plastic formulations can be varied to give almost any degree of flexibility, and any density from 0.5 lb/ft^3 to 70 lb/ft^3 in some materials. The foam structure can range from 95% closed cells to completely open cells (Gersten, 1965).

The use of foams for the solution of engineering problems has been extensive in recent years. They have been used on earth for the storage of hydrocarbon fluid in natural subterranean storage reservoirs (O'Brien, 1968). A glass-like foam, similar to plastic foams, produced by subjecting a hydrous solution of sodium or potassium silicate to either heat or vacuum, is being considered as material for the construction of

lunar shelters (Corp, 1967). There appears to have been little or no research on the use of foamed plastic as a means for stabilizing terrestrial soil, much less lunar soil. Our investigations to date, however, would suggest that the potential is very great.

There are five types of foamed plastics: expanded polystyrene, urethane, epoxy, silicon, and phenolic (Gersten, 1965). The requirements of impermeabilization and high strength, as well as the physical and environmental constraints in lunar application may best be satisfied through the use of urethane and epoxy foams. Urethane is a logical first choice between these two foamed plastics because of its greater versatility.

Urethanes are produced by the combination of a polyisocyanate with reactants which have at least some hydroxyl groups, e.g. polyols. Urethanes expand upon mixing to form a cellular structure and have an excellent strength-to-weight ratio, extremely low thermal conductivity, and significant compressive, shear, tensile, and flexural strengths. They also have a high dielectric strength, resistance to flame (with additives), very low water vapor transmission and water absorption, good vibration resistance, and resistance to oxygen, most solvents, and dilute acids. They are inert and non-abrasive materials that will not affect any substrate or metal with which they come in contact (Reference 7).

Both polyols and polyisocyanates are in liquid form. Foaming does not occur immediately after they are mixed, but can be delayed a predetermined amount of time by proper manipulation of the different components that make up the polyol and polyisocyanate solutions. The viscosity of the liquid before it foams can approach that of water. It is therefore possible that urethane foam plastic could be used to stabilize lunar soils of rather low permeability.

In a preliminary laboratory investigation it was determined that urethane plastic can be made to foam and set up within the pores of a uniform coarse sand, and that a greater volume of soil may be treated per unit weight of stabilizer than can be treated using more conventional chemical stabilization systems, e.g. AM-9 chemical group (Karol, 1957). The results of these preliminary tests were sufficiently encouraging that a detailed research program was planned and executed. This program has involved:

1) Study of the organic chemistry of urethane foamed plastic.
2) Development of urethane foamed plastic systems with (1) an initial low viscosity, (2) a controllable gel time, and (3) a high ratio of stabilized volume to weight of injected chemical.
3) Evaluation of the strength, permeability, and other pertinent mechanical properties of soils stabilized using foamed plastics.
4) Investigation of lunar environmental factors, primarily lack of an atmosphere and extreme temperature conditions, on the foaming process.
5) Formulation of conclusions and recommendations for the work completed so far.

Each of these phases is discussed in the following sections.

II. ORGANIC CHEMISTRY OF URETHANE FOAMED PLASTICS

Urethanes are produced by the reaction of polyhydroxy compounds with polyisocyanates. The general reaction is:

$$R - NCO + R' - OH \rightarrow R\left(\begin{matrix} H & O \\ | & || \\ N & - C \end{matrix}\right)OR' + \text{heat} \qquad (3\text{-}1)$$

where,

R - NCO = a polyisocyanate such as toluene diisocyanate

R = tolyl radical

R´ - OH = any polyhydroxyl compound (e.g. polyol, glycol, polyester, or polyether)

R´ = a non-reactive hydrocarbon radical

$\begin{pmatrix} H & O \\ | & || \\ N & - C \end{pmatrix}$ = the urethane linkage

The above reaction involves mono-functional reactants, however, if polyfunctional chemicals are used polymers result. Functionality refers to the number of reactive sites per molecule. For example, toluene diisocyanate (TDI) may be represented as NCO - R - NCO. Since there are two NCO groups per molecule, TDI is said to be di-functional. If a tri-functional polyol is used with a diisocyanate then a cross-linked structure results. This may be represented diagrametrically as follows:

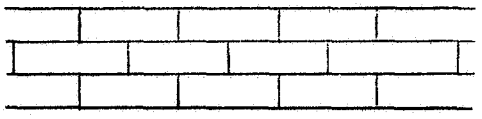

Quadrifunctional and 6-functional polyols are also available.

Catalysts, surfactants, and blowing agents may be incorporated in the reaction expressed by equation (3-1). Commonly used catalysts are tertiary amines and tin salts. They are added to control or accelerate the rate of reaction so that gelation will be synchronized with maximum rise of the foam. Surfactants control cell surface tension and thus can render the foam large-celled or fine-celled. Polyglycol-silicone polymers represent a general class of compounds that can be used as surfactants.

Blowing agents expand to form a gas in the polymer structure hence they are the agent responsible for the foam-like structure. Two classes of chemical blowing agents are possible. In the first the gas is produced by a chemical reaction within the polymer. In the second a chemical blowing agent decomposes in the presence of the exothermic heat of the reaction to produce the gas. Water and carboxylic acids would be in the former class of compounds. The gas produced in this instance is CO_2. Low boiling acetates or fluorocarbons would be in the latter class of compounds.

The flexibility or rigidity of urethane foamed plastic is controlled by the functionality and molecular weight of the polyol and isocyanate used. Rigid foams result when low molecular weight highly functional polyols are used. Conversely, flexible foams result when high molecular weight low functional polyols are used. Variations between these two extremes for specific applications are possible.

Ideally, the urethane linkage would be the only one found in the polymeric structure. This is not the usual case. There are several other important linkages that may be present. One of the most common subordinate linkages occurs when water is present. The general reaction is:

$$R - NCO + HOH \rightarrow R - \overset{H}{\underset{|}{N}} - H + CO_2\uparrow \qquad (3\text{-}2)$$

This reacts with another isocyanate as follows

$$R - NH_2 + R - NCO \rightarrow R - \overset{H}{\underset{|}{N}} - \overset{O}{\overset{||}{C}} - \overset{H}{\underset{|}{N}} - R \qquad (3\text{-}3)$$

where,

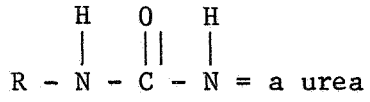

Another important subordinate reaction can occur when carboxylic groups are present. These groups may occur in the polyester polyols or may be added to the system. They react with diisocyonate as follows:

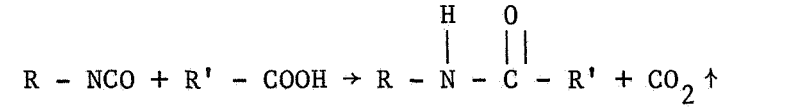

(3-4)

Further, a cross-linking reaction will occur when the hydrogen on the nitrogen atom of the urethane group reacts with an isocyanate group. This is known as the allophanate linkage and may be represented as follows:

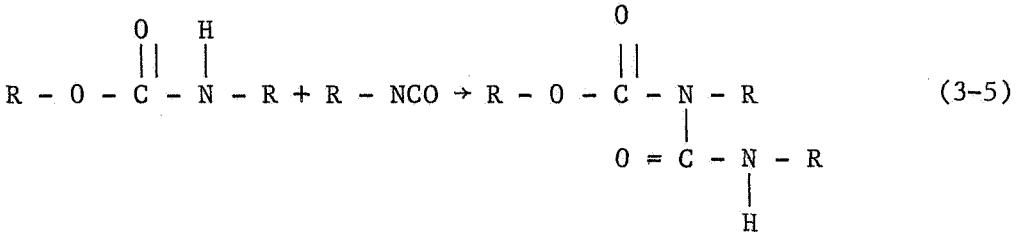

(3-5)

Pre-polymerization techniques enable the chemical system designer to direct the order of buildup in the polymeric structure and to reduce the heat of reaction. Pre-polymerization involves the mixing of a measured amount of polyol with an excess amount of polyisocyonate. Usually the resultant "pre-polymer" is in the ratio 5 equivalents of polyisocyanate to 1 equivalent of polyol.

The preceding paragraph summarizes the chemistry of urethane foamed plastics as it applies in this research program. More detailed treatments are presented by Dombrow (1963), Ferrigno (1963), and Phillips (1964).

III. DEVELOPMENT OF URETHANE FOAMED PLASTIC SYSTEMS

A. Analytical Laboratory Procedure

It was necessary first to determine what proportions of chemicals should be used for given polyol and polyisocyanate types. This was accomplished by developing a conceptual framework for the resultant urethane molecule. For example, suppose it is desired to form a urethane molecule with cross-linking in the polymer structure. A framework for such a system may be seen in Figure 3-1a. Figure 3-1b shows the unit cell for the framework. It is now a simple matter to count the number of molecules of the respective chemical types in the unit cell and then to multiply the number by the molecular weight of the actual chemical used to find the amount of a chemical necessary, in terms of gram molecular weights, to form the desired urethane molecule. For the unit cell of the urethane molecule in Fig. 3-1b there are 2-1/2 polyisocyanate groups, 1 difunctional polyol group, and 1 trifunctional polyol group. While the conceptual framework of the urethane molecule is an idealization of the actual urethane molecules formed in a given system, it is the most representative molecule for the system that can be visualized.

By simple proportions the amount of any chemical in a mix can be determined if the weight of any other component in the mix is known. Alternatively, the percentage by weight of the total molecule can be determined for each component. The latter approach has been followed in this research program. When chemicals were employed that were not a part of the original urethane molecule, their percentages are reported as a percentage (by weight) of the total weight of the chemicals making up the original urethane molecule. Chemicals such as the blowing agents

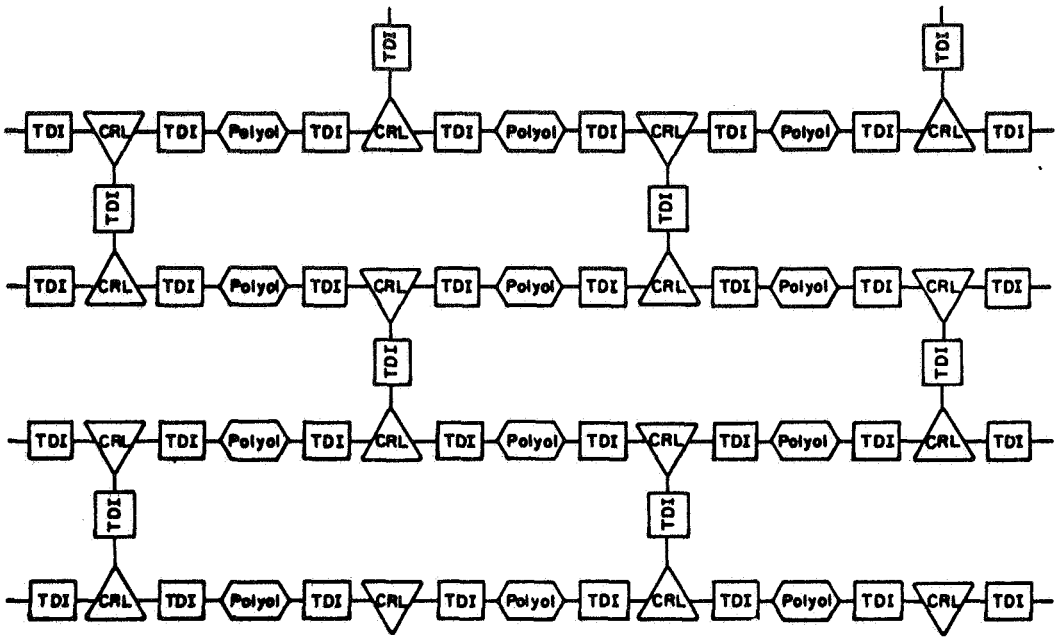

(a) TWO-DIMENSIONAL FRAMEWORK

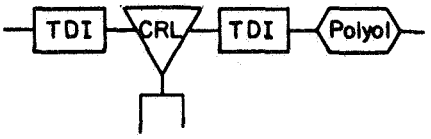

WHERE:

TDI = POLYISOCYANATE, SPECIFICALLY TOLYLENE DIISOCYANATE

Polyol = ANY DIFUNCTIONAL POLYOL (FUNCTIONALITY REFERS TO THE NUMBER OF REACTIVE SITES PER MOLECULE)

CRL = ANY TRIFUNCTIONAL POLYOL

(b) UNIT CELL

FIGURE 3-1 CONCEPTUAL FRAMEWORK FOR A CROSS-LINKED URETHANE POLYMER

surfactants, co-solvents, and most catalysts fall into this category.

Many different chemical systems were evaluated while trying to determine those which had an initial low viscosity, a controllable gel time, and a high ratio of stabilized volume to weight of injected chemical. Table 3-1 presents a listing of the chemicals used in these systems. Toluene diisocyanate (TDI) was common to every chemical system. It constituted from 30.3% to 70% of the total composition for the chemical systems tried. The polyols constituted from 30% to 69.7% of the total composition, depending on the given chemical system. Blowing agents and co-solvents were used in proportions up to 10% of the total weight of polyols + TDI.

Generally, the blowing agent and catalyst were premixed with the polyol, and the surfactant was premixed with the TDI. The original viscosity of the polyol or TDI did not change appreciably with addition of catalyst and surfactant. The initial viscosity of the polyol can be changed appreciably depending on the percentage of co-solvent or blowing agent added, however. For amounts of co-solvent and blowing agent greater than approximately 5% the viscosity was noticeably decreased.

It should be noted that a laboratory analysis indicated that 0.15 equivalents of carboxylic acid (COOH groups) were present per mole of triethylene glycol used in some of the experiments reported herein, specifically experiments 34, 35, 37, and 39. This implies some oxidation had taken place in this polyol. For the other experiments involving triethylene glycol a different sample was used which had not oxidized.

TABLE 3-1

CHEMICALS USED IN URETHANE SYSTEMS

Chemical	Molecular Weight	Boiling Point, °C (atmospheric pressure)
Polyisocyanate:		
toluene diisocyanate (TDI)	174.0	118-120
Polyols:		
castor oil #1	664.0	
1,3-propanediol	76.09	97-98
1,5-pentanediol	104.00	239
diethylene glycol	106.12	244.5
triethylene glycol	150.0	165-167
polyethylene glycol	≃400.0	
2-ethyl-2-(hydroxymethyl)-1,3-propanediol (TMP)	134.18	melting point 58-60
triethanolamine	149.19	278
Co-solvents:		
normal butanol	74.12	117.71
methyl cellosolve	76.09	124.3
Blowing agents:		
adipic acid	146.14	melting point 151-153
methyl ethyl ketone (MEK)	72.10	79.6
butyl acetate	116.	124-126
methyl butyl ketone		127
diacetone alcohol	116.	164-166
cellosolve acetate	132.	156.2
water	18.0	100.0
Catalysts:		
4-methylmorpholine	101.15	112-115
Surfactants:		
Union Carbide L-530	-	-
Union Carbide L-531	-	-

B. Experimental Laboratory Procedure

It was necessary to have a standard procedure for conducting laboratory tests so that results could be compared in order to determine the best chemical system. The mixing time (time from start of mixing of a chemical system to association*) and reaction time (time from onset of association to visible reaction) are greatly influenced by the efficiency of the mixer, the temperature of the components and the mixing container, and the size of the batch being processed. In this regard tests were conducted using a constant speed mixer, the same size glass container, and, generally, the same total weight of polyol plus TDI (20 grams total weight). Tests were conducted under a chemical hood since several of the components in the system are somewhat toxic.

C. Mixing and Reaction Times

Mixing and reaction times were determined using a stopwatch. Typically, a measured amount of TDI was poured into a glass jar containing the polyol. The combined system was then placed on a mixer and the stopwatch started. As soon as the chemicals associated the time was noted (mixing time). At the onset of "bubbling" or extreme heat the time was again noted (reaction time). The reaction time indicates the time that would be available to inject a chemical system into a soil mass. The results of these tests are presented in Table 3-2. All of these systems were developed by the "conceptual framework" approach previously explained.

One of the most significant findings illustrated by the data is that adding water to a given system decreases the reaction time. The decrease is in proportion to the amount of water added. It does not change the mixing time. Adding adipic acid also decreases the reaction time. The effect of adipic acid on the mixing time is uncertain. Adding the

*"Association" may be thought of as a chemical state in which the polyol and TDI molecules in a given system have come into alignment. That is to say, OH groups on the polyol molecules are in close proximity to the NCO groups on the TDI molecules. They have not at this time reacted in the sense of forming a polymeric structure, but there is a distinct formation of a homogeneous solution.

TABLE 3-2

MIXING AND REACTION TIMES FOR CHEMICAL SYSTEMS

Trial	Chemical System	Percent by Weight	Mixing Time (Sec.)	Reaction Time (Sec.)	Comments
34A	TDI	53.7			Strong, rigid, some foam due to vaporization of TDI
	Triethylene glycol	46.3	1'0"	1'30"	
34G	as 34A + water	1.0	1'0"	30"	strong, rigid, large celled - too much blowing agent
38A	as 34A + water	0.1	1'20"	50"	rigid but weak, uniform cell size, but unfoamed plastic at bottom
	L-531	0.5			
38B	as 34A + water	0.3	1'4"	40"	rigid but weak, uniform cell size but unfoamed plastic at bottom
	L-531	0.5			
34H	as 34A + water	1.0	1'0"	10"	rigid but weak uniform cell size but unfoamed plastic at bottom
	L-531	0.5			
38C	as 34A + water	0.2	1'25"	40"	rigid but weak, uniform cell size but unfoamed at bottom
	L-531	0.5			
	diacetone alcohol	0.4			
34T	as 34A + methyl butyl ketone	2.0	1'20"	1'15"	strong rigid, large celled - too much blowing agent
34J	as 34A + methyl butyl ketone	4.0	1'20"	1'30"	strong rigid, large celled - too much blowing agent unfoamed at bottom
	L-531	0.5			
35L	as 34A + methyl butyl ketone	4.0	1'20"	1'10"	strong, rigid, large celled - too much blowing agent, unfoamed at bottom
	L-531	1.0			
35U	as 34A + methyl ethyl ketone	0.5	1'20"	1'17"	rigid foam, uniform cell size, but unfoamed plastic at bottom
	L-531	0.5			
34K	as 34A + methyl ethyl ketone	0.5 4.0	1'15"	1'25"	strong rigid large celled - too much blowing agent

TABLE 3-2 (Con't.)

Trial	Chemical System	Percent by Weight	Mixing Time (Sec.)	Reaction Time (Sec.)	Comments
37L	as 34A + methyl butyl ketone diacetone alcohol L-531 4-methylmorpholine	0.5 0.5 0.5 0.2	37"	-	injected into soil
37M	as 37L		33"	-	40g, injected into soil
37N	as 37L		35"	-	40g, injected into soil
37P	as 37L		43"	-	40g, injected into soil
35V	as 34A+methyl butyl ketone diacetone alcohol L-531 4-methylmorpholine	0.5 0.5 0.5 0.2	28"	18"	strong, rigid, very good foam structure*
34B	TDI diethylene glycol	62.2 37.8	1'0" 1'20"	1'06" 1'10"	strong rigid plastic no blowing agent
36B	as 34B water L-531	0.1 0.5	1'55"	35"	no foam, strong and rigid, not enough blowing agent
36C	as 34B water L-531	0.2 0.5	1'55"	30"	rigid but very weak, foam cell size too large
36A	as 34B water L-531	1.0 0.5	1'20"	20"	rigid but very weak, friable foam, unfoamed at bottom
39A	TDI Triethylene glycol TMP	60.5 20.9 18.6	5'10"	33"	strong, rigid, some TDI vaporized
39D	as 39A + L-531 water	0.4 0.1	5'20"	26"	strong, rigid, but non-uniform cell size
39B	as 39A + water	0.2	5'17"	36"	strong rigid, large celled - too much blowing agent
39C	as 39A + L-531 water	0.4 0.3	4'20"	22"	strong, rigid, but non-uniform cell size

*See Footnote at end of table.

TABLE 3-2 (Con't.)

Trial	Chemical System	Percent by Weight	Mixing Time (Sec.)	Reaction Time (Sec.)	Comments
35P	as 34A + methyl ethyl ketone L-531 4-methylmorpholine	4.0 1.0 .25	21"	28"	strong, rigid, large celled - too much blowing agent
35N	as 34A + methyl butyl ketone L-531 4-methylmorpholine	4.0 1.0 0.5	10"	10"	strong, rigid, large celled - too much blowing agent
35S	as 34A + diacetone alcohol L-531	0.5 0.5	1'20"	1'10"	strong rigid foam untreated at bottom
35T	as 34A + methyl butyl ketone diacetone alcohol L-531	0.5 0.5 0.5	1'20"	1'20"	rigid foam, fairly uniform cell size, some plastic in bottom left unfoamed
37A	as 35T		1'20"	-	poured sand into jar with associated system
37H	as 35T		1'12"	-	injected into soil
37R	as 35T		1'13"	-	injected into soil
35W	as 34A + methyl butyl ketone diacetone alcohol L-531 4-methylmorpholine	0.5 0.5 0.5 0.1	45'	39"	strong rigid, uniform cell size, very good foam
37B	as 35W		48"	-	poured sand into jar with associated system
37C	as 35W		49"	-	injected into soil
37D	as 35W		53"	-	injected into soil
37E	as 35W		55"	-	injected into soil
37F	as 35W		57"	-	injected into soil
37G	as 35W		51"	-	injected into soil
37J	as 35W		52"	-	injected into soil

TABLE 3-2 (Con't.)

Trial	Chemical System	Percent by Weight	Mixing Time (Sec.)	Reaction Time (Sec.)	Comments
37K	as 35W		51"	-	injected into soil
37Q	as 35W		46"	-	injected into soil
34A1	TDI triethylene glycol	53.7 46.3	1'30" 1'15"	2'00" 2'10"	strong, but weak and friable, polyol oxidized
42A	TDI triethylene glycol water L-531	53.7 46.3 1.0 0.5	56"	30"	good foam* but too much blowing agent; react to bottom
42B	as 42A, but with water	0.5	1'22"	45"	good foam, bubbles too large, unfoamed at bottom
42K	as 42B		1'18"	48"	as 42B
42I	as 42A, but with water	0.3	1'20"	1'00"	good foam, unfoamed at bottom
42D	as 42A, but with water	0.2	1'18"	1'30"	poor foam*
42E	TDI triethylene glycol diacetone alcohol L-531	53.7 46.3 1.0 0.5	1'30"	2'30"	poor foam
42F	as 42E, but with diacetone alcohol	5.0	56"	1'35"	looks good, perhaps too much blowing, unfoamed at bottom
42M	as 42E + catalyst	0.2	22"	38"	not enough blowing agent, unfoamed at bottom
42N	as 42A, but with water catalyst	0.4 0.1	54"	28"	weak and friable, unfoamed at bottom
42P	TDI triethylene glycol water catalyst L-531	53.7 46.3 0.4 0.1 1.0	52"	31"	as 42N

TABLE 3-2 (Con't.)

Trial	Chemical System	Percent by Weight	Mixing Time (Sec.)	Reaction Time (Sec.)	Comments
42Q	as 42A, but with water diacetone alcohol MIBK	0.3 0.5 0.5	1'23"	1'19"	uniform, but large bubbles, unfoamed at bottom
42R	as 42Q, but with water	0.4	1'19"	1'01"	weak and friable, uniform foam w/medium bubbles
42S	as 42Q + catalyst	0.1	50"	38"	as 42R
43D	TDI triethylene glycol polyethylene glycol adipic acid L-531	53.7 46.3 1.5 3.0 0.5	1'30"	53"	very good foam, small bubbles, uniform, strong, not friable
43E	as 43D, but with adipic acid	2.0			good foam but not as well reacted as 43D
43F	as 43D, but with no polyethylene glycol		1'25"	45"	good foam, strong rigid, unfoamed at bottom
42H	as 43D, but with polyethylene glycol	0.5	1'25"	42"	as 43F
43G	as 43D, but with polyethylene glycol	3.0	1'21"	49"	as 43F
43I	as 43D, but with diacetone alcohol	0.5	1'30"	47"	as 43F
43J	TDI triethylene glycol polyethylene glycol adipic acid diacetone alcohol L-531 castor oil	53.7 46.3 1.5 3.0 0.5 0.5 5.0	1'07"	50"	strong, rigid good foam but perhaps a little too much blowing agent
43K	as 43J, but with L-531	1.0	1'06" 1'02" 1'02" 1'02"	48" 53" 55" 59"	very good foam, small, uniform, slightly unfoamed at bottom

TABLE 3-2 (Con't.)

Trial	Chemical System	Percent by Weight	Mixing Time (Sec.)	Reaction Time (Sec.)	Comments
43L	as 43K, but with diacetone alcohol	1.0	1'00"	55"	mixer speed faster than in 43J and 43K
43M	as 43J, but no diacetone alcohol		1'02"	55"	
43Q	as 43K, but with diacetone alcohol	3.0	51" 51"	1'10" 1'10"	as 43K, but perhaps too much blowing
46A	TDI triethylene glycol 1,5 pentanediol	57.8 24.9 17.3	1'19"	45"	unblown, strong, rigid - only some TDI vaporized
46B	as 46A, + L-531	 1.0	1'17" 1'13"	45" 42"	as 46A, but some small bubbles at surface
46C	as 46B + adipic acid	1.0	1'44"	26"	strong, rigid, small uniform, not enough blowing
46D	as 46B + adipic acid	2.0	1'24"	19"	as 46C
46E	as 46B + adipic acid	3.0	1'37"	11"	excellent foam but too fast
46F	as 46D, + polyethylene glycol	5.0	1'24"	22"	as 46C
46H	as 46B, + polyethylene glycol	2.0	1'29"	46"	as 46B
46G	as 46B, + polyethylene glycol	5.0	1'30"	54"	as 46B
46I	as 46B, + polyethylene glycol	10.0	1'08"	1'03"	as 46B
46J	as 46B, + polyethylene glycol	15.0	1'02"	1'15"	as 46B
46K	as 46B, + castor oil	2.0	1'16"	45"	as 46B
46L	as 46B, + castor oil	5.0	1'01"	52"	as 46B

TABLE 3-2 (Con't.)

Trial	Chemical System	Percent by Weight	Mixing Time (Sec.)	Reaction Time (Sec.)	Comments
46M	as 46B, + castor oil	10.0	1'00"	1'07"	as 46B
46N	TDI triethylene glycol 1,5 pentonediol castor oil adipic acid L-531	57.8 24.9 17.3 10.0 2.0 1.0	 55" 1'03" 1'02"	 24" 26" 27"	good foam, strong rigid, small bubbles, uniform, slightly unfoamed at bottom
46P	as 46N, but with adipic acid	1.0	58"	41"	poor foam
46DD	as 46N, but no adipic acid		45"	55"	poor foam
46R	as 46N, + diacetone alcohol	0.5	59"	1'16"	very poor foam
46Q	as 46N, + diacetone alcohol	1.0	58"	1'11"	very poor foam
46BB	as 46P, + diacetone alcohol	3.0	52"	40"	strong, rigid, too much blowing
46X	as 46N, + diacetone alcohol	4.0	46"	1'35"	poor foam
46CC	as 46P, + diacetone alcohol	4.0	47"	40"	as 46BB
46FF	as 46N, but with adipic acid	0.5	50" 54"	52" 51"	strong, rigid, too much blowing
46GG	as 46FF, but with adipic acid	0.3	52"	55"	strong, rigid, good foam
46HH	as 46N, but with adipic acid diacetone alcohol	 0.3 4.0	56"	56"	as 46BB but too much blowing
46II	as 46HH, but L-531	1.5	50"	54"	as 46HH, slightly smaller foam bubbles

TABLE 3-2 (Con't.)

Trial	Chemical System	Percent by Weight	Mixing Time (Sec.)	Reaction Time (Sec.)	Comments
46JJ	as 46HH, but L-531 adipic acid diacetone alcohol	 1.5 0.4 3.0	56"	52"	as 46HH
46KK	as 46JJ, but castor oil	15.0	49"	1'02"	strong, rigid, but large celled
46LL	as 46JJ, but castor oil adipic acid	 15.0 0.5	51"	55"	as 46KK
46MM	as 46JJ, but adipic acid diacetone alcohol	 0.5 3.5	51"	52"	as 46HH
46NN	as 46JJ but with adipic acid	1.0	49"	37"	too much blowing
46PP	as 46JJ, but with adipic acid	0.8	52"	45"	large celled, too much blowing
46QQ	as 46JJ, but with adipic acid diacetone alcohol	 0.8 2.0	51"	44"	good foam, strong, rigid, small celled, uniform

*The terms "very good foam," "good foam," "poor foam," "very poor foam," refer to a visual qualitative assessment of the suitability of the foam for lunar soil stabilization. If a foam is rigid, not friable, completely "blown," and of uniform cell size (approximately 1 mm in diameter in the mixing jar) it would be termed a "very good foam."

catalyst 4-methylmorpholine decreases both the mixing and reaction time. A system employing 0.5% catalyst is unworkable due to the extremely short mixing and reaction times. Adding either polyethylene glycol or castor oil decreases the mixing time and increases the reaction time. The surfactant, L-531, has no effect on the mixing or reaction time.

Systems other than those reported in Table 3-2 were tried. A 62.6% TDI, 37.4%, 1,5-pentanediol system associated after approximately 2 minutes mixing but reacted 15 seconds later, which is probably too fast for practical application. The 67.1% TDI, 32.9% 1,3-propanediol system never associated. The system would react, but when it did it produced an extremely weak, friable foam. It is now believed that the 1,3-propanediol may have been of a poor quality. Additional chemical systems with an uncontaminated sample of this polyol may be investigated subsequently.

The basic systems listed in Table 3-2 (34A, 34B, 39A, 43Q, 46PP) all have controllable mixing and reaction times and low initial viscosities. The decision as to which system would initially be injected into a laboratory soil mass was made on a qualitative basis. If the foam in a test jar could be made strong, not friable, uniform in cell size, small celled, and completely "blown" then it was felt it would have the greatest potential in actual lunar soil stabilization application. Pursuant to these criteria systems 34A, 39A, 43Q and 46PP were selected.

D. Viscosity Determination and Results

Viscosities of the separate chemical components and a mixture possibly suitable for stabilization were determined using a Stormer Viscosimeter. In this apparatus viscosities are measured by rotating a cylinder immersed in the sample. Table 3-3 presents the average viscosity

TABLE 3-3

VISCOSITY RESULTS

Chemical	Average Viscosity centipoise
TDI	5.8
Triethylene glycol	44.3
Diethylene glycol	28.3
1,5 pentanediol	87.8
46.3% triethylene glycol + 53.7% TDI	13.0
Water (at 20°C)	1.0

determined from six trials. As can be seen the viscosities of the components are rather high compared with water; however, they are still within a range that may be useful for injection of some soil types. The viscosity after association for a TDI, triethylene glycol system is also shown in the table. This is an average viscosity of only two runs, since it was found that rotating the cylinder in this sample decreased its reaction time to the extent that only two runs could be made. It is of interest that the viscosity of the system is intermediate between the viscosities of the two components but is substantially lower than that which would be calculated on a weighted proportion basis.

Time-viscosity relationships for times after association of various polyol, TDI systems would have been extremely hard to obtain due to the change in viscosity of the system, after association, with mixing, since only rotational type viscometers, which mix the system, were available for the research program.

E. Ratio of Stabilized Volume to Weight of Injected Chemicals

Table 3-4 presents data on ratios of stabilized volume to weight of chemical injected into soil masses in the laboratory. Also given is the void ratio (ratio of the volume of the voids of the soil mass to the volume of the solids), description of the soil, and the density of the foam in the voids. Typically the size of the foam bubbles produced in a glass jar for a given chemical system are considerably larger than the foam bubbles produced in a soil mass. The foam density is a useful parameter for comparing a polyurethane chemical system with a typical terrestrial chemical impregnation system for the same soil conditions.

TABLE 3-4

STABILIZED SOIL MASS DATA

Urethane Systems (refer to Table 3 for Formulations)	Soil Description	Soil Void Ratio, e	Mold Type	Foam Density gm/cm^3	Ratio: Volume of Stabilized Mass to Weight of Injected Grout cm^3/gm
11A	Coarse Monterey sand	.67	CBR	.224	11.1
11B	"	.65	CBR	.259	9.8
11C	"	.67	CBR	.229	10.9
12A	#20 Monterey sand	.61	CBR	.336	7.9
25A	Coarse Monterey sand	.66	CBR	.194	12.9
25E	#20 Monterey sand	.57	CBR	.257	10.7
27A	"	.60	CBR	.195	13.7
27B	Fine antioch sand	.87	CBR	.305	7.0
37D	#20 Monterey sand	.50	2" teflon	.550	5.45
37E	"	.56	"	.630	4.4
37F	"	.54	"	.740	3.9
37G	"	.72	1.375" teflon	.590	4.1
37H	"	.57	2" teflon	.697	3.95
37I	"	.69	1.375" teflon	.542	4.5
37K	"	.58	CBR	.422	6.45
37M	"	.68	1.375" teflon	.632	3.9
37N	"	.57	2" teflon	.640	4.3
37P1	"	.71	1.375" teflon	.765	3.2
37Q1	"	.71	1.375" teflon	.746	3.2
37Q2	"	.71	1.375" teflon	.655	3.7
37R1	"	.71	1.375 teflon	.625	3.9
37R2	"	.71	1.375" teflon	.646	3.7
39F1	"	.71	1.375" teflon	.668	3.6
39F2	"	.71	1.375" teflon	.752	3.2
44G	"	.64	1.375" polypropylene		4.14
44L	"	.64	"	.64	3.93
48A	"	.64	"	.605	4.16
48B	"	.64	"	.604	4.18
48C	"	.64	"	.592	4.29
48D	"	.64	"	.651	3.97
48E	"	.64	"	.614	4.14
48F	"	.64	"	.632	4.07

Specifically, for a soil with a given void ratio the density of a typical terrestrial grout would be approximately 1 gram/cc. If we have a foam density of 0.5 g/cc it means the foam system would use one-half the weight of chemicals to achieve the same stabilized volume.

For systems 11, 12, 25, and 37K injections into soil masses were made by placing the sand in a mold and then inserting a syringe cannula to a depth of 5 inches. A surcharge was added to the sand. A given urethane mixture was poured into the syringe and injected into the soil mass producing a spherical stabilized mass. For all other systems injections were made into soil contained in either a 1.4" or 2.0" diameter teflon mold. The procedure in this case was to insert a syringe cannula through a hole in a rubber stopper at one end of the mold to approximately the midpoint of the mold. The mold was filled with sand and a rubber stopper was placed at the other end to prevent any movement of the sand mass. The chemical system was injected into the mold, the syringe removed, and a large "C-clamp" fastened over both ends of the mold to prevent movement of the soil mass as the chemical reaction took place. In this type of injection it was determined experimentally that best results were achieved when the total weight of the chemical system was 40 grams. This yielded a stabilized mass approximately 6-1/2" long in the 1.4" diameter mold and approximately 3" long in the 2.0" diameter.

It should be noted that in tests 11, 12, 25, and 27 the data given are for chemical systems in which there was no visible association before injection. These systems also contained large proportions of blowing agents and/or co-solvents which were added in an attempt to reduce initial viscosities. It was concluded later that even though they produced low foam densities in the soil voids the quality of the system

could not be guaranteed. This is a consequence of injecting them in a dispersed state. Thus, these systems have been rejected for future use.

In systems 11 through 27 several different sand types were used ranging from a coarse Monterey sand to a fine Antioch river sand. For systems 37, 39, 44 and 48 a #20 Monterey sand (medium sand) was used.

No conclusions can be drawn at this time as to the relationship of foam density to catalyst content. The results indicate clearly, however, that low density foams can be formed in granular soils and that significant savings in stabilizer quantities may be realized relative to usual soil grouts.

IV. ENGINEERING PROPERTIES OF INJECTED SOIL MASSES

Engineering properties of injected soil masses were evaluated for the following four chemical systems: 34A, 39A, 43Q, and 46PP. To evaluate the extent to which the chemical systems could impermeabilize the soil, it was necessary to measure the permeability of an injected soil mass and to compare it to the permeability of the untreated soil. The permeability of the injected masses were determined using 1.4" diameter samples. The procedure used was to cut two 3" long samples from a 6-1/2" long stabilized cylinder of soil. These samples were then jacketed by rubber membranes and placed in a triaxial test cell (Seed, Mitchell, and Chan, 1960). A cell pressure was applied to the water surrounding the jacketed specimen. A back pressure (less than the cell pressure) was used to force water into the specimen. After saturation was achieved the permeability of the mass could be readily determined by establishing a pressure gradient across the sample and measuring the volume of water passing through the sample over a given period of time.

The permeability of the untreated soil (#20 Monterey sand) was determined with a falling head permeability apparatus (Gray, 1957). Figure 3-2 presents a comparison of the permeability of the injected soil masses and the untreated soil mass for various void ratios. For the treated soil masses the void ratios indicated are those determined before injection of the chemical system. It can be seen from this figure that a soil with an initial permeability of approximately 10^{-1} cm/sec had its permeability reduced to 10^{-5} cm/sec by two of the chemical systems. A soil with a permeability of 10^{-5} would be a fairly effective barrier to fluid flow. For system 48 the soil mass was apparently made impermeable. This, of course, is the desired state.

Figures 3-3 and 3-4 present the results of several unconfined compressive tests conducted on grouted samples 3" long and 1.4" in diameter. Untreated and unconfined sand would have no strength. Figure 3-3 shows the effect of variations in catalyst content on the stress-strain behavior of system 37. It should be noted that as catalyst content increases the strength increases. These samples tended to fail on moderately well defined failure planes or along axial planes (axis in the direction of loading). Figure 3-4 presents stress-strain curves for system 39. One might expect that such a system (highly cross-linked polymeric structure) would yield considerably greater strengths than those in which there was no crosslinking (such as Figure 3-3 systems). However, the system in Figure 3-4 was too "brittle" due to the extremely high degree of cross-linking and this tended to reduce the strength considerably. Table 3-5 summarizes the strength and permeability results of these tests and tests 44 and 48.

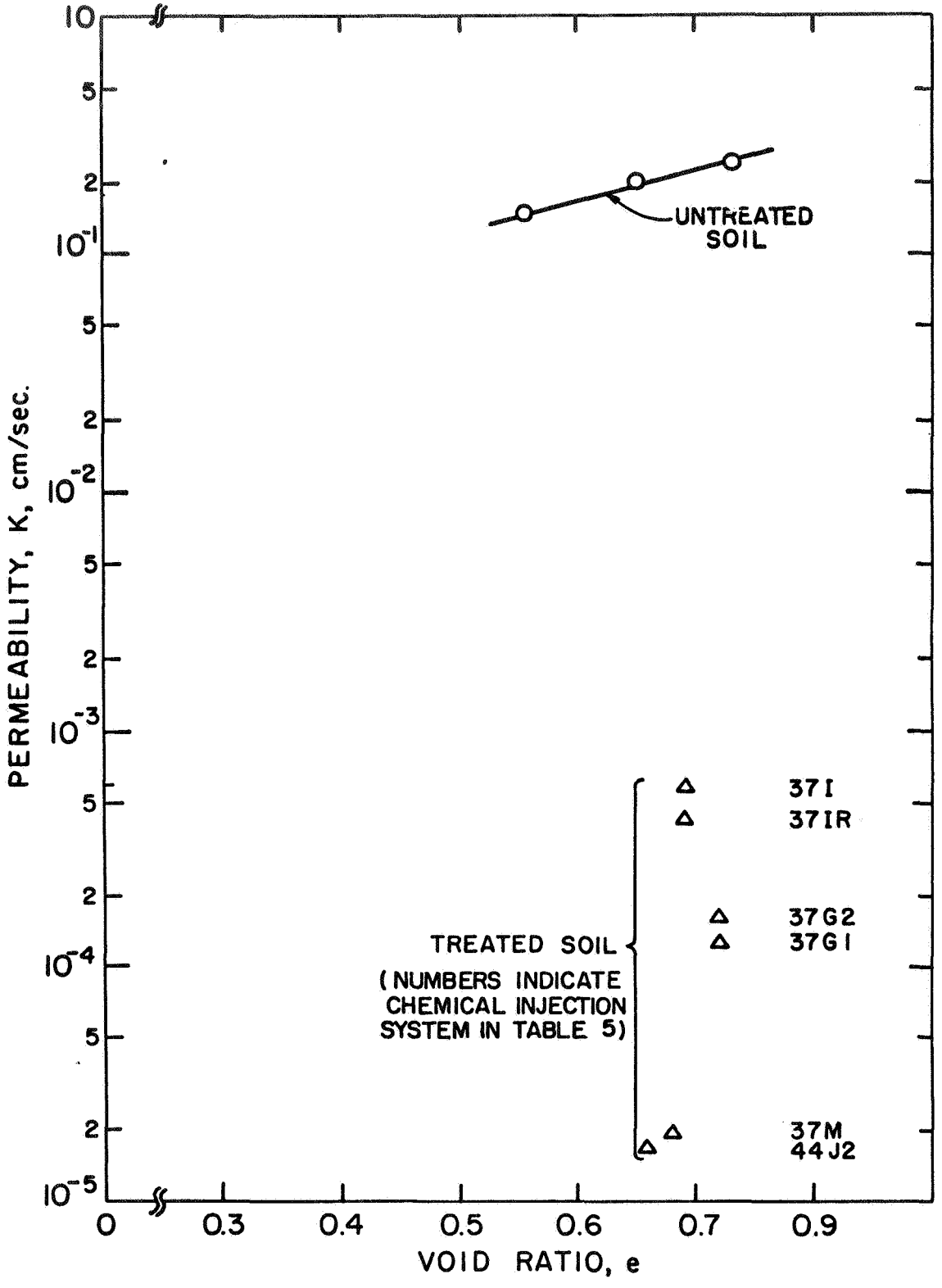

FIGURE 3-2 PERMEABILITY (TO WATER) VS VOID RATIO FOR NO. 20 MONTEREY SAND AND INJECTED SOIL MASSES.

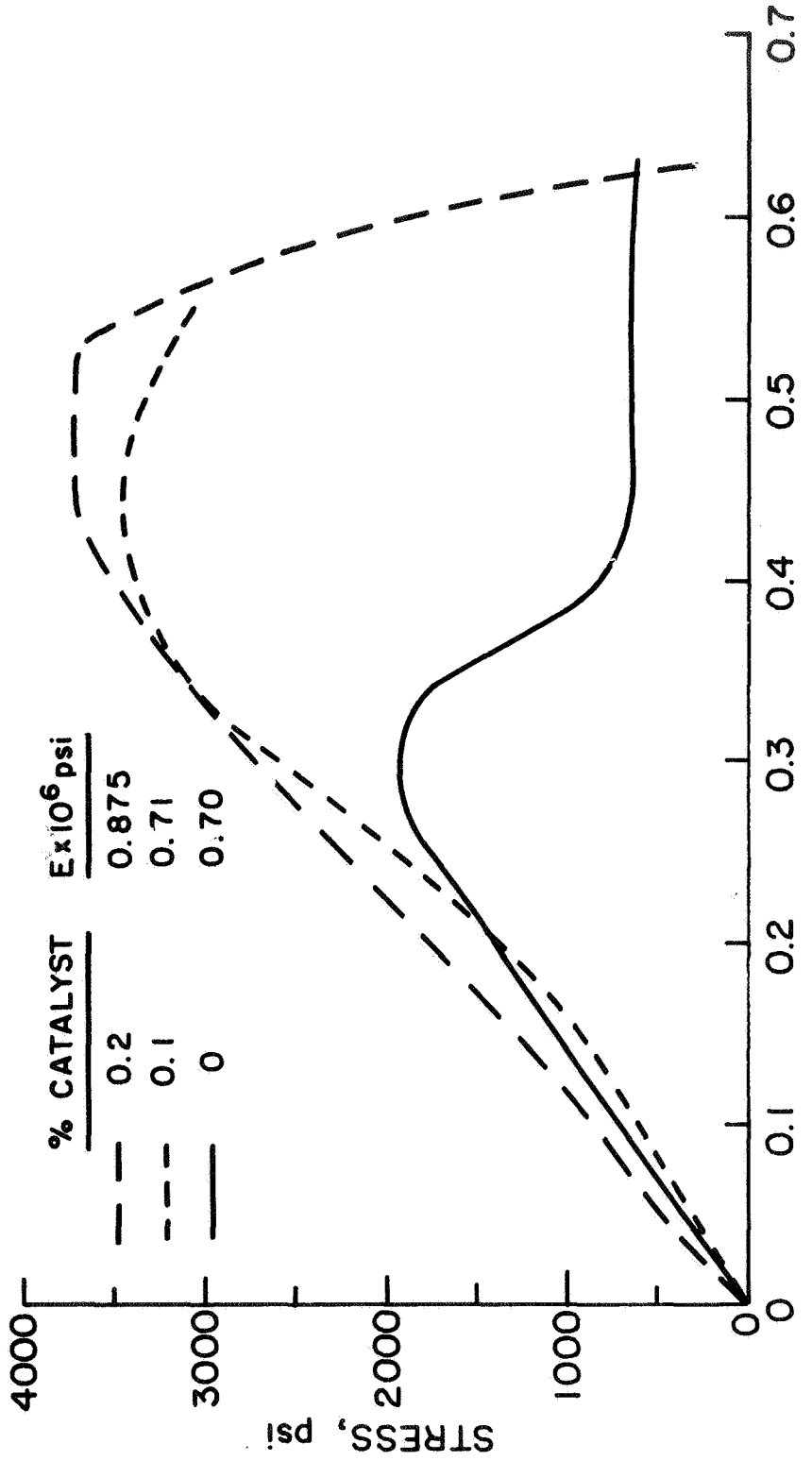

FIGURE 3-3 STRESS STRAIN BEHAVIOR OF 1.4-INCH DIAMETER, NO. 20 MONTEREY SAND SAMPLES INJECTED WITH 46.3% TRIETHYLENE GLYCOL, 53.7% TDI CHEMICAL SYSTEM

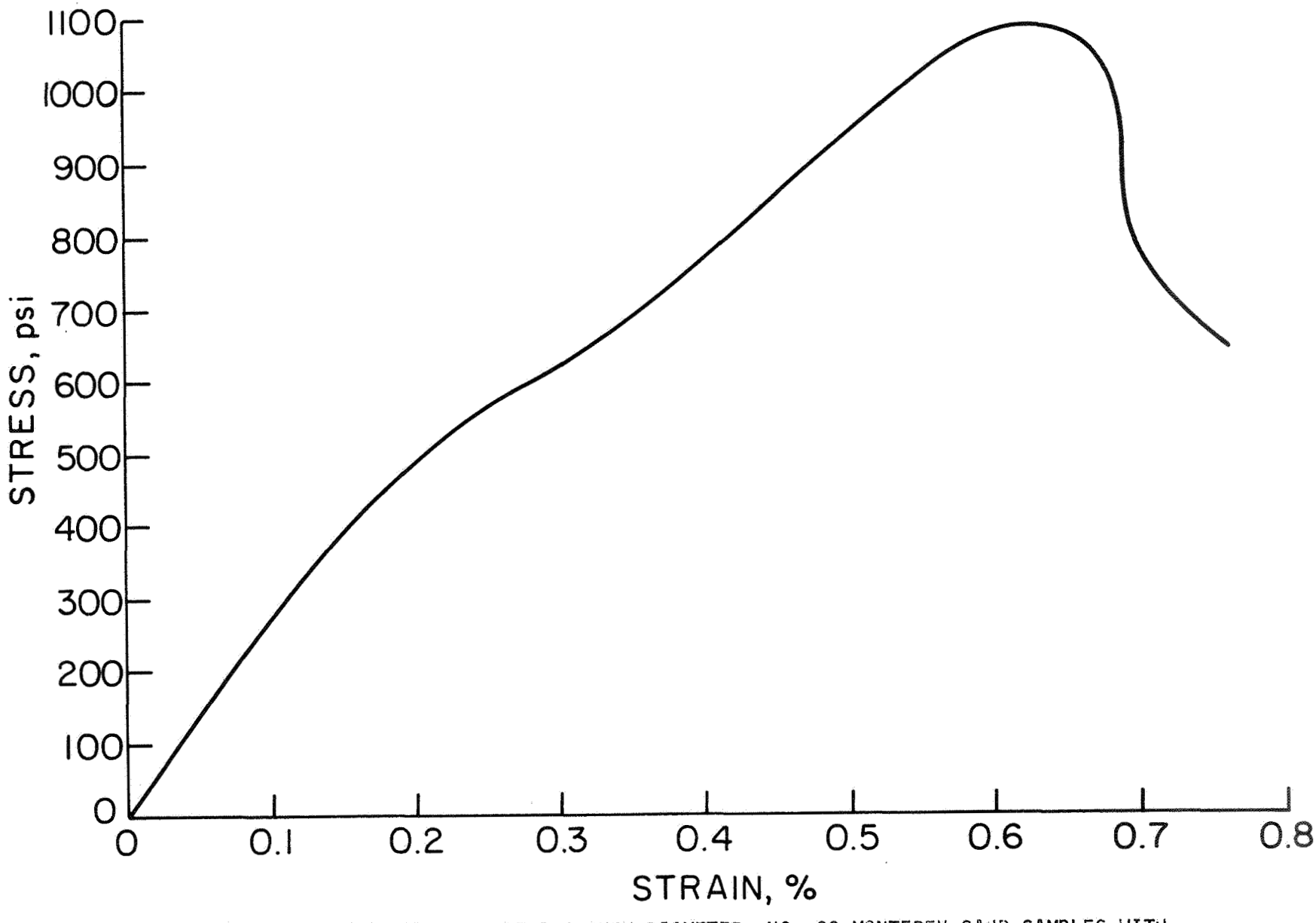

FIGURE 3-4 STRESS-STRAIN BEHAVIOR OF 1.4-INCH DIAMETER, NO. 20 MONTEREY SAND SAMPLES WITH 20.9% TRIETHYLENE GLYCOL, 18.6% TMP, 60.5% TDI CHEMICAL SYSTEM

TABLE 3-5

RESULTS OF STRENGTH AND PERMEABILITY TESTS
ON STABILIZED MONTEREY SAND SOIL CYLINDERS

Test No.	Chemical System	Unconfined Compressive Strength, psi	Permeability cm/sec
37I	53.7% TDI 46.3% triethylene glycol 0.5% (of total weight) L-531 0.5% (of total weight) diacetone alcohol 0.5% (of total weight) MIBK		5.10×10^{-4}
37G1	as in 37I + 0.1 (of total weight) catalyst		1.28×10^{-4}
37G2	as in 37I + 0.1 (of total weight) catalyst		1.65×10^{-4}
37M1	as in 37I + 0.2 (of total weight) catalyst		0.85×10^{-5}
37M2	as in 37I + 0.2 (of total weight) catalyst		2.96×10^{-5}
37R1		1960	
37Q1	as 37G1 or 37G2	3460	
37P1	as 37M1 or 37M2	3700	
39F1	60.5% TDI 20.7% triethylene glycol 18.6% TMP	1080	
44G1	53.7% TDI 46.3% triethylene glycol 1.5% (of total weight) polyethylene glycol (MW=400) 3.0% (of total weight) adipic acid 0.5% (of total weight) diacetone alcohol 5% (of total weight) castor oil 1% (of total weight) L-531	5240	
44H1	as 44G1	5265	
44J1	as 44G1	5190	
44J2	as 44G1		2.77×10^{-5}

TABLE 3-5 (Con't)

Test No.	Chemical System	Unconfined Compressive Strength, psi	Permeability cm/sec
48A1	57.8% TDI 24.9% triethylene glycol 17.3% 1,5 pentanediol 10.0% (of total weight) castor oil 0.8% (of total weight) adipic acid 3.0% (of total weight) diacetone alcohol 1.0% (of total weight) L-531	5140	
48B1	as 48A1	4780	
48D1	as 48A1	4540	
48D2	as 48A1		Impermeable

The results of the research to this point established clearly that under atmospheric conditions:

(1) Urethane foams could be made to form in the pores of granular soils.

(2) Injected soil masses could be obtained which were nearly impervious and exhibited appreciable strength.

(3) The weight of stabilizer needed per unit volume of treated soil was considerably less than would be required using conventional soil grouts.

These results were sufficiently encouraging that the next phase of the research was investigation of the formation of foamed plastics in vacuo. This phase is described in the next section.

V. DEVELOPMENT OF FOAMED PLASTIC SYSTEMS FOR USE IN VACUO

A. Behavior of a Foamed Plastic Bubble in Vacuo.

If a foamed plastic bubble is formed under atmospheric conditions it will tend to expand to the point where the internal gas pressure is in equilibrium with the atmospheric pressure and the tensile stress in the bubble skin. In vacuo the bubble formation mechanism is exactly the same except the internal gas pressure is restrained only by the tensile stress in the bubble skin. Hence, in vacuo, the tensile strength in the bubble skin must be sufficient to contain the internal gas pressure or the bubble will burst. These conditions are illustrated in Figure 3-5.

B. Required Chemical System in Vacuo.

To effectively solve the problem of producing a foam in vacuo it was necessary first to define a potentially suitable chemical system. Such a system should meet the following general requirements:

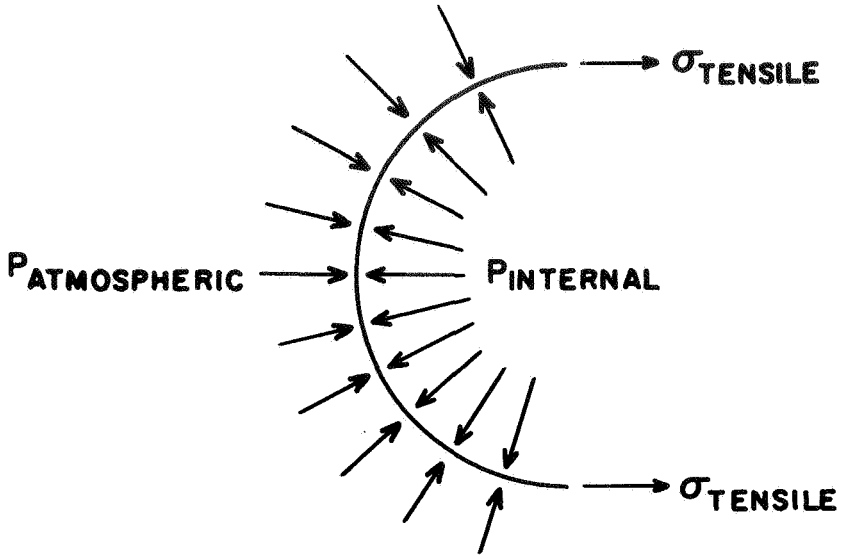

A. ATMOSPHERIC CONDITIONS.

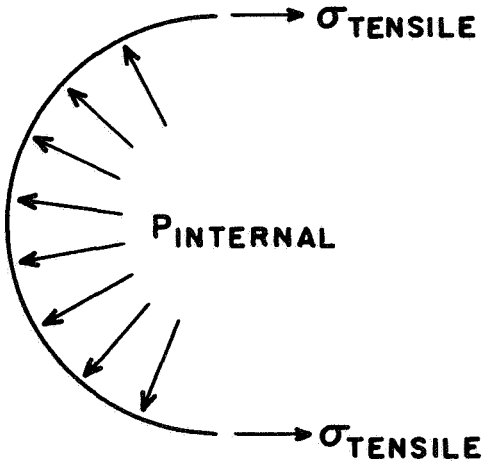

B. IN VACUO, TENSILE STRESS IN SKIN LESS THAN TENSILE STRENGTH.

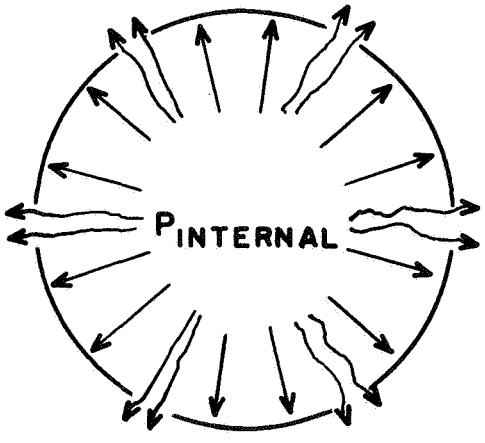

C. IN VACUO, TENSILE STRESS IN SKIN GREATER THAN TENSILE STRENGTH.

FIGURE 3-5 BEHAVIOR OF A FOAMED PLASTIC BUBBLE

1. It should have a rapid polymer formation ability. This will enable the gas produced in the polymeric structure to be used immediately in bubble formation. If the system didn't have rapid polymer formation the gas would merely go to the surface of the associated chemical system and be evacuated. Additional considerations are:
    a. The wall strength of the foam bubble must be sufficient to withstand the internal gas pressure.
    b. The reactants must be able to proceed in polymer formation once the reaction is initiated.
    c. There must be a high degree of alignment in the associated system. This will aid in the rapid buildup of the polymer structure.
2. The foam should be semi-rigid. A flexible foam would allow relief of initial gas pressure by expansion but would collapse too much when the internal and external pressures equalized. A rigid foam wouldn't allow any relief of gas pressure by expansion but wouldn't collapse as the internal and external pressures equalized. A semi-rigid foam would allow some relief of the initial internal gas pressure but wouldn't collapse too much when the internal and external pressures equalized.

Additional considerations are:

a. The structure must be slightly cross-linked.
b. The structure must employ a "flexible" polyol.

The fact that the chemical system must be designed to meet the specific demands of the environment cannot be overemphasized. The non-reactive constituents that may be added to the system such as the catalyst

and the surfactant can only change the properties of a given system within limits. The system must first be properly selected then the non-reactive constituents can be used for refinement. Table 3-6 presents a list of several chemical systems that were reacted in vacuo to exemplify this point. These systems all produce good foams under atmospheric conditions. Typically, however, in vacuo, the gas produced as the chemicals reacted formed bubbles that went immediately to the surface of the associated chemical system and burst. The resultant foam was not a foam at all but only a hardened mass of urethane plastic.

Finally, it is known that the vaporization temperature of certain chemicals decrease as the pressure in their surroundings decrease. This is true for the toluene diisocyanate (TDI) common to all urethane chemical systems. To accommodate this fact a small excess of TDI should be added to any chemical system designed. In general, the polyols in the chemical systems will not vaporize under vacuum.

C. Example of Design of Chemical System for Vacuum Condition.

As indicated above it is desirable to develop a semi-rigid foam with a rapid polymer formation ability for vacuum applications. Two possible diagrammatic structures of a semi-rigid foam are shown in Figures 3-6a and 3-6b. Figures 3-6c and 3-6d show the same structures after bubble formation. This is an over-simplified representation. However, it is readily seen that the structure in Figure 3-6d would tend to yield spherical foam bubbles whereas the structure in Figure 6c would tend to yield elongated and irregularly shaped foam bubbles. The spherical foam bubble would offer the greatest stability in vacuo, therefore, it is logical to use Figure 3-6b as the blueprint for a conceptual framework.

TABLE 3-6

UNSUCCESSFUL URETHANE FOAM SYSTEMS IN VACUO

Test No.	Chemical System	Initial Vacuum
43K1	53.7% TDI 56.3% triethylene glycol 3% (of total weight) adipic acid 1.5% (of total weight) polyethylene glycol (MW=400) 5.0% (of total weight) castor oil 1.0% (of total weight) L-531	5×10^{-3} mm Hg
43K2	53.7% TDI 46.3% triethylene glycol 2% (of total weight) adipic acid 1.5% (of total weight) polyethylene glycol (MW=400) 5.0% (of total weight) castor oil 10.0% (of total weight) L-531	7×10^{-3} mm Hg
43P1	53.7% TDI 46.3% triethylene glycol 1% (of total weight) L-531 0.2% (of total weight) catalyst	3×10^{-2} mm Hg
4D	44.5% TDI 30.7% polyethylene glycol (MW=600) 24.8% 2-ethyl-2-(hydroxymethyl)-1,3-propanediol 1% (of total weight) catalyst 2.0% (of total weight) diacetone alcohol 2.0% (of total weight) L-531	3×10^{-2} mm Hg
4E	44.5% TDI 30.7% polyethylene glycol (MW=600) 24.8% 2-ethyl-2-(hydroxymethyl)-1,3-propanediol 5% (of total weight) catalyst 1% (of total weight) adipic acid 1% (of total weight) L-531	3×10^{-2} mm Hg

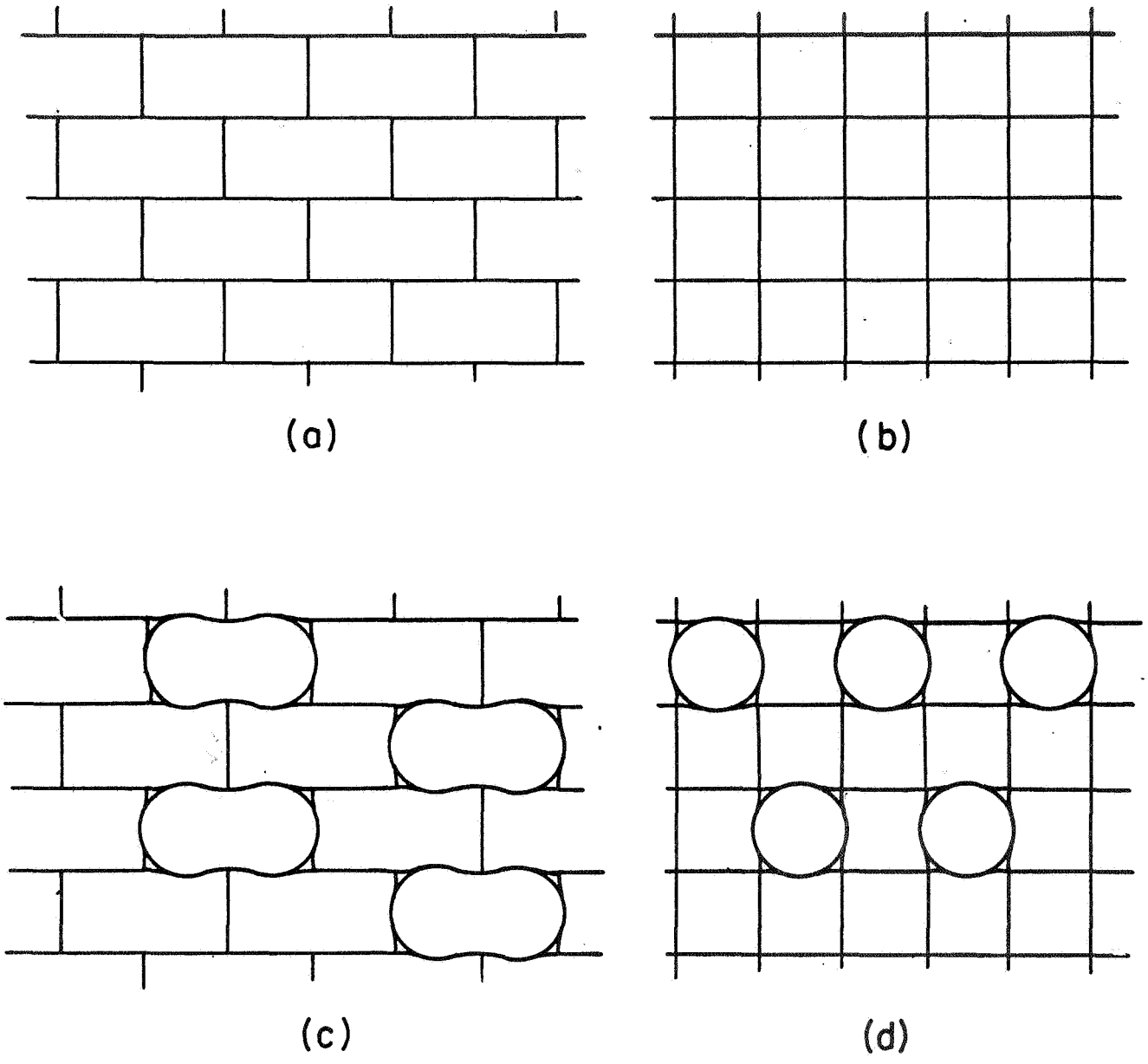

FIGURE 3-6 DIAGRAMMATIC STRUCTURES OF TWO POSSIBLE SEMI-RIGID FOAMS

Rapid polymer formation ability is a function primarily of the relative rate of reactivity of TDI with various constituents in the chemical system. Table 3-7 presents a scale of relative reactivity rates for TDI with different molecular groups. For our purposes it would be desirable to have a group similar to $-CH_2OH$. It has been found by experience that this should allow the buildup of the polymeric structure at a rate sufficiently fast to produce a workable foam in vacuo.

Figure 3-7 presents a conceptual framework showing selected urethane chemical species that incorporate both of the concepts mentioned in the last two paragraphs. Triethylene glycol is used in the structure to insure that some degree of flexibility will be present.

D. Laboratory Apparatus Used for Vacuum Systems

Figure 3-8 shows a schematic diagram of the apparatus used for study of the formation of plastic foams in vacuum. The TDI and polyol are introduced into a mixing jar in the vacuum desiccator through separate lines. Mixing of the chemicals is accomplished by an air magnetic stirrer placed under the vacuum desiccator. The stirring bar magnet is placed in the jar. The vacuum in the system is measured before the chemicals are introduced in the vacuum desiccator. The range of the McLeod gage used was not sufficient to measure the vacuum after the chemicals were introduced together with a small amount of air. It is felt, however, that the vacuum during foaming remained sufficiently low to allow meaningful interpretation of the results to be made.

E. Results of Laboratory Tests in Vacuo

One urethane system was developed that formed a foam in vacuo. It consisted of 60.9% TDI, 26.0% triethanolamine, 13.1% triethylene glycol 0.5% (of total wt.) surfactant, and 0.5% (of total weight) adipic acid.

TABLE 3-7

RELATIVE REACTIVITY RATES OF TDI

WITH VARIOUS MOLECULAR GROUPS

$-NH_2$	amine	Most reactive
$=NH$		
$-CH_2OH$	alcohol	
$=CH-OH$	approximately equal	
$-COOH$	acid (carboxyl)	Least reactive

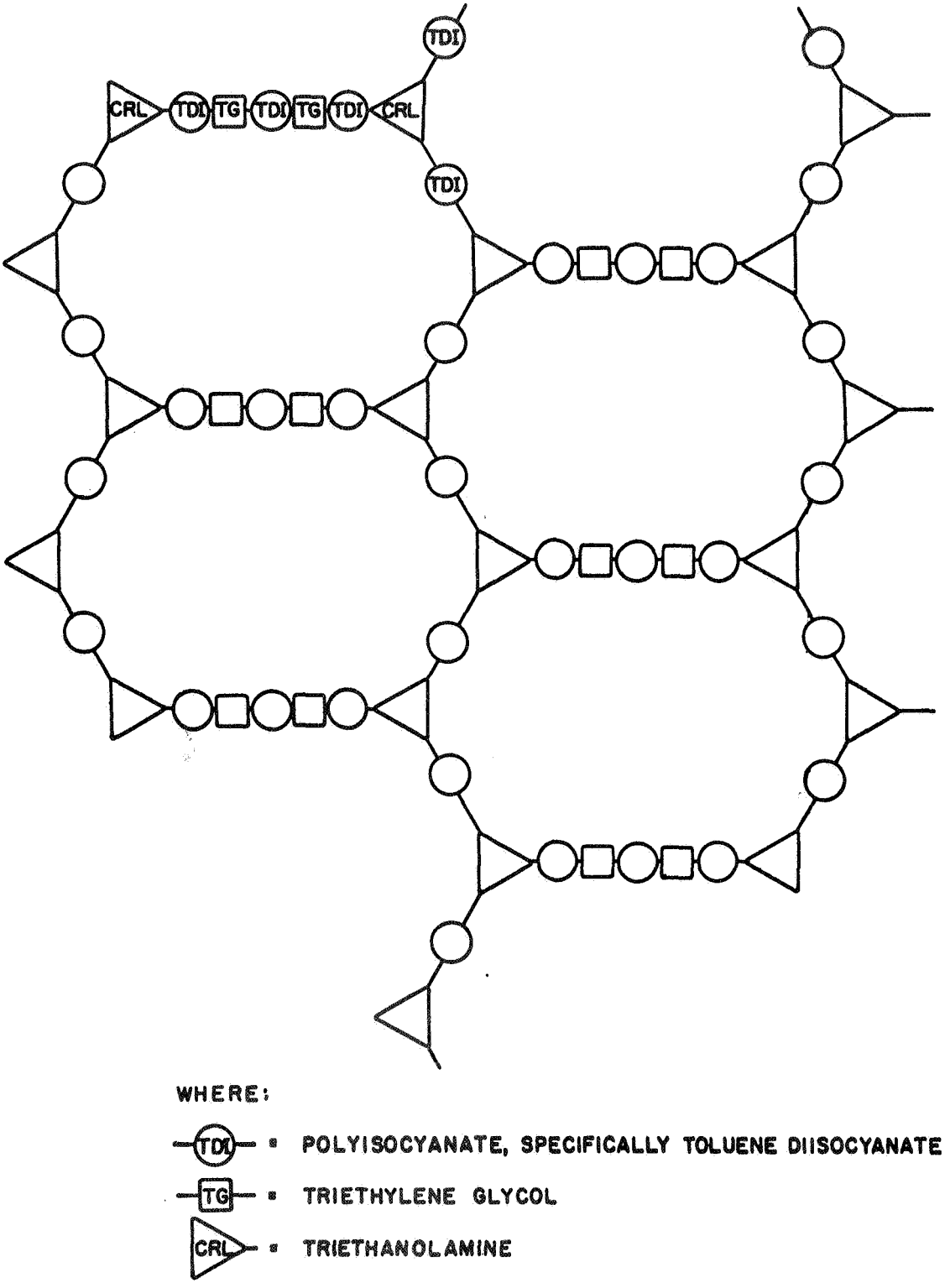

FIGURE 3-7 TWO-DIMENSIONAL CONCEPTUAL FRAMEWORK

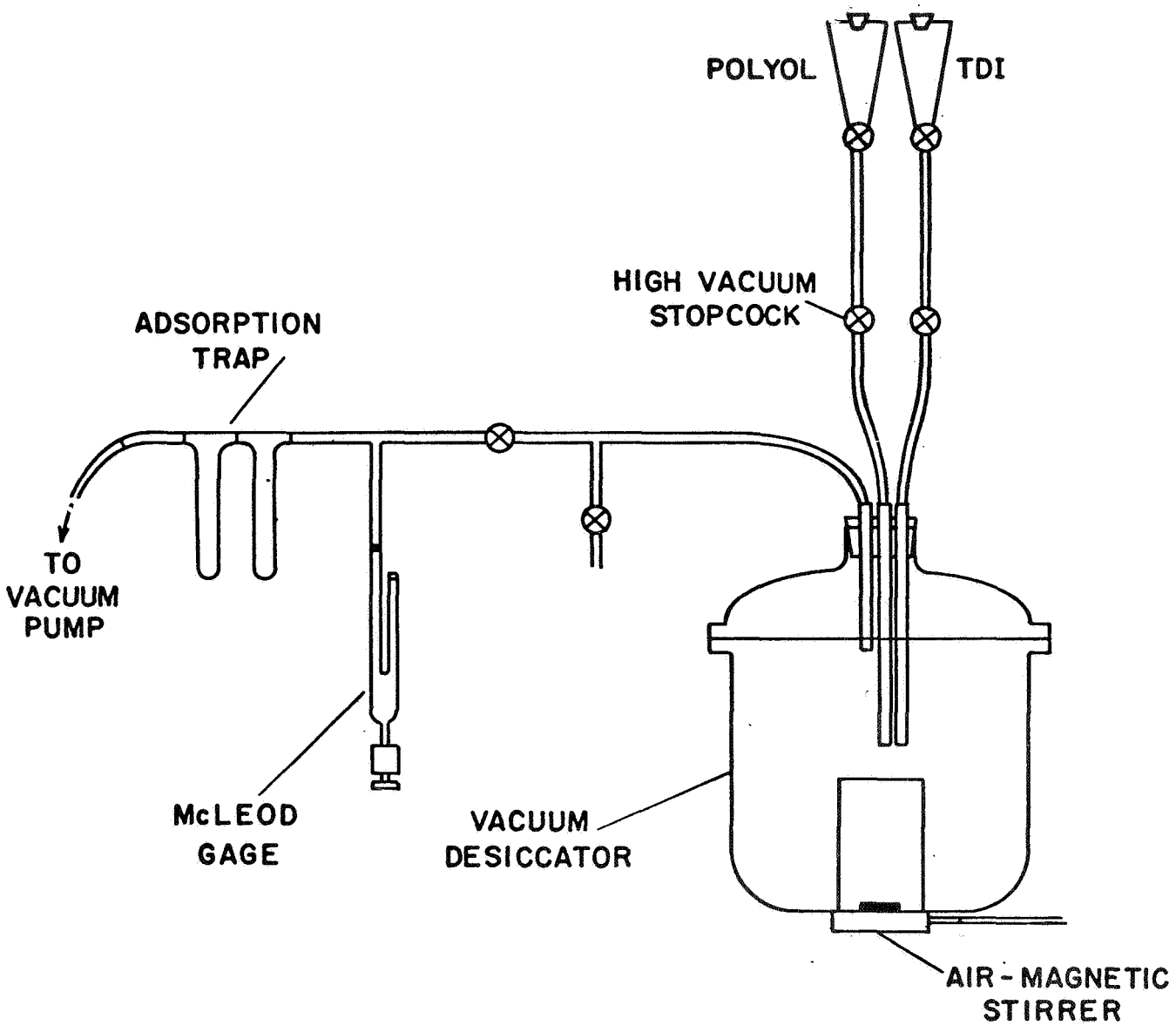

FIGURE 3-8 DIAGRAMMATIC REPRESENTATION OF VACUUM SYSTEM

This is the same system shown in the conceptual framework of Figure 3-7. The texture of the foam was coarse and might not be the most desirable in lunar application. However, it is evidence that a foam can be produced in vacuo. Tests on this type of system are continuing.

VI. CONCLUSIONS AND RECOMMENDATIONS

The encouraging results of the engineering performance tests on stabilized soil cylinders and the successful formation of urethane foamed plastic in vacuo suggest that the potential lunar engineering applications of urethane foamed plastics might become realities. However, the techniques developed to this point fall far short of those necessary in full-scale lunar application. Among many proposals to be considered further in the research program the following emerge as the most critical:

(1) The continued development of foamed plastic chemical systems for use in vacuo.

(2) Study of the effect of extreme temperature conditions on the foaming process and the subsequent development of chemical systems to operate effectively under these conditions.

(3) Study of the relationship of the properties of stabilized soil cylinders to those of stabilized soil deposits as simulated by larger scale tests.

(4) Combining the results of the research on (1), (2), and (3) for stabilization of a simulated lunar soil deposit under simulated lunar environmental conditions.

Concurrent with this research it would be desirable, although secondary in importance, to investigate the following:

(1) Characteristics of stabilized soil that might be achieved by mixing a chemical foamed plastic system directly with soil.

(2) The use of foamed plastic for protection and preservation of lunar surface material samples for earth-return operations.

With respect to this we have found that the simulated lunar soil described in Vol. 1, Chapter 1 is too fine-grained for stabilization by injection with any liquid system. It has been possible to encapsulate "undisturbed" samples of this material with foamed plastic, however, thus suggesting a possible technique for preserving samples for earth return. Such a technique might result in less disturbance than sampling with core tubes or drills.

If the actual lunar soil proves to be as impervious as the simulated soil, injection grouting will not be a suitable means for stabilization, although direct mixing with foamed plastics might be. Injection of jointed rock masses and rubble may still be desirable objectives. Furthermore direct application of foams to the walls of cavities on structures may be useful for sealing and insulating purposes. Because of the versatility and adaptability of these materials for such purposes, continued serious study is recommended in conjunction with planning for extended lunar exploration and future development of the moon.

REFERENCES

1. Corps. E. C., (1967) "Multidisciplinary Research Leading to Utilization of Extraterrestrial Resources," United States Department of the Interior, Bureau of Mines, July.

2. Dombrow, B. A., (1963), Polyurethanes, Reinhold Publishing Corporation.

3. Ferrigno, T. H., (1963) Rigid Plastic Foams, Reinhold Publishing Corporation.

4. Gerstin, H. (1965) "How to evaluate the rigid plastic foams," Product Engineer, June 21.

5. Gray, H. (1957) "Suggested Method of Test for Permeability of Porous Granular Materials by the Falling-Head Permeameter," Procedures for Testing Soils, ASTM Committee D-18, Dec. 1964.

6. Karol, R. H., (1957) "Development of a New Chemical Grout," Proceedings of ASTM, Vol. 57, 1957, p. 1219

7. Modern Plastics Encyclopaedia, (1967) McGraw-Hill, September.

8. O'Brien, L. J. (1968) United States Patent Office, Patent 3,379,260 April 23.

9. Phillips, L. N. and Parker, D. B. V., 1969) Polyurethanes, The Plastics Institute.

10. Seed, H. B., J. K. Mitchell and C. K. Chan, (1960) "The Strength of Compacted Cohesive Soils," Research Conference on Shear Strength of Cohesive Soils, ASCE, Boulder, Colorado, Appendix.